LIVE MICROSCOPY OF RNA GRANULE SORTING IN HIPPOCAMPAL NEURONS IN SPACE AND TIME

Karl Emory Bauer

Graduate School of
Systemic Neurosciences

LMU Munich

Dissertation
der Graduate School of Systemic Neurosciences
der Ludwig-Maximilians-Universität München

April, 2019

Supervisor
Prof. Dr. Michael A. Kiebler
BioMedizinisches Centrum/ Lehrstuhl Zellbiologie
Ludwig-Maximilians-Universität München

First Reviewer: Prof. Dr. Michael A. Kiebler
Second Reviewer: Dr. Oliver Griesbeck
External Reviewer: Prof. Dr. Gunter Meister

Date of Submission: 30.04.2019
Date of Defense: 10.09.2019

Table of Contents

Abbreviations

Arc	Activity-regulated cytoskeleton-associated protein
ALS	Amyotrophic lateral sclerosis
BicD	Bicaudal-D
Btz	Barentsz
Calm	Calmodulin
CamKII	Calcium/Calmodulin-dependent protein kinase II
CLIP	Cross-linking and immunoprecipitation
CPE	Cytoplasmic polyadenylation elements
CPEB1	Cytoplasmic polyadenylation element binding protein 1
DEAD	Asp-Glu-Ala-Asp
DIV	days in vitro
dsRBD	double-stranded RNA-binding domain
dsRBP	double-stranded RNA-binding protein
E17	embryonic day 17
eGFP	enhanced green fluorescent protein
Egl	Egalitarian
FISH	Fluorescent in situ hybridization
FMRP	Fragile X Mental Retardation Protein
FP	fluorescent protein
GPCR	G-protein coupled receptor
hnRNP	Heterogeneous Nuclear Ribonucleoprotein
IP	Immunoprecipitation
ISH	In situ hybridization
KIF1A	Kinesin family member 1A
KIF5	Kinesin family member 5
KD	knock-down
lncRNA	long non-coding RNA
LTD	Long-term depression

LTP	Long-term potentiation
MAP	Microtubule-associated protein
MCP	MS2-coat protein
mGluR	metabotropic glutamate receptor
RNA	ribonucleic acid
miRNA	micro RNA
mRNA	messenger RNA
NLS	nuclear localization signal
ORF	open reading frame
P-bodies	Processing-bodies
PSF	polypyrimidine tract binding protein-associated splicing factor
Pur	Purine-rich element binding protein
qRT-PCR	quantitative reverse transcriptase (real-time) PCR
RBD	RNA-binding domain
RBP	RNA-binding protein
RFP	red fluorescent protein
Rgs	Regulator of G-protein signaling
RISC	RNA-induced silencing complex
RNP	Ribonucleoprotein particle
shRNA	short hairpin RNA
smFISH	single molecule fluorescence *in situ* hybridization
smiFISH	single molecule inexpensive fluorescence *in situ* hybridization
SMN	survival of motor neuron protein
Stau	Staufen
SYNCRIP	Synaptotagmin Binding Cytoplasmic RNA Interacting Protein
tdMCP	tandem MS2-coat protein
UTR	untranslated region
Xrn1	5´-3´ exoribonuclease 1
ZBP	Zipcode-binding protein

1. Introduction

1.1 Overview

The ability to learn and form memory is of vital importance, not only for basic survival, but also as a basis for higher cognitive functions. This ability is attributed to the cells of the nervous system that comprise the brain, *i.e.* neurons and glial cells. It is well established today that neurons possess the ability to form special functional connections, termed synapses, that are used to transmit directional signals such as action potentials form one cell to the next (Albright et al., 2000). In addition, glia have a vital role in the maintenance and regulation of synaptic strength (Allen and Lyons, 2018; Eroglu and Barres, 2010). Various anatomical regions of the brain and the neuronal connections between them have been linked to learning and memory. A core role is attributed to the hippocampus, which has been shown to be essential for the retention of new information and the formation of long-term memory (Albright et al., 2000). Long-term memory goes hand in hand with long lasting synaptic strengthening or weakening based on previous electrophysiological activity patterns, called long-term potentiation (LTP) and long-term depression (LTD). The ability of synapses to change their transmission strength is termed synaptic plasticity. On a molecular level, we can distinguish (at least) two phases in this process: an early phase over the first few hours (1-3 h), which is protein-synthesis independent and a late phase (up to 24 h), which depends on new protein synthesis (Bailey and Chen, 1983; Bailey et al., 2015; Frey et al., 1988; Stanton and Sarvey, 1984; Sutton and Schuman, 2006). Therefore, the synthesis of new protein is essential for the development of long-term memory. Moreover, it is understood today that new protein synthesis can occur locally at active synapses (Kang and Schuman, 1996; Yoon et al., 2016). This is accomplished by the translation of locally available messenger ribonucleic acid (mRNA), which would allow the synthesis of the encoded protein and its direct integration into the synapse, changing the synaptic proteome, and directly affecting synaptic plasticity (Doyle and Kiebler, 2011).

However, the biological relevant processes enabling local protein synthesis are not well known. How is mRNA made readily available at synapses and how is it regulated in the complex morphological structure of a neuron? This dissertation aims to characterize mRNA transport processes in living neurons and to understand how

neuronal activity and RNA-binding proteins (RBPs) regulate the subcellular localization of two different types of RNA granules (RNA-protein complexes), *i.e.* dendritic transport granules and processing bodies (P-bodies). These processes are the foundation of synaptic plasticity, and therefore, essential for learning and memory formation.

1.2 mRNA and RBPs in learning and memory formation

1.2.1 mRNA transport, localized translation and synaptic plasticity

The translation of localized mRNA is a critical process, by which cells can target protein expression to certain intracellular subcompartments (Buxbaum et al., 2015a; Medioni et al., 2012). Thereby, a protein can be synthesized by ribosomes at a defined subcellular location, restricting its function both in space and time. This is an essential mechanism for many biological processes, such as embryonic axis formation, cell division or cell migration (St Johnston, 2005). In neurons, mRNA localization has been implicated in several processes such as axonal outgrowth and regeneration, dendritic branching, synapse morphology and in higher order functions such as learning and the formation of memory (Klann and Dever, 2004; Sahoo et al., 2018; Willis et al., 2005; Yoon et al., 2016).

Previous work in multiple model systems has demonstrated how mRNA localization governs these essential processes, and its miss-localization can have severe impact at the cellular level or on the entire organism. For instance, in the oocyte of the fruit fly *Drosophila melanogaster* the correct spatial and temporal regulation of key mRNAs such as *oskar*, *bicoid* or *gurken* are essential in axis formation and the further body patterning of the animal (Riechmann and Ephrussi, 2001). Previous studies have shown that the mechanisms used to achieve precise transcript localization are diverse and that mRNA distribution patterns can appear strictly ordered or more intricate (Lecuyer et al., 2007; St Johnston, 2005). For instance, mRNA can be diffusely localized to one cellular pole, it can be found in discrete mRNA granules or be localized in different cellular compartments. These findings indicate that mRNA localization is not random, but highly regulated and dependent on the transcript itself. Furthermore, the localization of an mRNA usually

coincides with a similar localization pattern of the equivalent protein, and the disruption of mRNA localization in turn also disrupts the localization of the protein (Lecuyer et al., 2007; Riechmann and Ephrussi, 2004). Therefore, initial protein localization is often directly linked to the localization of its mRNA. After translation however, a protein can undergo its own transport, or be degraded, altering its distribution independent of the original transcript.

To achieve proper localized protein expression, mRNA might be tightly regulated throughout its lifetime: during transcription, splicing, nuclear export, transport, translation and ultimately degradation. All these processes are accomplished by the combination of *cis*-acting factors such as mRNA sequences and/or structures, *trans*-acting factors such as RBPs or microRNAs (miRNAs), and intra- or extracellular cues (Huang et al., 2003; Rook et al., 2000; Zhang et al., 1999). The processes leading up to localized translation, are illustrated in a neuron in **Fig. 1.1,** based on previously proposed models (Doyle and Kiebler, 2011; Wilhelm and Vale, 1993). Particularly, RBPs play an essential role in regulating important processes involved in posttranscriptional gene regulation such as mRNA transport or translation (Fernandez-Moya et al., 2014). It is proposed that an mRNA is exported from the nucleus after transcription and splicing, where it is packaged into ribonucleoprotein particles (RNPs), also termed RNA granules, via the binding of RBPs and associated factors (**Fig. 1.1A**). The presence of certain *trans*-acting factors may depend on mRNA sequence or structure, providing specific binding sites, or the cooperative and competitive binding of additional factors, e.g. adaptors or motor proteins. In addition, extracellular cues will have an effect as well. Upon packaging, the RNPs are transported along cytoskeletal structures by motor proteins. Multiple lines of evidence suggest, that RNPs are not simply transported directly to one pre-determined destination, but that they can be dynamically transported in multiple directions (Knowles et al., 1996; Köhrmann et al., 1999; Tübing et al., 2010). In neurons, for instance, this behavior has been proposed to resemble a *sushi-belt* like transport in dendrites, as an anecdotal comparison to the transport of sushi on a circulating conveyor belt to the customers in a restaurant (Doyle and Kiebler, 2011). The *sushi-belt* model suggests that RNPs (the sushi) patrol dendrites in multiple directions and that they are not irreversibly anchored at one destination (the synapse, here being the customer), allowing multiple transport phases (**Fig. 1.1B**). A specific cue, such as synaptic activity, would result in the local capture of an RNP, where the mRNA

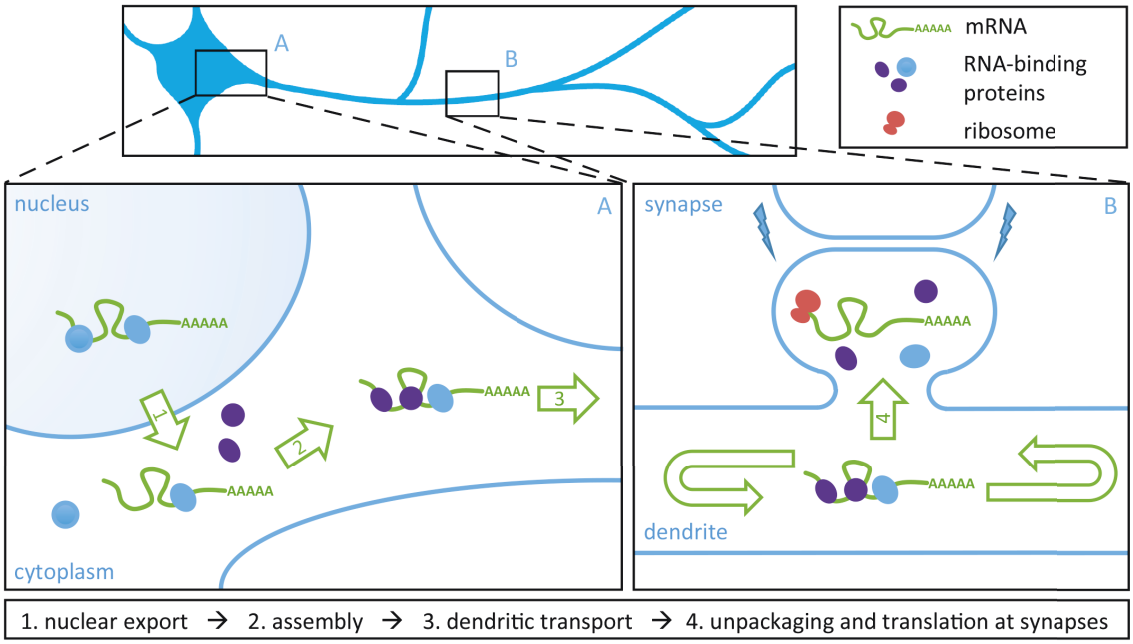

Figure 1.1: Model of neuronal mRNA transport and local translation at synapses. Insets A and B represent the soma (**A**) and dendritic compartment (**B**) of a schematic neuron. Neuronal mRNA transport, processing and translation is illustrated step by step by numbered green arrows. In B, synaptic signaling is signified via lightning bolts. This model is based on Doyle and Kiebler, EMBO Journal, 2011.

may be released from associated factors to permit translation by localized ribosomes. After translation the mRNA might eventually be repackaged and transported to a new destination for another round of translation. This model of mRNA transport and translation would be an efficient and economical way for a cell to rapidly deal with local protein demand at sites far from the soma.

The following chapters will take a closer look at relevant scientific insight into mRNA transport and translation, and its regulation.

1.2.2 mRNA transport is a motor-driven process

The first report of intracellular mRNA transport of a specific transcript in living cells was made by Ainger et al. (Ainger et al., 1993). The authors injected *in vitro* transcribed fluorescently labeled *myelin basic protein* (*MBP*) mRNA into cultured oligodendrocytes and observed that the initially diffuse mRNA eventually formed distinct granules, which moved along microtubules. In neurons, the use of the cell-permeable RNA dye SYTO14 first showed the transport of RNA granules along dendrites of cortical neurons (Knowles et al., 1996). Multiple types of transport behaviors can be observed in cells *in vivo* (Ainger et al., 1993; Fusco et al., 2003; Knowles et al., 1996; Park et al., 2014). These are classically categorized as stationary (no displacement over a define threshold), diffusive (displacement in line with Brownian motion or random walk), corralled (confined movement in a small restricted area) or directed transport (unidirectional transport over a threshold). The occurrence of these categories has been analyzed in different organisms and for different mRNA molecules. Importantly, a single transcript may undergo multiple transitions between these transport behaviors upon sufficiently long observation time (Monnier et al., 2015). Although the process of diffusion and local anchoring has also been proposed as a method to achieve specific mRNA localization patterns (St Johnston, 2005), it is the motor-driven directed transport in neurons, which is understood to be the basis of regulated dendritic localization. This motor-driven transport occurs by the displacement of motor proteins along cytoskeletal structures (Ainger et al., 1993; Knowles et al., 1996; Köhrmann et al., 1999), as microtubule-depolymerizing drugs reduce the transport of mRNAs and RBPs in dendrites (Knowles et al., 1996; Köhrmann et al., 1999; Rook et al., 2000). The motor proteins

kinesin and dynein have been implicated in this process (Gagnon and Mowry, 2011; Kanai et al., 2004; Ma et al., 2011; McClintock et al., 2018; McKenney et al., 2014). For instance, knock-down of the kinesin heavy chain KIF5B disrupts the transport of *MBP* mRNA into processes of oligodendrocytes (Ainger et al., 1993), or *Arc* and *CaMKIIα* mRNAs in dendrites (Kanai et al., 2004), while KIF5B overexpression has the opposing effect, *i.e.* an increase in dendritic mRNA localization (Kanai et al., 2004). Furthermore, KIF5B is found in RNA granules together with the dendritic mRNAs *Arc* and *CaMKIIα*. In addition, the observed velocities of RNPs in various publications are all consistent with motor-driven transport (Köhrmann et al., 1999 6.4 µm/min; Park et al., 2014, 1.3 µm/s). If dependent on motor proteins, the directed displacement of RNPs along microtubules is an ATP dependent process and must be regulated on a cellular level. To date it is yet unknown, how a motor protein is linked to an RNP and which factors mediate the association. The study of this process is complicated in dendrites, which have microtubules of mixed polarity, making it difficult to easily discern plus- or minus-end directed transport (Baas et al., 1988; Burton, 1988; Kanai et al., 2004).

1.2.3 Regulation of mRNA localization by RNA-binding proteins

Multiple studies have demonstrated the displacement of RNPs via the visualization of fluorescently tagged RBPs, such Staufen2 (Stau2), the Zipcode-Binding Protein 1 (ZBP1) or heterogeneous nuclear ribonucleoprotein A2 (hnRNP A2) (Han et al., 2010; Köhrmann et al., 1999; Tang et al., 2001; Zhang et al., 1999). However, it is essential to identify the individual components of these granules, and to investigate how they interact with each other. The biochemical purification of RNPs has brought more detailed insight into the composition of these RNA granules. For instance, Kanai et al. characterized *Activity-regulated cytoskeleton-associated protein* (*Arc*) and *Ca^{2+}/calmodulin-dependent protein kinase IIα* (*CaMKIIα*) mRNA granules, and found that the associated proteins Staufen1 (Stau1), Purine-rich element binding protein α (Purα), heterogeneous nuclear Ribonucleoprotein U (hnRNP U) and polypyrimidine tract binding protein-associated splicing factor (PSF) are involved in their dendritic localization (Kanai et al., 2004). Moreover, the proteins Synaptotagmin Binding Cytoplasmic RNA Interacting Protein (SYNCRIP, hnRNP-Q1)

and Fragile X Mental Retardation Protein (FMRP) were identified as well. This study proved that transport RNPs can be composed of many *trans*-acting factors, some of which are necessary for proper mRNA transport. Another study isolated *ß-actin* mRNA granules from the developing rat brain and identified a large number of associated proteins (Elvira et al., 2006), including RBPs such Staufen2 (Stau2). The RBP ZBP1, previously shown to be involved in the localization of *ß-actin* mRNA was identified as well (Zhang et al., 2001). In addition, *ß-actin* mRNA granules contained stalled ribosomes, indicating that translation is stopped in motile granules (Elvira et al., 2006). Both aforementioned screenings identified a quantity of overlapping proteins, such as SYNCRIP or the family of DEAD box helicases, but differed in others such as ZBP1 (Elvira et al., 2006; Kanai et al., 2004). Taken together, these publications provided first evidence that RNPs might be composed of different proteins depending on the presence of specific mRNAs, tissue specificities or developmental variations. Moreover, aside of transport RNPs, which deliver transcripts to specific subcellular locations in a translationally silent state, there are other types of RNA granules, which are distinct in their protein composition, function, localization and morphology, such as processing bodies (P-bodies), stress granules or the RNA-induced silencing complex (RISC) (**Fig. 1.2**) (Fernandez-Moya et al., 2014; Kiebler and Bassell, 2006; Kosik, 2006), that can be categorized by the presence or absence of certain proteins. Recent studies have contributed to our understanding of RNP composition under different conditions or in different cellular compartments (Cajigas et al., 2012; Fontes et al., 2017; Schanzenbacher et al., 2018), showing that RNP composition does not only vary across different cell types or conditions, but also within the same system. Although many components of RNPs are conserved across species, a comparison of neuronal Staufen2 (Stau2) and Barentsz (Btz) containing granules has shown that these RNPs are more heterogeneous than expected, with only about a third of common proteins (Fritzsche et al., 2013; Kiebler and DesGroseillers, 2000). Similarly, a recent study explored the protein composition of different axonal RNPs, dependent on mRNAs and heterogeneous nuclear ribonucleoproteins (hnRNPs) (Lee et al., 2018). The authors found that RNPs form distinct functional groups dependent on their interaction with different hnRNPs. Together, these studies indicate that different RNPs have different biological functions, suggesting that RNA granules are highly dynamic in their

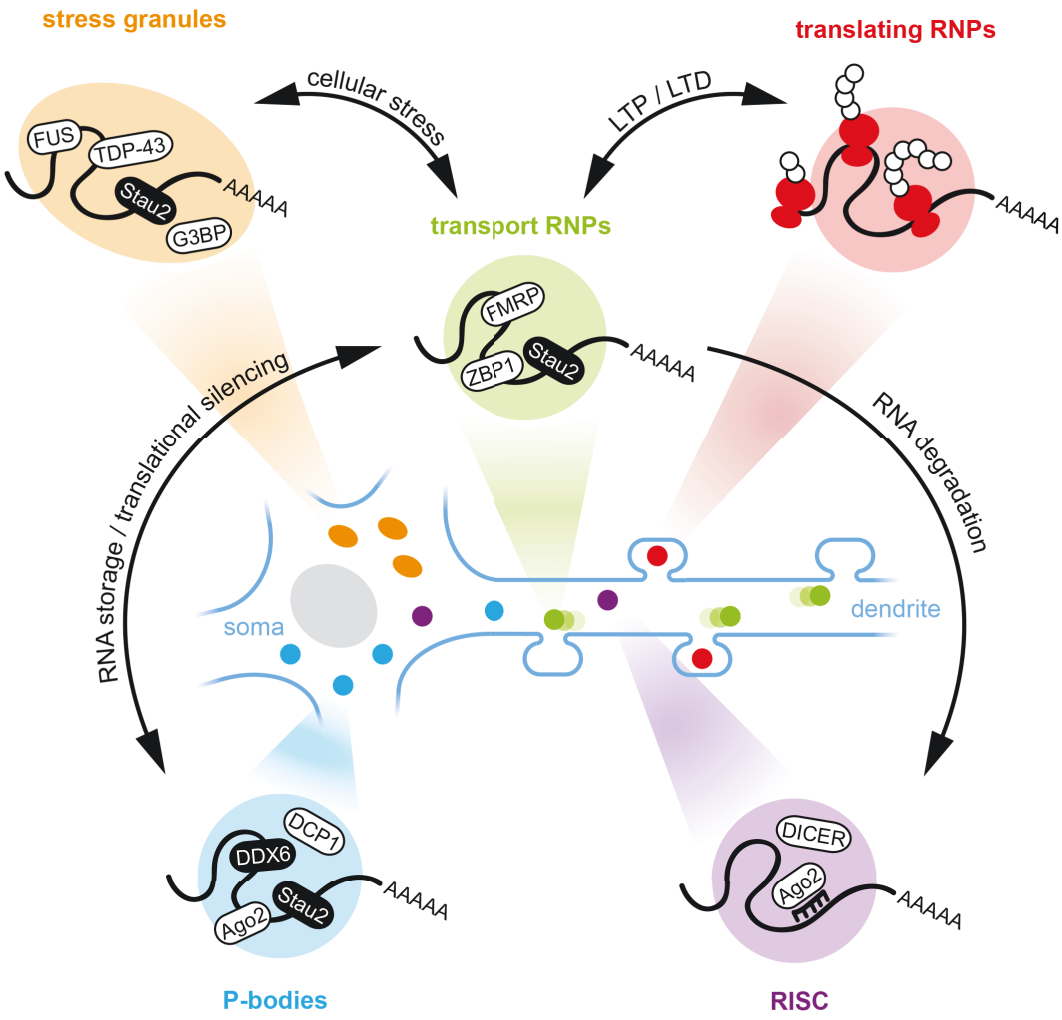

Figure 1.2: Schematic overview of representative examples of known mRNA granules in neurons. For simplicity, only soma, a dendrite and mushroom-shaped spines are shown. Types of mRNA granules are color coded: stress granules (orange), transport RNPs (green), translating RNPs (red), P-bodies (blue) and RISC (purple). Physiological relevant interplay resulting in mRNA or protein reorganization between granule types are indicated, with a focus on transport RNPs. RNPs = ribonucleoprotein particles, LTP = long-term potentiation, LTD = long-term depression, RISC = RNA-induced silencing complex.

composition. Importantly, in neurons, neuronal activity can have an effect on RNP composition (Fontes et al., 2017; Schanzenbacher et al., 2018).

Certain RBPs regulate the transport and localization of their target mRNAs, as mentioned above for *Arc, CaMKIIα* and *ß-actin* mRNA (Kanai et al., 2004). To mediate localization, RBPs recognize and bind RNA sequences or structures termed *cis*-elements or zip codes, often, but not exclusively located in the 3´-untranslated region (3´-UTR) of mRNA (Jambhekar and Derisi, 2007). For instance, the cytoplasmic polyadenylation element binding protein 1 (CPEB1) binds the cytoplasmic polyadenylation elements (CPEs) located in the 3´-UTR of *CaMKIIα* mRNA to mediate dendritic localization (Huang et al., 2003). Neurons cultured from mice deficient for CPEB1 display a decrease in dendritic localization of mRNA reporters carrying CPEs in their 3´-UTRs. Additionally, *CaMKIIα* and *Microtubule-associated protein 2* (*MAP2*) mRNAs are reduced in synaptosomal preparations of neurons expressing a dominant negative CPEB protein. Such RNA zip codes or localization elements have been identified for other mRNAs as well (Heraud-Farlow et al., 2013; Rook et al., 2000; Zhang et al., 2001).

The interaction of specific RBPs with their target mRNAs might be an essential part of correct RNP assembly. Little is still known about the regulation and maintenance of RNP assembly. However, examples of individual proteins and mRNAs suggest this process is essential, as in the case of survival of motor neuron protein (SMN) and *ß-actin* mRNA. SMN is involved in the assembly of spliceosomal RNPs (Monani, 2005). The neuromuscular disorder spinal muscular atrophy is a consequence of the hereditary loss of SMN. A mouse model of this disease shows the mislocalization of *ß-actin* mRNA in axonal growth cones (Rossoll et al., 2003).

To ultimately modify the local proteome and exert a spatially restricted function, RNPs need to regulate the translatability of the transcripts they carry. The possibility of local translation came up with the discovery of factors related to the translation machinery in dendritic processes (Klann and Dever, 2004; Tiedge et al., 1993). Therefore, the regulation of translation during RNP transport and localization has been of increasing interest. Multiple lines of evidence have shown that local translation is related to signaling activity in neurons (Krichevsky and Kosik, 2001; Sutton and Schuman, 2006; Yoon et al., 2016). Moreover, local neuronal translation is involved in long-term potentiation (LTP) and long-term depression (LTD), which are

considered the basis for learning and memory formation (Sutton and Schuman, 2006).

In conclusion, previous research has established that RBPs play a key role in the processing and regulation of their target RNA, and that their absence or dysfunction can have severe consequences for an organism, including learning and memory impairments. As highlighted here, one aspect of this regulation is the targeting and transport of RNA to a specific subcellular location. However, how specific RBPs achieve this and which other factors determine their function are less known.

1.3 The Staufen2 protein in mRNA transport, learning and memory formation

1.3.1 Staufen structure and RNA-binding

The double-strand RBP (dsRBP) Staufen2 (Stau2) is a *trans*-acting factor that has been identified in multiple studies and shown to play a vital role in neurons (Duchaine et al., 2002; Goetze et al., 2006; Heraud-Farlow and Kiebler, 2014; Heraud-Farlow et al., 2013). Staufen was first described in *Drosophila* (St Johnston et al., 1991), and is highly conserved across species. Vertebrates carry two homologs, termed Stau1 and Stau2. Stau1 is ubiquitously expressed, while Stau2 is highly enriched in the nervous system and only present at low levels in other tissues (Duchaine et al., 2002). Mammalian Stau2 consist of five RNA-binding domains (RBDs) (**Fig. 1.3A**). However, RBD5 is inverted in Stau2, but not Stau1, compared to the *Drosphila* staufen homolog. Interestingly, it is generally assumed that the RNA-binding capability of RBD5 is compromised, though it plays a role in *oskar* mRNA translation initiation at the posterior pole of the *Drosophila* oocyte, but not in the transport of the transcript (Micklem et al., 2000). Moreover, RBD5 has been shown to bind the Miranda protein in *Drosophila*, an interaction important for *prospero* and *bicoid* mRNA localization (Irion et al., 2006; Schuldt et al., 1998). In addition to the five RBDs, mammalian Staufen proteins contain a tubulin-binding domain (TBD) and a nuclear localization signal (NLS), which are not present in *Drosophila* staufen (Macchi et al., 2004). In addition, the 52 kD and 59 kD isoforms contain a nuclear export signal (NES), generated by alternative splicing (Miki and Yoneda, 2004). Interestingly, point mutations of the dsRBD3, which disrupt RNA binding,

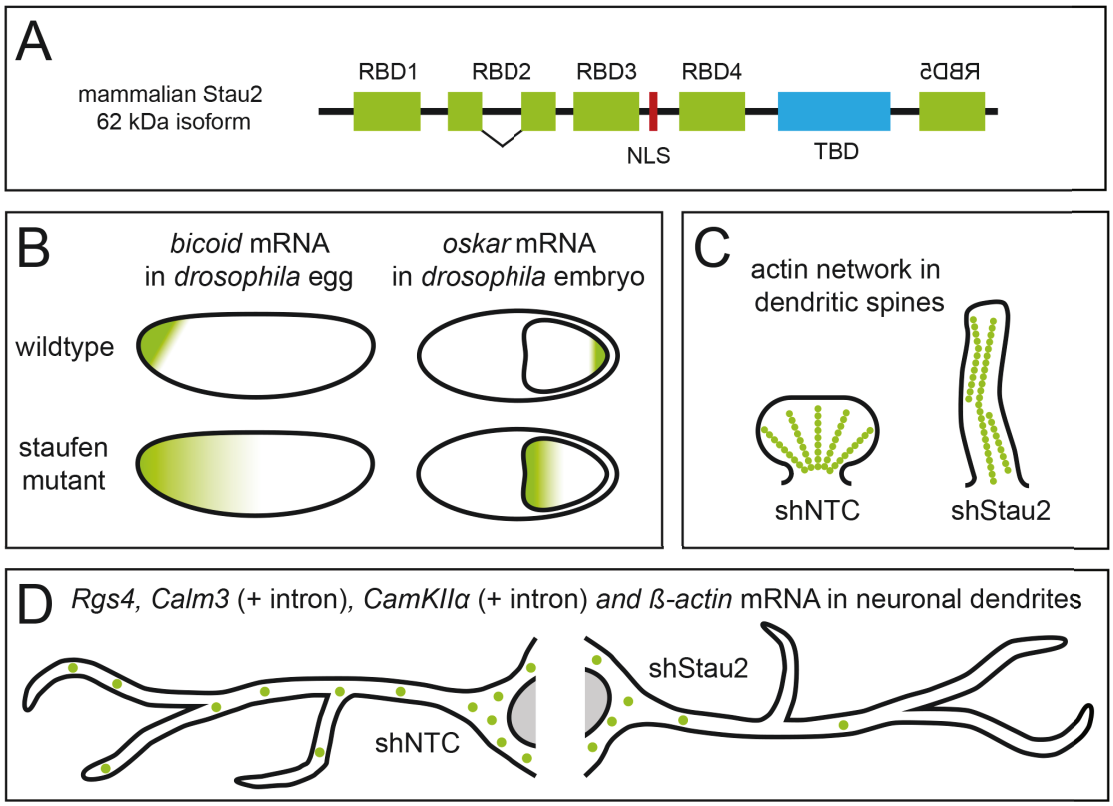

Figure 1.3: The role of the double-stranded RNA-binding protein Staufen2 (Stau2) in mRNA localization and dendritic spine morphogenesis. **(A)** Schematical representation of the domains of the 62 kD Stau2 isoform. RBD = RNA-binding domain, NLS= nuclear localization signal, TBD = tubulin binding domain. Mirrored RBD5 indicates inversion of mammalian Stau2 compared to *Drosophila* staufen. **(B)** Illustration of staufen dependent bicoid and oskar mRNA localization (green gradient) in the development of *Drosophila*. Based on Ferrandon et al., Cell, 1994. **(C)** Illustration of Stau2 dependent dendritic spine morphology and actin (green dots) network remodeling. Based on Goetze et al., JCB, 2006. **(D)** Illustration of Stau2-dependent Rgs4, Calm3 (intron containing, + intron), *CaMKII* α (intron containing, + intron) and *ß-actin* mRNA granules (green dots) localization to neuronal dendrites. shNTC = short hairpin non-targeting control, shStau2 = short hairpin Stau2. Based on Heraud-Farlow et al., Cell Rep., 2013, Sharangdhar et al., EMBO Rep., 2017, Ortiz et al., Cell Rep., 2017, and Goetze et al, JCB, 2006.

cause Stau2 to accumulate almost exclusively in the nucleolus (Macchi et al., 2004). Mammalian Stau2 expresses four isoforms of 52 kD, 56 kD, 59 kD, and 62 kD, that vary in their N- and C-terminal domains, *i.e.* truncations of RBD1 and RBD5, due to alternative splicing. It is thought that these isoforms have different functions in the cell. A study investigating the developing chicken eye found that the knock-down of Stau2 leads to a reduction in eye size (Cockburn et al., 2012). Interestingly, different Stau2 isoforms rescued the phenotype to a varying degree, where the longest 62 kD isoform performed a full rescue and the smallest 51 kD isoform a partial rescue. Together, these findings indicate possible different regulatory roles for the isoforms during eye development.

In contrast to most RBPs, which bind RNA in a sequence specific manner, double-strand RBPs (dsRBPs), such as Staufen, recognize double-stranded RNA and are reported to bind primarily to the sugar-phosphate backbone rather than a specific nucleotide sequences (Ryter and Schultz, 1998). A conserved αββββα structure in the dsRBD is responsible for this interaction. In the case of the *Drosophila* staufen dsRDB3, a 12 bp stem-loop with no unpaired bases and a tetraloop presents the ideal binding site (Ramos et al., 2000). Analysis by mutagenesis revealed five conserved amino acids necessary for RNA binding and a region in the α1 helix that might facilitate the interaction via a UUCG tetraloop. A recently developed computational algorithm has been used to successfully identify staufen binding sites by structure in *Drosophila* (Laver et al., 2013) and to define Stau2 binding sites in the mammalian nervous system (Heraud-Farlow et al., 2013). Interestingly, one study found the formation of a Stau1-binding site, via the base-pair interaction of a long non-coding RNA (lncRNA) with the 3´-UTR of an mRNA, streamlining the mRNA for Stau1-mediated RNA decay (Gong and Maquat, 2011). This finding presents an intriguing cooperative mechanism, which could regulate Staufen binding. Moreover, a recent study identified intramolecular long-range RNA duplexes that act as binding sties for Stau1 (Sugimoto et al., 2015). These duplexes can have loop lengths longer than 100 (57% of identified duplexes) or 500 base pairs (20% of identified duplexes). Interestingly, these long-range duplexes were often formed between the beginning and end of the coding sequence (CDS) or 3´-UTR, possibly enabling the interaction of factors bound to these regions. These examples emphasize the importance to consider mRNA structure *in vivo* and to development of new techniques, such as hiCLIP (RNA hybrid and individual-nucleotide resolution UV

cross-linking and immunoprecipitation), to reliably identify dsRNA-binding sites. However, the apparent lack of sequence specificity and the possibility of long-range RNA duplexes make the prediction of local binding sites difficult.

1.3.2 The role of Staufen in mRNA localization

Both Stau1 and Stau2 localize in distinct cytoplasmic RNPs in the soma and dendrites of neurons (Duchaine et al., 2002; Kiebler et al., 1999). The mRNA composition of such Stau2-containg granules has been described in the developing rat brain (Heraud-Farlow et al., 2013), including the *regulator of G protein signaling 4* (*Rgs4*) mRNA. Furthermore, Stau1 and Stau2 have been implicated in the localization of mRNA transcripts (Heraud-Farlow et al., 2013; Ortiz et al., 2017; Sharangdhar et al., 2017; Tang et al., 2001). Staufen is required for the localization of *oskar, bicoid*, and *prospero* mRNAs in the developing *Drosophila* oocyte and embryo (St Johnston, 2005) (**Fig. 1.3B**). Staufen knock-down leads to mislocalization of these mRNAs and their encoding proteins (Ephrussi et al., 1991; Ferrandon et al., 1994; Kim-Ha et al., 1991; Li et al., 1997). Mammalian Stau1 and Stau2 form granules that are dynamically transported in dendrites of hippocampal neurons in culture (Köhrmann et al., 1999; Zeitelhofer et al., 2008) and localize close to synapses (Stau1 Kiebler et al. 1999; Stau2: Duchaine et al., 2002). The overexpression of a dominant-negative Stau2, lacking the microtubule-binding domain and the inverted RBD5, decreases the amount of global RNA located in dendrites, visualized by ethidium bromide staining (Tang et al., 2001). Similarly, Stau2 depletion results in the reduction of multiple mRNAs in dendrites (Goetze et al., 2006; Heraud-Farlow et al., 2013; Ortiz et al., 2017; Sharangdhar et al., 2017) (**Fig. 1.3D**). This data points to a conserved role for the Staufen proteins in the spatial regulation of their target-RNAs. It is intriguing to consider how the predominantly neuronal mammalian Stau2 might act in mRNA transport in neurons.

1.3.3 The role of Staufen2 in learning and memory

Importantly, Stau2 has been implicated in neuronal signaling, synaptic plasticity and memory. Stau2 is required for DHPG-induced protein synthesis depended long-term depression (LTD) via mGluR, linking it directly to learning and memory (Lebeau et al., 2011). Here, the lack of Stau2 results in transport defects of *Map1b* mRNA via its 3´-UTR, and a reduction of the encoding protein necessary for the maintenance of metabotropic Glutamate Receptor (mGluR)-LTD. Furthermore, Stau2 knock-down results in a reduction of the amplitude of miniature excitatory postsynaptic currents (mEPSCs) in young neurons, along with a reduction in the number of dendritic spines and synapses, and an altered dendritic actin network (**Fig. 1.3C**) (Goetze et al., 2006). A recent study observed additional electrophysiological defects *in vivo*, including favored LTP and impaired LTD in Stau2 deficient rats (Berger et al., 2017). The role of Stau2 in synaptic plasticity and memory formation *in vivo* is corroborated by behavioral studies in rats and mice. The forebrain specific knock-down of Stau2 in a transgenic rat resulted in defects in spatial working memory, spatial novelty detection and associative learning and memory (Berger et al., 2017). Furthermore, mice with a reduction in Stau2 protein levels display reduced locomotion, and the inability to distinguish between familiar and novel objects (Popper et al., 2018). Another study investigating olfactory memory identified transcriptionally regulated genes, including staufen, during memory formation in *Drosophila* (Dubnau et al., 2003), raising the question if the Staufen proteins might have a conserved role in memory. Together, these studies show that Stau2 is not only essential in the expression and spatial regulation of its target mRNAs, but also has a fundamental impact on synaptic plasticity, learning and memory formation.

1.4 Rgs4 and receptor mediated signaling in the central nervous system

1.4.1 G-protein coupled receptor signaling in the central nervous system

The Kiebler lab has previously identified the *regulator of G protein signaling 4* (*Rgs4*) mRNA as a high confidence target of the double-stranded RNA-binding

protein Stau2 in the E17 rat brain (Heraud-Farlow et al., 2013). This was accomplished by immunoprecipitation of endogenous Stau2-containing RNA granules followed by microarray analysis and independent verification via qRT-PCR. Further analysis revealed that *Rgs4* was one of eight significantly enriched Stau2 target-mRNAs that function in the G protein-coupled receptor (GPCR) signaling pathway. This data indicates that Stau2 might regulate the production of proteins of common function. At neuronal synapses, the GPCR signaling pathway regulates neurotransmitter release and synaptic transmission, playing a role in both pre- and postsynaptic regulation (Betke et al., 2012; Rojas and Dingledine, 2013; Tedford and Zamponi, 2006). The ligand-dependent activation of the receptor of heterotrimeric G proteins (Gαβγ) leads to the exchange of GDP to GTP at the Gα subunit, which results in the release of Gα from Gβγ, both of which can affects downstream second messengers (**Fig. 1.4**) (Bourne et al., 1990; Hamm, 1998; Simon et al., 1991). Importantly, Gβγ activates G protein-coupled inwardly rectifying potassium (GIRK) channels, which leads to cell hyperpolarization, affecting the excitability of the neuron (Dascal, 1997). The Rgs4 protein and other members of the regulator of G protein family act as negative regulators of the GPCR pathway (Abramow-Newerly et al., 2006; Gerber et al., 2016). Here they function as GTPase activating proteins (GAPs), facilitating the hydrolysis of GTP to inactive GDP on the Gα subunit (G_q and G_i α-subunits), terminating downstream signaling of both Gα and Gβγ (**Fig. 1.4**) (Abramow-Newerly et al., 2006; Berman et al., 1996; De Vries et al., 2000; Hepler et al., 1997; Huang et al., 1997; Ross and Wilkie, 2000; Willars, 2006). The regulation by Rgs4 affects multiple receptors, such as glutamate, serotonin and dopamine receptors (Gu et al., 2007; Saugstad et al., 1998; Taymans et al., 2004). In the hippocampus, Rgs4 inhibits neuronal signaling through group I metabotropic glutamate receptors (mGluRs), by blocking the inhibition of potassium currents by mGluR5 in neurons of the CA1 region (Saugstad et al., 1998). These receptors have been linked to Stau2 during protein synthesis-dependent LTD (Lebeau et al., 2011). In addition, the Rgs4 gene is linked to neurodegenerative diseases, such as schizophrenia or Parkinson's disease and neuropathic pain (Ding et al., 2006; Erdely et al., 2006; Garnier et al., 2003; Harrison and Weinberger, 2005).

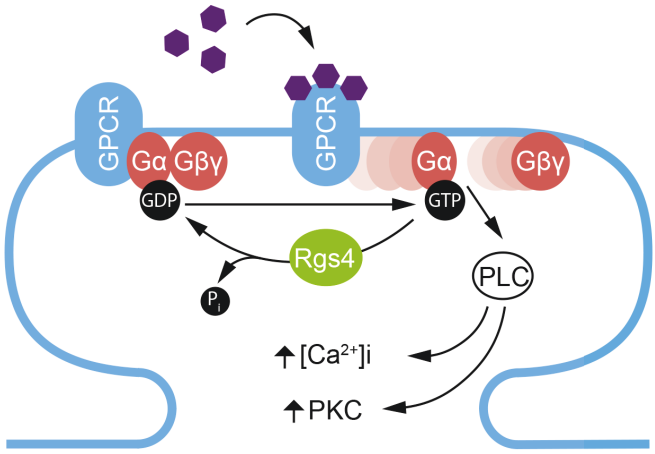

Figure 1.4: Schematically representation of G-protein coupled receptor (GPCR) activation and its regulation by Rgs4 at the postsynaptic site. Ligand activation (purple hexagons) of GPCRs results in the exchange of guanosin diphosphate (GDP) to guanosin triphosphate (GTP) at the G-protein α-subunit, leading to the dissociation of Gα and Gβγ and the activation of downstream signaling pathways. Rgs4 inhibits Gαβγ dissociation at group I metabotropic glutamate receptors (mGluRs) by activating Gα GTPase activity and the hydrolysis of GTP to GDP. Thereby, Rgs4 blocks activation of phospholipase C (PLC) and the downstream release of intracellular Ca2+ ([Ca2+]i) and the stimulation of protein kinase C (PKC). Pi = Phosphate. Modified from Heraud-Farlow et at., Cell Reports, 2013.

1.4.2 Staufen2 regulates Regulator of G-protein signaling 4 mRNA

Rgs4 is a ~24 kD protein with a single RGS domain and is expressed in multiple brain regions including the hippocampus (Gold et al., 1997; Heraud-Farlow et al., 2013; Saugstad et al., 1998). Among the RGS proteins, Rgs4 has the highest expression in the brain (Larminie et al., 2004). Investigation into the subcellular localization of *Rgs4* mRNA in hippocampal neurons via fluorescence *in situ* hybridization (FISH) shows that endogenous *Rgs4* mRNA is present in distinct granules in both the cell body and neurites (Heraud-Farlow et al., 2013). Knock-down of Stau2 results in a reduction of total *Rgs4* mRNA levels, both *in vitro* and *in vivo* (Berger et al., 2017; Heraud-Farlow et al., 2013). FISH experiments revealed that Stau2 silencing induced a strong reduction in fluorescence intensity in the cell body and a near complete depletion of *Rgs4* mRNA granules from dendrites (**Fig. 1.3**) (Heraud-Farlow et al., 2013). Importantly, the depletion of Stau2 from primary cortical neurons, results in a significant down regulation of *Rgs4* mRNA as well. Additionally, a translation assay using an *Rgs4* 3´-UTR luciferase reporter in cortical neurons revealed that Stau2 regulates *Rgs4* mRNA via its 3´-UTR. Stau2 knock-down significantly decreases the expression of the luciferase reporter, indicating that Stau2 may indeed regulate *Rgs4* mRNA stability via its 3´-UTR.

Computational analysis previously used to identify Staufen-recognizing structures (SRSs) in *Drosophila* revealed an enrichment of type III SRSs (stem consisting of at least 10 of 12 paired bases and no more than 2 unpaired bases) in the 3´-UTR of identified Stau2-target mRNAs (Heraud-Farlow et al., 2013; Laver et al., 2013). Stau2-regulated mRNAs have significantly larger 3´-UTRs than the median rat 3´-UTR. The 3´-UTR of *Rgs4* has a length of 2.2 kb, making it much longer than the median rat 3´-UTR of 496 bases, and contains two Type III SRSs (Heraud-Farlow et al., 2013). In addition, the *Rgs4* 3´-UTR contains several *in vivo* cross-linking sites for Stau2 (Sharangdhar et al., 2017). The presence of multiple binding sites raises the question, whether Stau2 might regulate other aspects of the *Rgs4* mRNA lifecycle via its 3´-UTR. A recent study reported a significant increase in Rgs4 protein in response to the induction of chemical long-term potentiation (LTP) by forskolin and high concentrations of calcium and potassium in acute mouse hippocampal slices (Fontes et al., 2017). Taken together, this data argues that Rgs4 might have an essential role in the regulation of synaptic plasticity, learning and memory.

1.5 P-bodies and the RNA-helicase Rck in the central nervous system

1.5.1 P-bodies and mRNA regulation

Transport RNPs, which deliver transcripts to specific subcellular locations in a translationally silent state, interact with other types of mRNA granules and share functional protein components with them. Such mRNA granules include P-bodies, stress granules or the RNA-induced silencing complex (RISC) (**Fig. 1.2**) (Balagopal and Parker, 2009; Fernandez-Moya et al., 2014). Although such RNA granules have overlapping components and functions, they can be categorized by the presence or absence of specific proteins, which will determine whether they are marked for transport, translation, storage or degradation. In their physiological state, all such granules can be both stable or have a high turnover of their components (Barbee et al., 2006; Kedersha et al., 2000). This dynamicity is related to the phenomenon of phase separation, as researched extensively in previous years (Brangwynne et al., 2009; Hyman et al., 2014; Molliex et al., 2015). By phase separation a cell can separate molecular processes in membrane-less droplets with liquid properties, based on the local concentration of the involved components. Physiological phase separation can be perturbed by the formation of aberrant solid-state aggregates, which have been linked to neurological pathologies such as amyotrophic lateral sclerosis (ALS) or frontotemporal dementia (FTD).

P-bodies, also termed GW- or DCP-bodies, are large granules that appear as distinct cytoplasmic foci, clustered more densely in the perinuclear region and less in distal parts of the cell (Aizer et al., 2008; Bashkirov et al., 1997; Yang et al., 2004). In neurons, P-bodies are predominantly present in the soma, but can also be found in dendrites (Vessey et al., 2006; Zeitelhofer et al., 2008). P-bodies are composed of a number of proteins, including (i) components of the mRNA decay machinery (*e.g.* Dcp1, Dcp2, Xrn1, Lsm1p-7p complex), (ii) translational regulators (*e.g.* Rck, Dhh1p) and (iii) components of the RISC complex (*e.g.* Argonaute1, Argonaute2) (Behm-Ansmant et al., 2006; Chu and Rana, 2006; Ding et al., 2005; Liu et al., 2005; Parker and Sheth, 2007). P-bodies are considered sites of transient mRNA storage and degradation, and therefore have a key role in regulating the degradation and translatability of mRNA (Cougot et al., 2004; Lian et al., 2006; Liu et al., 2005; Parker and Sheth, 2007; Sheth and Parker, 2003). These functions suggest an essential role

for P-bodies in neuronal development, synaptic plasticity, learning and memory (Ashraf et al., 2006; Schratt et al., 2006). Previous research has shown that P-bodies are localized to dendrites of rat hippocampal neurons, but are distinct from transport mRNPs and are not co-transported together (Vessey et al., 2006; Zeitelhofer et al., 2008). However, the observation of docking events between the P-body marker DCP1a and the mRNP marker Stau2 suggests an interaction between these two RNA-carrying granules. Importantly in the context of neurons, chemical stimulation of neuronal activity results in a reduction in dendritically localized P-bodies (Zeitelhofer et al., 2008). Taken together, this data shows that P-bodies are an essential RNA granule and are expected to have a profound impact on other types of RNA granules and their regulation in the cell.

1.5.2 The Rck protein and its function in the central nervous system

One key component of P-bodies is the ATP-dependent RNA helicase Rck, also termed DDX6, p54 or HLR2 (Lu and Yunis, 1992) . Rck is a member of the DEAD box protein family, characterized by a conserved Asp-Glu-Ala-Asp (DEAD) motif. Though DEAD box proteins are a family of putative RNA helicases, Rck has been shown to be a true ATP-dependent helicase (Akao et al., 2003; Lu and Yunis, 1992). As an RNA helicase, Rck has been linked to processes involving changes in RNA structure, such as translation initiation, splicing or mRNA degradation and stability (Broytman et al., 2009; Fenger-Gron et al., 2005; Smillie and Sommerville, 2002; Zhang and Wu, 1996). In neuronal stem cells, Rck induces neuronal differentiation by activating the miRNA Let-7 (Nicklas et al., 2015). Furthermore, Rck is required for translationally regulated dendrite morphogenesis in *Drosophila* (Barbee et al., 2006). Rck has been identified in complexes together with Stau2 in the rodent brain (Fritzsche et al., 2013), suggesting a role for Rck independent from P-bodies. Further research on Rck relevant to the data presented in this dissertation will be discussed in chapter 3.2.

1.6 RNA live cell imaging and the MS2 system

1.6.1 An overview of mRNA imaging techniques and challenges

The imaging of RNA expression in fixed cells or tissue is traditionally achieved by *in situ* hybridization (ISH) of the endogenous RNA with a labeled-antisense probe (Hougaard et al., 1997). The method can be applied as whole-mount ISH on small organisms, on tissue slices or single cells. The sensitivity of this approach was further improved by methods such as fluorescence *in situ* hybridization (FISH), single molecule fluorescence *in situ* hybridization (smFISH) or single molecule inexpensive fluorescence *in situ* hybridization (smiFISH) (Levsky and Singer, 2003), that all allow the quantification of individual RNA molecules. Additional adaptations of these methods have made it possible not only to image endogenous mRNAs, but also miRNAs or long-noncoding RNAs (Tsanov et al., 2016). The exposure of biological replicates to different conditions (e.g. chemical treatments) or the fixation of samples at different time-points has made this method a powerful tool in the field of cell and molecular biology.

However, many essential biological questions require to be addressed in living cells or organisms. It is in this aspect that the imaging of RNA presents a comparative challenge. To achieve the imaging of RNA in living samples, some hurdles must be overcome. Most importantly, (i) the applied method may not destroy, damage or affect the sample in a way that would influence the biological readout, but (ii) needs to introduce a detectable reporter into the cell, which (iii) specifically labels an RNA. Multiple methods have been developed, that meet these criteria to a varying degree. Some successfully applied examples are cell permeable RNA-binding agents, molecular beacons, pre-labeled in vitro transcribed mRNAs, genetically encoded systems such as the MS2-system or recently even the CRISPR-Cas system (reviewed in Bauer et al., 2017 or Mikl et al., 2010; **Fig. 1.5**). A system for the live visualization of endogenous mRNA, which has been employed successfully over the past years, is the use of molecular beacons, which recognize RNA by antisense and only emit fluorescence upon binding (Turner-Bridger et al., 2018). Importantly, such methods display a varying success rate dependent on the sample they are applied to. An especially limiting factor is the means of delivery of the reporter system to the cell or organism. This is particularly relevant when working with neurons, which

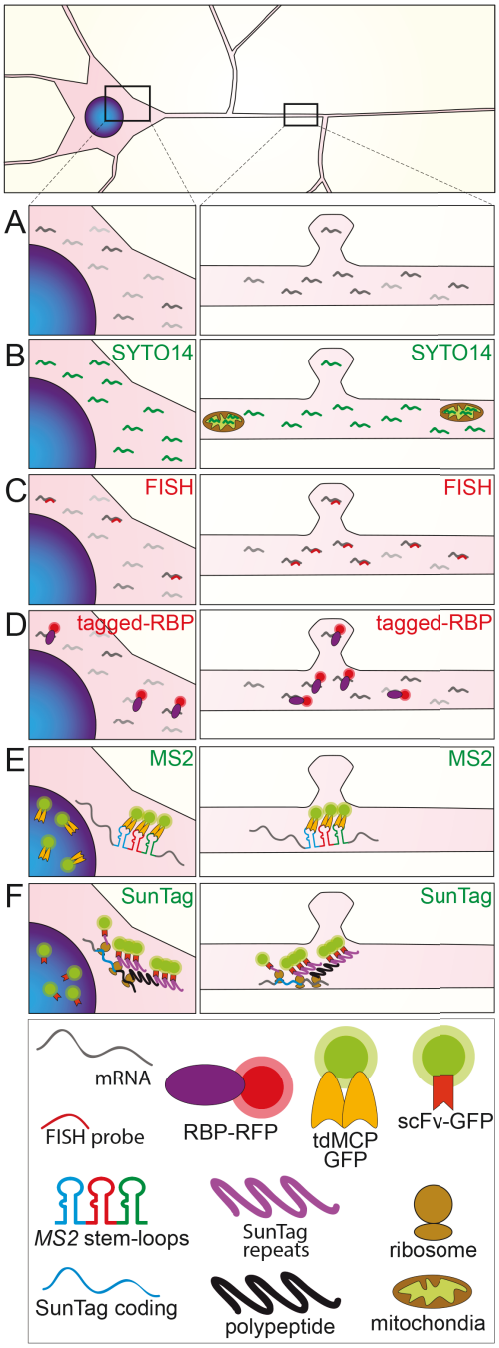

Figure 1.5: Methods to study mRNA granule transport and local translation. Schematic representation of a neuron, showing the soma (left panels) and a dendritic segment (right panels), indicating cytoplasmic mRNA molecules (grey) **(A)** that can be detected with a sequence unspecific dye for nucleic acids such as SYTO 14 **(B)** or, alternatively, by sequence specific fluorescent in situ hybridization (FISH) **(C)**. **(D)** Schematic representation of the MS2-MCP system to visualize pre-labeled mRNAs. **(E)** Schematic representation of RNA granule visualization by FP-tagged RBP (in red). **(F)** Schematic representation of the SunTag system to visualize local protein synthesis. Modified from Bauer et al., Methods, 2017.

are extremely susceptible to cellular stress. Methods that rely on the microinjection of individual cells to deliver probes or other agents can be tedious and harmful to neurons (Tübing et al., 2010). Conversely, cell permeable nucleic acid dyes are not specific in labeling single mRNA transcripts. A more suitable approach for neurons is the use of genetically encoded systems, such as the MS2-, PP7- or λN/BoxB-system, which rely on similar principles (Bauer et al., 2017; Mikl et al., 2010). Such methods allow the use of classical transfection based delivery methods to generate transient expression in cells, such as calcium phosphate co-precipitation or viral transduction, or even the generation of transgenic cell lines or animals. This approach based on genetically encoded systems causes low cellular stress, while still labeling specific single transcripts. Moreover, it allows further flexibility in addressing biological questions by *e.g*. introducing mutations to the genetically encoded reporter. The MS2 system has been well established and greatly improved upon in the last decades (Bauer et al., 2017; Bertrand et al., 1998). To date, the system has been modified to address multiple biological questions, presenting a flexible toolbox to inquire multiple aspects of mRNA metabolism in the living cell.

1.6.2 The MS2 system for mRNA live cell imaging

The MS2-system is derived from the MS2 bacteriophage. It makes use of a 19 nucleotide RNA stem-loop structure and the MS2-coat protein (MCP), which binds to this stem-loop with high specificity and affinity (**Fig. 1.6A**). The MCP can be fused to a fluorescent protein such as GFP (**Fig. 1.6B**). Thereby, it will fluorescently mark the RNA stem-loop when binding to it. The stem-loops are introduced as an array of multiple repetitive stem-loops, and can be introduced into an mRNA sequence of interest to generate a reporter mRNA. It is usually added to the 3´-UTR, to avoid disrupting the open reading frame or impairing translation initiation. When both the mRNA reporter and the fluorescently tagged MCP (MCP-FP) are co-expressed together in the same cell, the MCP-FP will recognize and specifically bind to the RNA stem-loops, marking the mRNA reporter for direct inspection under the microscope (**Fig. 1.6C**). By using an array of multiple RNA stem-loop repeats, the number of MCP-FP molecules that can bind to the RNA reporter increases, resulting in more

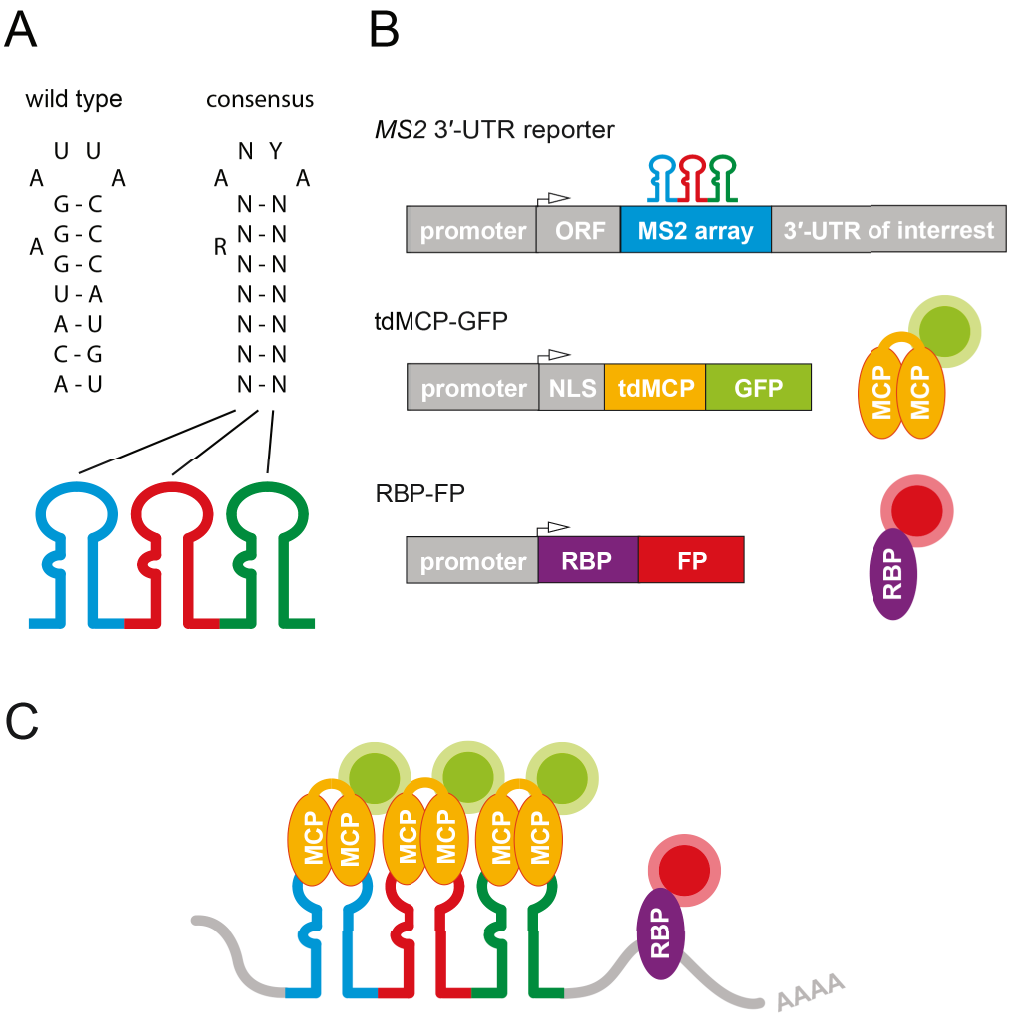

Figure 1.6: The MS2-system for RNA live-cell imaging. **(A)** Wilde-type and consensus sequence of the 19 nucleotide MS2 RNA stem-loop. A = Adenosine, U = Uracil, C = Cytosine, G = Guanine, N = nucleotide, R = Purine, Y = Pyrimidine. Modified from Schneider et al., J. Mo. Bio.,1992. **(B)** Schematic representation of conventional DNA expression cassettes making use of the MS2-system for RNA live-cell imaging and the corresponding mRNA MS2 reporter and fluorescently labeled proteins (MCP-GFP for mRNA, and RBP-FP for protein visualization). ORF = open reading frame, UTR = untranslated region, NLS = nuclear localization signal, tdMCP = tandem MS2 coat protein, RBP = RNA-binding protein, (G)FP = (green) fluorescent protein. **(C)** Illustration of the MS2-system for simultaneous imaging of mRNA and a bound RBP. AAAA indicates polyA-tail.

MCP-GFP recruitment and therefore in an improved detectable signal. Importantly, the MCP has a high specificity in recognizing the RNA stem-loop and a high affinity for binding to it (Horn et al., 2004; Schneider et al., 1992; Stockley et al., 1995). As both the stem-loop and the MCP originate from the MS2 phage, the MCP should not bind to other nucleotide sequences in *e.g.* mammalian cells, which are often the focus of research.

The MS2-system was first used in 1998 to investigate the intracellular transport of an *ASH1* mRNA reporter in the budding yeast *Saccharomyces cerevisiae* (Bertrand et al., 1998). Using this method, the authors were able to demonstrate the 3´-UTR dependent transport of this mRNA from the mother to the daughter cell during bugging. In addition, this transport was impaired in strains deficient for the She1 and Myo4 proteins. This example nicely illustrates the strength of live cell imaging in addressing relevant biological questions, which cannot be answered by other means. Over the years, additions and modifications have been made to the components of the MS2 system, to enhance detectability or address new biological questions. The most important of these adaptations will be discussed for the MCP and the stem-loop array below.

1.6.3 Advancement of the MS2 RNA imaging system

In respect to the MCP, it is important to consider that unbound, diffusing MCP-GFP in the cell will significantly increase background fluorescence, making the detection of individual MS2 RNA granules challenging. To address this issue, nuclear localization signals (NLS) have been added to the protein sequence to shuttle unbound MCP-GFP to the nucleus, thereby reducing fluorescent background in the cytoplasm. Such an NLS can be added or omitted, dependent on the compartment of interest. Another important advance was developed based on the fact that the MCP binds to the MS2 stem-loops as a dimer (Wu et al., 2012). The DNA sequence for the MCP was cloned twice in frame to create a single-chain tandem dimer (tdMCP), with increased labeling efficiency and uniformity (Wu et al., 2012). The development of the tdMCP was an essential step in reducing fluorescent background and increasing the detectability of the MS2 reporter, and greatly facilitated the research presented in this dissertation.

On the RNA side, the array of repetitive RNA stem-loops is used to recruit multiple GFP-molecules to the reporter mRNA via the GFP-tagged MCP. To increase the GFP signal bound to the mRNA the number of stem-loops can simply be increased, thereby providing additional binding sites for MCP-GFP. Following this strategy, various numbers of stem-loops, including 6, 24, 32 or even 132 MS2 hairpins have been integrated into the reporter mRNA, ultimately increasing the GFP signal intensity and signal to noise ratio (Bertrand et al., 1998; Park et al., 2014; Pichon et al., 2016; Tantale et al., 2016; Wu et al., 2015). However, it is important to note that a full coverage of all stem-loops cannot be expected. For instance, when 24 stem-loops are used, on average only 13 were found to be bound by tdMCP in the cell (Wu et al., 2012).

Another aspect to consider is that repetitive sequences, as present in the stem-loop array, are prone to recombination, resulting in a possible loss of stem-loops during the cloning process. This may affect proper detection of the reporter mRNA and affect the biological readout of an experiment. To circumvent this issue, such sequences are often cloned in stable high-efficiency competent cells with reduced recombination activity and optimal growth at lower temperatures, such as the Stabl2 cells available from Invitrogen. An alternative approach is to alter the sequence of the MS2 array to make it less repetitive. The consensus sequence of the MS2 RNA stem-loop shows that parts of the hairpin head, as well as an unbound nucleotide in the stem are necessary for MCP binding, while other nucleotides need to conserve the hairpin structure but are not sequence specific (Horn et al., 2004; Schneider et al., 1992; Wu et al., 2012) (**Fig. 1.6A**). To reduce repetitiveness, the consensus sequence was used to design sequence optimized MS2 arrays of either 24 or even 128 repeats (Pichon et al., 2016; Wu et al., 2015). These sequences can now be cloned in classical competent cells, with little to no complications. Another alteration to the MS2 sequence that has been reported is a mutation to the hairpins loop (AUUA → AUCA), which causes increased binding stability of the MCP (Rowsell et al., 1998). In addition, the MS2 system has been combined with the PP7 system, where different fluorescent proteins visualize the respective stem-loops, allowing the visualization of mRNA translation and mRNA degradation in localized transcripts (Halstead et al., 2016; Horvathova et al., 2017). To detect the first round of translation, an array of PP7 stem-loops was designed that could be translated and placed in frame with the ORF. In addition, an MS2 array was placed in the 3´-UTR.

During translation, the ribosome would knock-off the PCP-FP from the in frame PP7 stem-loops, thereby only leaving the MCP-FP to be detected (Halstead et al., 2016). RNA degradation was visualized by placing both an array of PP7 and MS2 repeats in the 3´-UTR, which are separated by two viral pseudo-knots which block 5´-3´ exoribonuclease 1 (Xrn1). Blocking of Xrn1 would prevent further degradation beyond this point (Horvathova et al., 2017). Therefore, degradation fragments blocked by the pseudo-knots would only carry the PCP-FP, indicating degradation was initiated. These examples illustrate how these genetically encoded systems can be used to address essential biological questions. Similar approaches could for instance address alternative splicing or simply visualize two mRNAs in the same cell.

In summary, the MS2 system has proven itself to be flexible and applicable to answer diverse research questions. It has been successfully used in multiple systems and is the method of choice for the live visualization of mRNA today. Especially in the recent past, multiple alterations have been made to the system to improve its applicability and the biological readout. It will be interesting to see which future applications will be developed.

1.7 Aims

Based on current scientific knowledge and the extensive previous work by the Kiebler lab as outlined in preceding chapters, two separate projects were designed to address the intracellular sorting of both mRNA and RBPs. The first project aimed to investigate intracellular 3´-UTR dependent mRNA transport via the neuronal Stau2-target mRNA *Rgs4*. The second project is based on my own previous work in the Kiebler lab (master's thesis available from the University of Vienna; http://othes.univie.ac.at/29195/), where a number of RBPs were screened and their localization was investigated during aging/maturation in cell culture. Investigating RBPs allows to address how different types of RNA granules behave in the cell, complementing the approach taken in the first project. Therefore, this second project aspired to unravel changes in subcellular RNP granule localization of the RBP Rck, which is also found in neuronal Stau2 granules and P-bodies.

Specific aims for each project are defined as follows.

Aims Project 1

1.1 Is mRNA transported in a sushi-belt like fashion?

1.2 Does the 3´-UTR of *Rgs4* mediate sequence specific mRNA transport dynamics and localization?

1.3 Does neuronal activity influence *Rgs4* 3´-UTR mediated transport dynamics and localization?

1.4 Does Staufen2 regulate *Rgs4* transport via its 3´-UTR?

Aims Project 2

2.1 Does the localization of Rck change during neuronal maturation in culture?

2.2 Does neuronal activity play a role in age-dependent alterations in Rck localization?

2.3 Does helicase activity affect Rck localization?

2. Manuscript 1:

Live cell imaging reveals 3´-UTR dependent mRNA sorting to synapses

(Currently under revision at Nature Communications, April 24th 2019)

Karl E Bauer[1], Inmaculada Segura[1], Imre Gaspar[2,4], Volker Scheuss[1], Christin Illig[1], Georg Ammer[1,5], Saskia Hutten[1], Eugénia Basyuk[3,6], Sandra M Fernández-Moya[1], Janina Ehses[1], Edouard Bertrand[3] and Michael A Kiebler[1,*]

[1] BioMedical Center, Medical Faculty, Ludwig Maximilians University, Großhaderner Str. 9, 82152 Planegg-Martinsried, Germany

[2] EMBL, Meyerhofstraße 1, 69117 Heidelberg, Germany

[3] Institut de Génétique Moléculaire de Montpellier, CNRS UMR5535, 1919 route de Mende, 34293 Montpellier, France

[4] Current address: Institute of Molecular Biotechnology, Dr. Bohr-Gasse 3, 1030 Vienna, Austria

[5] Current address: MPI of Neurobiology, Am Klopferspitz 18, 82152 Martinsried, Germany

[6] Current address: Institut de Génétique Humaine de Montpellier, CNRS UMR9002, 141 rue de la Cardonille, 34396 Montpellier, France

* Correspondence: mkiebler@lmu.de (MAK)

No. of Figures: **6 Figures**
6 Supplementary Figures

Key words: mRNA granules, Staufen2, MS2 system, Rgs4, 3´-UTR, dendritic mRNA transport, mRNA localization, synaptic activity-dependent recruitment, sushi-belt model

Running title: Dendritic mRNA sorting to synapses

Author contribution: Dr. Inmaculada Segura conducted experiments relevant to Supplementary Figure 2.6A. Dr. Imre Gaspar provided analysis relevant to Figure 2.4D-H and Supplementary Figure 2.4E-N. Dr. Volker Scheuss provided experiments relevant to Figure 2.5 and Supplementary Figure 2.5. Christin Illig conducted experiments relevant to Figure 2.3F-G, Supplementary Figure 2.3A-F and Supplementary Figure 2.4Q-T. Dr. Georg Ammer provided preliminary experiments not included in this manuscript. Dr. Saskia Hutten provided experiments relevant to Figure 2.1B and Supplementary Figure 2.1D. Dr. Eugénia Basyuk designed the 32xMS2 and 128xMS2 sequence. Janina Ehses and Dr. Sandra M Fernández-Moya cloned lentiviral plasmids and generated lentiviral particles used for experiments relevant to Figure 2.5 and Supplementary Figure 2.5. Dr. Edouard Bertrand designed FISH probes used in experiments relevant to Figure 2.1B and Supplementary Figure 2.1B,D.

2.1 Abstract

mRNA transport restricts translation to specific subcellular locations, which is the basis for many cellular functions. However, the precise process of mRNA sorting to synapses in neurons remains elusive. Here, we used *Rgs4* mRNA as a model to investigate 3´-UTR-dependent transport by MS2 live-cell imaging. The majority of RNA granules displayed bidirectional transport in dendrites, independent of the 3´-UTR. Importantly, the *Rgs4* 3´-UTR caused an anterograde transport bias, which required the Staufen2 protein. Moreover, the 3´-UTR mediated dynamic, sustained mRNA recruitment to synapses. Visualization of these processes at high temporal resolution enabled us to show that mRNA patrols dendrites allowing transient interaction with multiple synapses, in agreement with the sushi-belt model. Modulation of neuronal activity by chemical silencing or local glutamate uncaging regulated both the 3´-UTR-dependent transport bias and synaptic recruitment. This dynamic and reversible mRNA recruitment to active synapses would allow translation and synaptic remodeling in a spatially and temporally adaptive manner.

2.2 Introduction

Messenger RNAs (mRNAs) display a variety of subcellular localization patterns in a plethora of model systems (Buxbaum et al., 2015b; Holt and Bullock, 2009; Palacios and St Johnston, 2001), including the dendritic compartment of the hippocampus (Cajigas et al., 2012). Several distinct mechanisms have been proposed to explain how the sorting of specific mRNAs to subcellular locations can be achieved (Andreassi and Riccio, 2009; Holt and Bullock, 2009; Palacios and St Johnston, 2001), from simple diffusion to the more complex *sushi-belt* model of dendritic mRNA trafficking (Doyle and Kiebler, 2011). The latter proposes that mRNA granules patrol dendrites in a highly dynamic multidirectional fashion, without being irreversibly anchored at a single specific location. Multiple approaches demonstrated that specific transcripts can be actively transported along cytoskeletal structures (Dynes and Steward, 2007; Saxton, 2001; Tübing et al., 2010). Such active and directed transport has been hypothesized to be the driving force that mediates mRNA sorting to specific distal locations in neurons, such as postsynaptic sites or axonal growth cones, where it may become available for local translation (Dictenberg et al., 2008; Dynes and Steward, 2012; Eliscovich et al., 2017; Terenzio et al., 2018; Wu et al., 2016; Yoon et al., 2016). This allows the tightly regulated production of the resulting protein, both spatially and temporally. Localization of mRNA and subsequent local translation are particularly important in neurons, where synapses containing a specific proteome can be located at distal dendrites far from the site of transcription. Ultimately, local protein synthesis at synapses is fundamental for learning and the formation of long-term memory (Doyle and Kiebler, 2011; Jung et al., 2014; Palacios and St Johnston, 2001; St Johnston, 2005).

Previous studies investigated the role of neuronal stimulation on these processes and reported the activity-induced unpacking of mRNAs, allowing local translation in dendrites of primary hippocampal neurons (Buxbaum et al., 2014; Cougot et al., 2008; Wang et al., 2016; Wu et al., 2016). In addition, Singer and colleagues showed that glutamate uncaging induced *ß-actin* mRNA recruitment in dendrites, where it is eventually translated and the newly produced actin participates in dendritic spine remodeling (Yoon et al., 2016). However, we are only beginning to understand how mRNA sorting to synapses takes place.

Sorting signals, usually within the 3´-untranslated region (3´-UTR) of the mRNA, play a crucial role in mRNA localization (Holt and Bullock, 2009; Martin and Ephrussi, 2009; Mayr, 2017; Meer et al., 2012). Such signals are able to interact with specific RNA binding proteins (RBPs), such as ZBP1, FMRP or Staufen2 (Stau2), to form neuronal RNA granules (Dictenberg et al., 2008; Fernandez-Moya et al., 2014; Kiebler and Bassell, 2006). Thereby, Stau2 and ZBP1 regulate the dendritic localization of *Calm3* and *ß-actin* mRNA, respectively (Eom et al., 2003; Sharangdhar et al., 2017). Through these processes RBPs significantly contribute to synaptic function (Dictenberg et al., 2008; Goetze et al., 2006; Kao et al., 2010).

The *negative regulator of G protein signaling 4* (*Rgs4*) mRNA is a previously identified physiological target mRNA of Stau2 in the brain (Heraud-Farlow et al., 2013). It encodes a GTPase activating protein of the G protein-coupled receptor (GPCR) pathway, and therefore modulates receptor mediated neuronal signaling at the synapse (Gerber et al., 2016; Pacey et al., 2011; Saugstad et al., 1998). Fluorescent *in situ* hybridization (FISH) has shown that *Rgs4* mRNA is present in cytosolic RNA granules localized in distal dendrites. Further analysis confirmed the presence of *Rgs4* mRNA in Stau2 granules (Heraud-Farlow et al., 2013). As the long *Rgs4* 3´-UTR contains *in vivo* cross-linking sites for Stau2 (Sharangdhar et al., 2017), it might provide key binding sites for a direct interaction with Stau2. Silencing of Stau2 induces a reduction of endogenous *Rgs4* mRNA both *in vitro* and *in vivo*, suggesting an involvement of Stau2 in the regulation of *Rgs4* mRNA levels (Berger et al., 2017; Heraud-Farlow et al., 2013).

To evaluate the role of the 3´-UTR in mediating proper subcellular sorting in mature neurons, we used *Rgs4* as a model, and generated an mRNA reporter combining the *Rgs4* 3´-UTR with an improved MS2 RNA live-cell imaging system (Bertrand et al., 1998; Pichon et al., 2016). This reporter system allowed us to perform long-term mRNA tracking in dendrites and to (i) unravel the underlying mRNA transport dynamics mediated by a specific 3´-UTR and investigate (ii) neuronal activity and (iii) Stau2 dependency. Together, our results support a model of active, directed mRNA trafficking in a *sushi-belt* like fashion promoting synaptic recruitment of mRNA, which would lead to activated translation. This in turn may trigger synaptic remodeling, which ultimately impacts synaptic function.

2.3 Results

2.3.1 The *Rgs4* 3´-UTR localizes an MS2 reporter mRNA to distal dendrites

To test whether the 3´-UTR of *Rgs4* is sufficient for dendritic localization and to unravel the underlying dynamics of subcellular mRNA sorting, we employed the MS2 system (Bertrand et al., 1998) in cultured rat hippocampal neurons. This system makes use of the high affinity and specificity interaction of the MS2 coat protein (MCP) with the *MS2* RNA stem-loop structure. We designed reporters containing the *LacZ* open reading frame that includes a stop codon followed by an array of either 32 or 128 *MS2* stem-loops(Pichon et al., 2016) and the *Rgs4* 3´-UTR (**Fig. 2.1A**). A second MS2 reporter mRNA lacking the *Rgs4* 3´-UTR was generated (termed '*MS2 only*' throughout). Together, these reporter mRNAs allowed us to assess the specific contribution of the *Rgs4* 3´-UTR to dendritic mRNA transport. To visualize these reporter mRNAs in living cells, we co-transfected the reporter plasmid with an expression vector encoding a C-terminally green fluorescent protein (GFP)-tagged tandem MCP (tdMCP-GFP) (Wu et al., 2012), containing a nuclear localization signal (NLS) sequestering excess tdMCP-GFP into the nucleus (Bertrand et al., 1998; Dynes and Steward, 2007; Park et al., 2014; Rook et al., 2000; Wu et al., 2012) (**Fig. 2.1A**; **Supplementary Fig. 1A**). Single molecule FISH (smFISH) (Fusco et al., 2003), targeting the *MS2* repeats, demonstrated that the *MS2+Rgs4* 3´-UTR reporter mRNA localized to dendrites (**Supplementary Fig. 2.1B**), resembling the pattern of endogenous *Rgs4* mRNA (Heraud-Farlow et al., 2013). Control reporter mRNAs with no known function in dendrites, *i.e. MS2 only* or *MS2+histone-3.3* 3´-UTR, all displayed dendritic localization (**Supplementary Fig. 2.1C**). This suggests that dendritic localization is not exclusively dependent on the 3´-UTR, but that other sequences or different expression levels might possibly contribute as well. Therefore, we inquired how specific subcellular sorting within dendrites might be achieved. To further validate the MS2-MCP system in neurons, we co-transfected both the *MS2+Rgs4* 3´-UTR MS2 reporter and tdMCP-GFP plasmids. GFP fluorescence was clustered in discrete cytoplasmic granules that colocalized with the *MS2* smFISH signal (**Fig. 2.1B**, **Supplementary Fig. 2.1D**), confirming that we reliably detected reporter mRNAs, thereby allowing the visualization of intracellular mRNA transport in living cells.

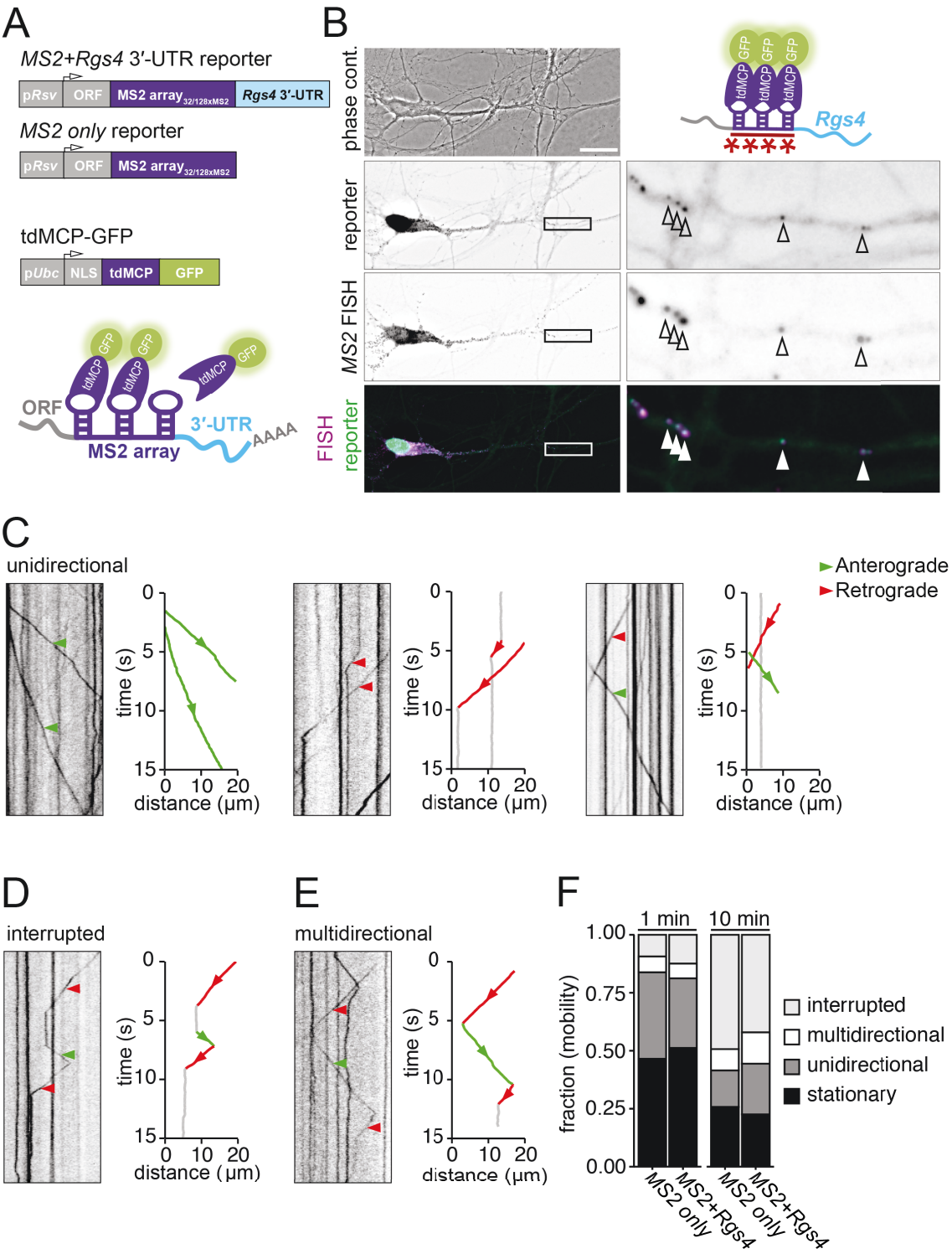
A
MS2+Rgs4 3′-UTR reporter
pRsv
ORF
MS2 array32/128xMS2
Rgs4 3′-UTR
MS2 only reporter
pRsv
ORF
MS2 array32/128xMS2
tdMCP-GFP
pUbc
NLS
tdMCP
GFP
ORF
tdMCP
GFP
3′-UTR
AAAA
MS2 array
B
phase cont.
reporter
MS2 FISH
FISH reporter
Rgs4
C
unidirectional
Anterograde
Retrograde
time (s)
distance (μm)
D
interrupted
E
multidirectional
F
1 min
10 min
fraction (mobility)
interrupted
multidirectional
unidirectional
stationary
MS2 only
MS2+Rgs4
MS2 only
MS2+Rgs4

←

Figure 2.1: Reporter mRNAs display directed dendritic transport dynamics in primary hippocampal neurons. (**A**) Scheme of both *MS2 only* and *MS2+Rgs4* MS2 reporter constructs and tdMCP-GFP expression cassettes (upper) and the MS2 system (lower). Abbreviations: pRSV = Rous sarcoma virus promoter, pUBC = Ubiquitin C promoter, ORF = open reading frame, NLS = nuclear localization signal, tdMCP = tandem MS2 coat protein, UTR = untranslated region. (**B**) Phase contrast, GFP fluorescence (reporter), MS2 single molecule FISH and overlay in a rat hippocampal neuron expressing both tdMCP-GFP and *MS2+Rgs4* MS2 reporter mRNA (scheme). Arrowheads indicate overlapping tdMCP-GFP bound MS2 reporter mRNA and MS2 smFISH. Fluorescent images were deconvolved to assess overlap (for unprocessed images see Supplementary Fig. 1C). Scale bar 20 µm. Boxed region is magnified in right panels. (**C-F**) Representative kymographs (left) and extracted tracks (right) illustrating differences in unidirectional *MS2+Rgs4* 3´-UTR mRNA granule transport speed, displacement and directionality (**C**), as well as interrupted (**D**) and multidirectional transport (**E**). Anterograde and retrograde transport are indicated in green or red arrowheads and lines, respectively. (**F**) Quantification of relative transport dynamics of *MS2 only* and *MS2+Rgs4* 3´-UTR reporter mRNAs in 1 and 10 minute time-series acquisitions, respectively.

2.3.2 The *Rgs4* 3´-UTR mediates an anterograde transport bias to distal dendrites

To investigate the underlying transport dynamics, time-lapse imaging of single neurons expressing the MS2 system was performed for 1 minute at 15.3 fps (frames per second) with a spinning disk microscope. To analyze the characteristics of single RNA granule trafficking, we generated kymographs of dendritic regions at a minimal distance of 20 µm from the soma and traced single trajectories (**Fig. 2.1C-E; 2.2A-C; movies 2.1-2.8**). This revealed diverse RNA transport patterns, independent of a 3´-UTR. We observed mobile mRNA granules with differences in transport speed, displacement length and directionality (**Fig. 2.1C**, **movies 2.1-2.3**). Furthermore, two

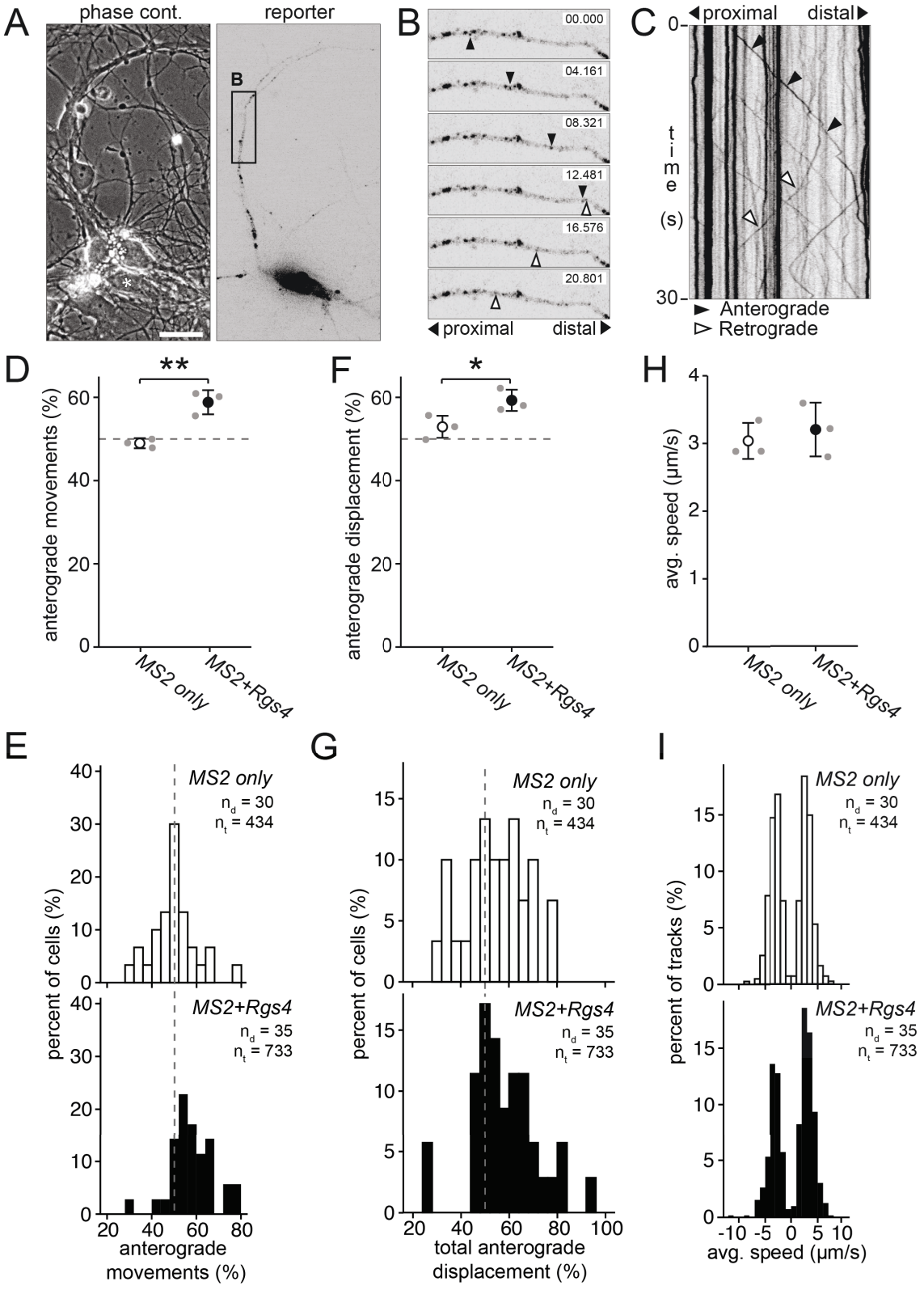
A
phase cont.
reporter
B
B
00.000
04.161
08.321
12.481
16.576
20.801
proximal
distal
C
proximal
distal
0
30
time (s)
Anterograde
Retrograde
D
**
anterograde movements (%)
MS2 only
MS2+Rgs4
F
*
anterograde displacement (%)
MS2 only
MS2+Rgs4
H
avg. speed (µm/s)
MS2 only
MS2+Rgs4
E
MS2 only
n_d = 30
n_t = 434
MS2+Rgs4
n_d = 35
n_t = 733
percent of cells (%)
anterograde movements (%)
G
MS2 only
n_d = 30
n_t = 434
MS2+Rgs4
n_d = 35
n_t = 733
percent of cells (%)
total anterograde displacement (%)
I
MS2 only
n_d = 30
n_t = 434
MS2+Rgs4
n_d = 35
n_t = 733
percent of tracks (%)
avg. speed (µm/s)

←

Figure 2.2: *Rgs4* 3´-UTR mediates an anterograde transport bias. (**A**) Representative phase contrast and GFP fluorescence of hippocampal neuronal culture co-transfected with the *MS2+Rgs4* 3´-UTR reporter and tdMCP-GFP constructs. Scale bar 20 µm. Asterisk denotes GFP positive cell. (**B**) Time series of the dendritic boxed region in A. Representative anterograde (black arrowheads) and retrograde (white arrowheads) moving mRNA granules are indicated. (**C**) Kymograph of the dendritic region in B. Arrowheads indicate mRNA granules signified in B. (**D-I**) Dot plots (**D,F,H**) and histograms (**E,G,I)** displaying percentage of anterograde moving granules (**D-E**), percentage of total anterograde travel distance (**F-G**) and average speed (**H-I**) for *MS2 only* or *MS2+Rgs4* 3´-UTR reporter mRNAs, detected by tdMCP-GFP. In (I), positive values indicate anterograde and negative values indicate retrograde transport. Data represents mean ± standard deviation of three independent experiments (individual experiments shown as gray dots). Asterisks represent *p*-values obtained by Student's t-test (**p* < 0.05, ***p* < 0.01). Data was obtained from 40 µm dendritic segments at a minimal distance of 20 µm from the cell body. At least 10 dendrites/condition/experiment were analyzed. Total number of dendrites (n_d) and tracks (n_t) analyzed per condition are indicated. Only displacements ≥ 1.5 µm were considered for analysis.

additional distinct types of mRNA granule mobility were detected. We found that mRNA granules may undergo interruptions in their movement before reinitiating transport (**Fig. 2.1D**, **movie 2.4**, *interrupted*) or may display multiple changes in direction without interrupting transport (**Fig. 2.1E**, **movies 2.5-2.6**, *multidirectional*). Additionally, we observed mRNA granules that reversed direction at branch points to move between different dendritic segments (**movie 2.7**). Such transport behaviors support the *sushi-belt* model of dendritic mRNA trafficking, which proposed that mRNA granules patrol dendrites in a highly dynamic multidirectional fashion, without being irreversibly anchored at a single specific location (Doyle and Kiebler, 2011). We quantified the frequencies of these transport behaviors and found that half of the mRNA granules remained stationary during the one-minute acquisition period. In

contrast, the mobile fraction of granules traversed the dendrites in a highly dynamic way, including unidirectional, interrupted and multidirectional movements, independent of the 3´-UTR present (**Fig. 2.1F**). Increasing the acquisition time to 10 minutes reduced the fraction of stationary and unidirectional granules in favor of interrupted and multidirectional movements, demonstrating that a large fraction of RNA granules indeed undergo transport in a *sushi-belt* like fashion. The fraction of the stationary population is consistent with previously published data for the *ß-actin* mRNA as well as for Staufen1 granules in the time frames analyzed (Köhrmann et al., 1999; Yoon et al., 2016). Statistical analysis by Chi-squared test could not establish any difference in the frequency of these events between *MS2 only* or *MS2+Rgs4* 3´-UTR reporter mRNAs, suggesting that the 3´-UTR of the transcript does not regulate the types of motility exhibited by the reporters.

As both *MS2+Rgs4* and *MS2 only* reporter mRNAs were found to be localized in dendrites, we decided to reinvestigate the underlying regulation of dendritic mRNA sorting, which ultimately fine-tunes trafficking to achieve specific localization upon demand. We investigated multiple parameters of 3´-UTR-dependent mRNA granule transport, including speed, displacement and directionality in dendrites (**Fig. 2.2; Supplementary Fig. 2.2; movie 2.8**). When exploring transport directionality, the *MS2 only* mRNA displayed an equal number of mRNA granules moving in the anterograde (48.9 ± 1.2 %) or retrograde direction (**Fig. 2.2D-E**). Interestingly, the *MS2+Rgs4* 3´-UTR mRNA mediated a significant anterograde transport bias, with 58.8 ± 2.9 % of mRNA granules moving towards more distal dendritic regions (**Fig. 2.2D-E**; p = 0.0056). Moreover, when the percentage of total anterograde travel distance of all mRNA granules was investigated, we observed a similar transport bias for the *MS2+Rgs4* 3´-UTR (59.1 ± 2.5 %) compared to the *MS2 only* (52.8 ± 2.6 %) mRNA reporter (**Fig. 2.2F-G**; p = 0.0399). Directional transport has previously been observed for other mRNAs, such as *ß-actin*, *Arc*, and *CaMKIIα*, in hippocampal neurons or *oskar* in the *Drosophila* oocyte, with a preferential transport direction towards the distal or the posterior part of the cell, respectively (Dynes and Steward, 2007; Park et al., 2014; Rook et al., 2000; Zimyanin et al., 2008). In contrast, we observed no differences in either average transport speed or in average displacement length of single events, indicating that the *Rgs4* 3´-UTR did not affect these parameters of mRNA transport (**Fig. 2.2H-I; Supplementary Fig. 2.2A-B**). The distribution of single data points showed that most RNA granules underwent short

displacement events and only few particles traveled long distances at a time, often longer than the 40 µm analyzed (**Supplementary Fig. 2.2B**). To exclude that the NLS included in the tdMCP protein might potentially affect transport as previously reported (Salman et al., 2005), we generated a tdMCP lacking the NLS and repeated the previous experiment. Although the fluorescent signal had higher background, we still observed an anterograde transport bias mediated by the *Rgs4* 3´-UTR (**Supplementary Fig. 2.2C,D**), showing that the NLS did not affect trafficking in our hands.

In conclusion, our live cell imaging data suggests that the *Rgs4* 3´-UTR was responsible for the observed anterograde transport bias, affecting both anterograde moving mRNA granule number and anterograde travel distance in dendrites. Importantly, the results establish the 3´-UTR as a key determinant as the bias was not observed in the absence of the *Rgs4* 3´-UTR.

2.3.3 Inhibition of neuronal activity abolishes the *Rgs4* 3´-UTR dependent anterograde transport bias

Next, we asked whether neuronal activity might regulate dendritic mRNA transport. As mature neurons display endogenous neuronal activity in culture, we chemically silenced activity by simultaneously inhibiting AMPA receptors, NMDA receptors and voltage-gated sodium channels via bath application of CNQX, AP5 and TTX, respectively (Sharangdhar et al., 2017). Neurons transfected with either *MS2 only* or *MS2+Rgs4* 3´-UTR reporters were left untreated or pre-incubated for 1 h with either vehicle or CNQX/AP5/TTX, and then imaged during continuous treatment (**Fig. 3A**). No differences in speed, displacement or transport directionality were observed for the *MS2 only* mRNA reporter, independent of the treatment (**Fig. 2.3B-C, Supplementary Fig. 2.3A,B,G,H** and *data not shown*). However, the anterograde transport bias mediated by the *MS2+Rgs4* 3´-UTR was completely abolished when neuronal activity was inhibited (46.7 ± 2.3 %), compared to vehicle treated (55.1 ± 2.9 %, p = 0.00431) or untreated neurons (56.3 ± 2.3 %, p = 0.00187) (**Fig. 2.3D-E;** $F_{2,9}$ = 0.00136). Moreover, the inhibition of neuronal activity alleviated the anterograde bias observed in respect to total travel distance (50.2 ± 2.5 %), compared to vehicle treated samples (56.0 ± 3.0 %, p = 0.02884) (**Supplementary Fig. 2.3C-D**). Importantly, these effects were not due to neuronal toxicity, as 1h

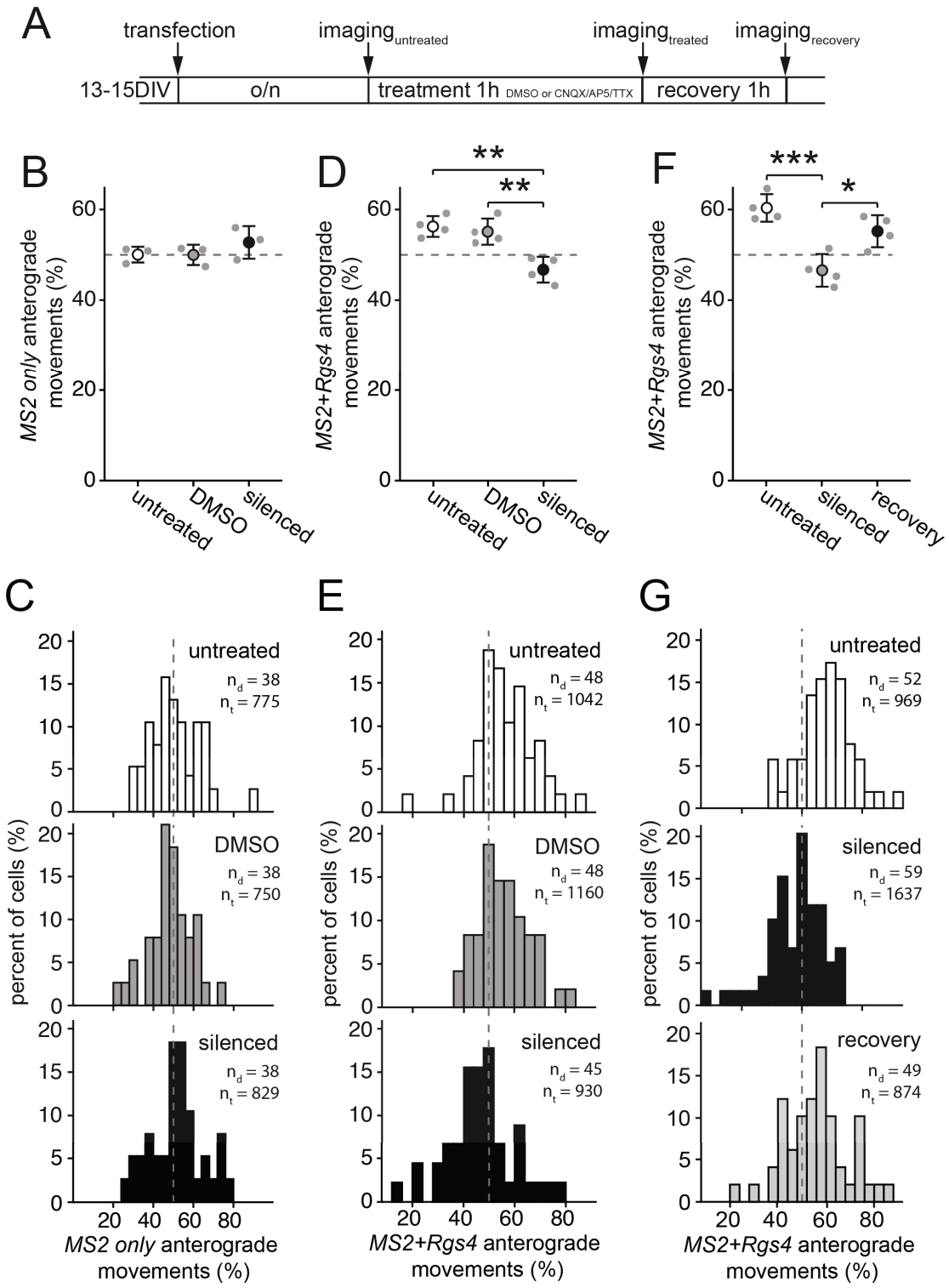
A
transfection
imaging untreated
imaging treated
imaging recovery
13-15DIV
o/n
treatment 1h DMSO or CNQX/AP5/TTX
recovery 1h
B
MS2 only anterograde movements (%)
untreated
DMSO
silenced
D
MS2+Rgs4 anterograde movements (%)
**
**
F
MS2+Rgs4 anterograde movements (%)
***
*
recovery
C
E
G
percent of cells (%)
untreated
n_d = 38
n_t = 775
DMSO
n_d = 38
n_t = 750
silenced
n_d = 38
n_t = 829
MS2 only anterograde movements (%)
n_d = 48
n_t = 1042
n_d = 48
n_t = 1160
n_d = 45
n_t = 930
MS2+Rgs4 anterograde movements (%)
n_d = 52
n_t = 969
n_d = 59
n_t = 1637
n_d = 49
n_t = 874

←

Figure 2.3: Chemical inhibition of neuronal activity abolishes *Rgs4* 3´-UTR dependent transport bias. (**A**) Scheme of experimental outline. (**B-G**) Dot plots (**B,D,F**) and histograms (**C,E,G**) displaying percentage of anterograde moving *MS2 only* (B-C) or *MS2+Rgs4* 3´-UTR (D-G) reporter mRNA granules in rat hippocampal neurons, untreated, vehicle treated (DMSO) or silenced (100µM CNQX, 50µM AP5, 1µM TTX) and after 1 hour recovery. Data represents mean ± standard deviation of 3-4 independent experiments (individual experiments shown as gray dots). Asterisks represent *p*-values assessed by Tukey's test post-hoc to one-way ANOVA analysis (* $p < 0.05$, ** $p < 0.01$, *** $p < 0.001$). Data was obtained from 40 µm dendritic segments at a minimal distance of 20 µm from the cell body. At least 10 dendrites/condition/experiment were analyzed. Total number of dendrites (n_d) and tracks (n_t) analyzed per condition are indicated. Only displacements ≥ 1.5 µm were considered for analysis.

wash-off of chemical inhibition induced recovery of the transport bias ($F_{2,9} = 0.00093$, $p = 0.01456$ for silenced *vs* wash-off, $p = 0.00074$ for silenced *vs* untreated, **Fig. 2.3F-G)**. Displacement of anterograde movements of *MS2+Rgs4* 3´-UTR mRNA granules partially recovered after 1h wash-off ($F_{2,9} = 0.021$, $p = 0.424$ for silenced *vs* wash-off, $p = 0.017$ for silenced *vs* untreated, **Supplementary Fig. 2.3E-F**). Moreover, fractions of mRNA granule mobility, categorized as stationary, unidirectional, interrupted and multidirectional, remained unaffected by inhibition of neuronal activity (**Supplementary Fig. 2.3I-J**). Together, this data demonstrates that the transport bias of the reporter mRNAs not only depended on the *Rgs4* 3´-UTR, but on neuronal activity as well. Importantly, the movement of the *MS2 only* mRNA reporter remained unaffected by synaptic inhibition, suggesting that neuronal silencing did not reduce the mRNA transport bias in general, but that the effect was indeed dependent on the *Rgs4* 3´-UTR.

2.3.4 *Rgs4* 3´-UTR dependent mRNA sorting to synapses

As inhibition of neuronal activity abolished the *Rgs4* 3´-UTR dependent anterograde transport bias in distal dendrites, we next investigated whether mRNA was recruited to dendritic synapses. To visualize endogenous excitatory synapses in dendrites, we generated a fluorescent synaptic marker by tagging the postsynaptic density protein 95 kD (PSD-95) with tagRFP-t (PSD-95−RFP). Mature neurons were co-transfected with PSD-95−RFP, tdMCP-GFP and either *MS2 only* or *MS2+Rgs4* 3´-UTR mRNA reporters. To analyze whether synapses might affect mRNA granule transport, we co-imaged both mRNA reporters and the synaptic marker by time-lapse dual-color microscopy in single cells for one minute. We generated kymographs for each separate channel and created dual-color overlays (**Fig. 2.4A; movies 2.9-2.10**). We identified the positions, where mRNA granules were found to either interrupt (termed *docking*) or reinitiate transport (termed *undocking*), and measured the distance to the closest PSD-95−RFP positive cluster. Importantly, co-expression of the fluorescent reporters together with either *MS2 only* or *MS2+Rgs4* 3´-UTR reporter mRNA did not modify synaptic density (**Supplementary Fig. 2.4A**). Moreover, we found no difference in the ratio of mRNA granules docking or undocking between *MS2 only* and *MS2+Rgs4* 3´-UTR reporter mRNAs, respectively (**Supplementary Fig. 2.4B**). While both reporter mRNAs were recruited to synapses, *MS2+Rgs4* 3´-UTR reporter mRNAs on average docked closer than *MS2 only* reporter mRNAs (1.11 ± 0.01 µm for *MS2 only vs.* 0.67 ± 0.02 µm for *MS2+Rgs4* 3´-UTR; p = 4.25E^{-6}, **Fig. 2.4B-C**). Similar results were obtained for mRNA granules undocking after a previous stationary phase (**Supplementary Fig. 2.4C-D**). Together, these results suggest a dynamic sorting process as the *Rgs4* 3´-UTR mediated mRNA recruitment and eventual release close to synapses.

To further investigate how *MS2 only* and *MS2+Rgs4* 3´-UTR RNA reporters behave at the synapse, we acquired longer dual-color videos (3.5 minute, at ~ 4.7 fps) of neurons co-transfected with either *MS2 only* or the *MS2+Rgs4*, tdMCP-GFP and the synaptic marker PSD-95−RFP. We tracked PSD-95−RFP positive clusters over time and measured GFP fluorescence of reporter mRNAs in equivalent areas. This allowed us to specifically analyze dynamic changes in GFP fluorescence intensity caused by docking or undocking reporter mRNAs at single synapses (see *Methods* for details). During the time analyzed, we observed at least one docking or

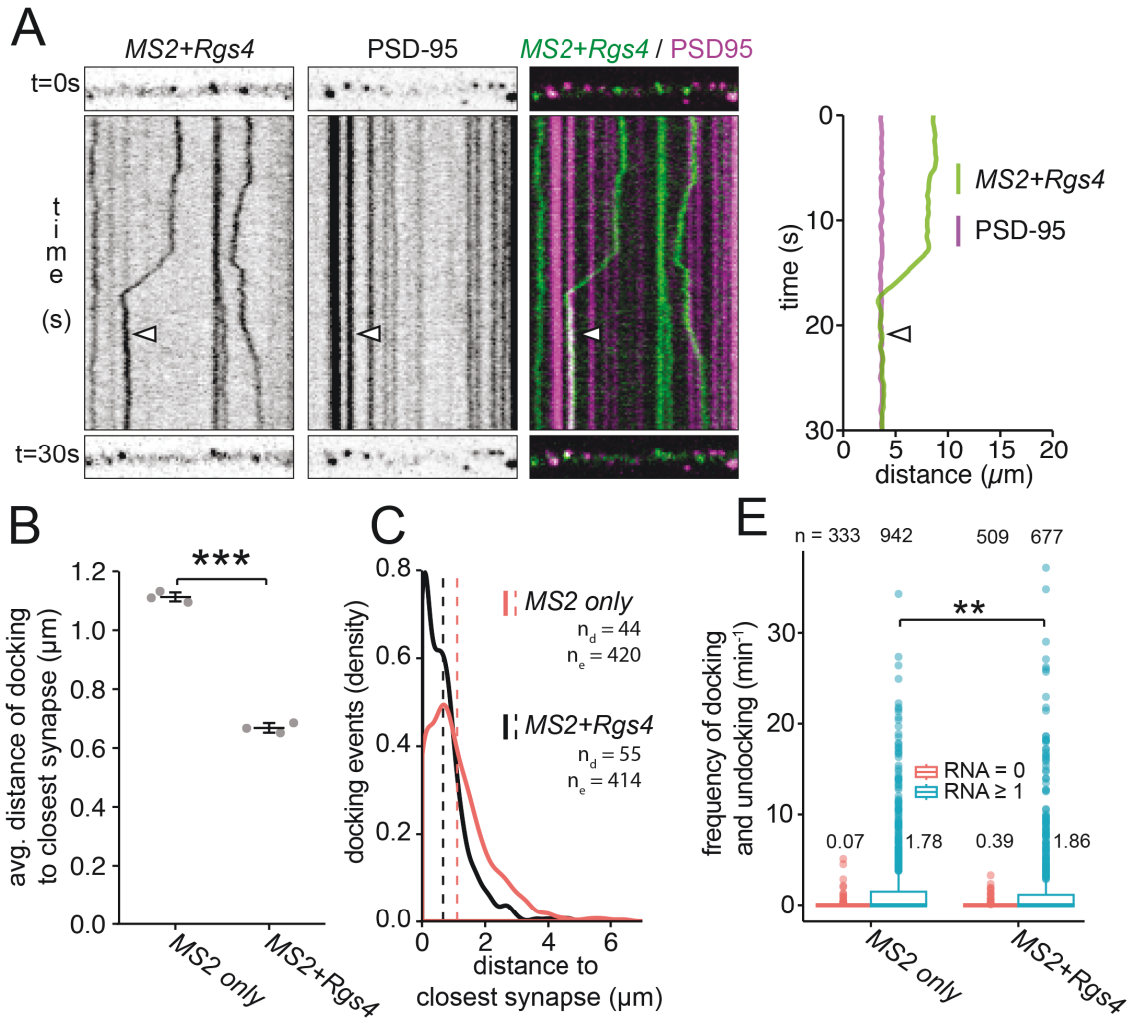

D

	somatic synapses		dendritic synapses	
	RNA ≥ 1	RNA = 0	RNA ≥ 1	RNA = 0
MS2 only	143 (97.2%)	4	942 (73.9%)	333
MS2+Rgs4	78 (100%), $p = 0.3$	0	677 (57.1%), $p < 0.0001$	509

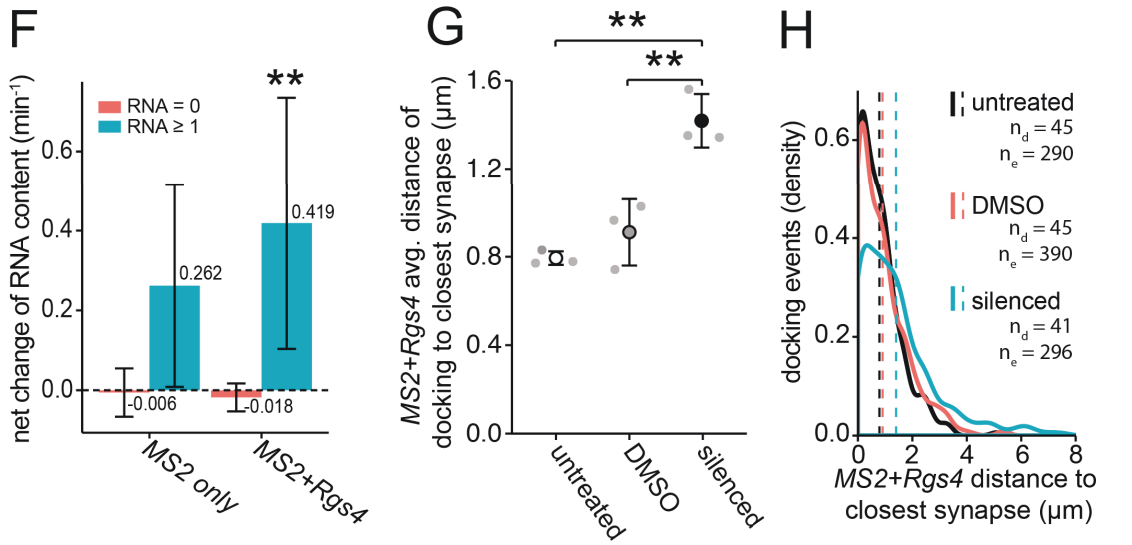

←

Figure 2.4: *Rgs4* 3´-UTR mediates mRNA recruitment to synapses dependent on neuronal activity. (**A**) Representative dual-color kymograph showing *MS2+Rgs4* 3´-UTR reporter mRNA (green) and TagRFPt tagged PSD-95 (magenta) from a dendrite of a rat hippocampal neuron. First and last frames are shown at top and bottom. Extracted track (right) for an mRNA granule docking at a PSD-95 positive area is indicated by arrowheads. (**B-C**) Distance between *MS2 only* or *MS2+Rgs4* 3´-UTR reporter mRNA docking events and closest PSD-95 positive cluster in co-transfected rat hippocampal neurons is displayed as dot plot (**B**) and density plot (**C**). (**D**) Distribution of *MS2 only* or *MS2+Rgs4* reporter mRNA-positive (estimated RNA number ≥ 1) and -negative (RNA < 1) PSD-95-TagRFPt clusters in soma and dendrites. *P-values* of Chi^2 tests against the control are indicated. (**E**) Integrated frequency of reporter docking and undocking events in dendritic synapses per min. Number of observations and population means are indicated. (**F**) Average net change of *MS2 only* or *MS2+Rgs4* mRNA content at mRNA reporter-positive or -negative synapses per min, calculated from the estimated reporter molecules that dock or undock at synapses per event, respectively. Numbers indicate mean value of net RNA level change. Error bars represent 95% confidence intervals. ** indicates significant ($p<0.01$) difference compared to zero (no net flux, null hypothesis). (**G-H**) Distance between *MS2 only* and *MS2+Rgs4* 3´-UTR reporter mRNA docking events and closest PSD-95 positive cluster displayed as dot plot (**G**) and density plot (**H**). Plots display *MS2+Rgs4* 3´-UTR reporter mRNA under untreated, vehicle (DMSO) or silenced (100 µM CNQX, 50 µM AP5, 1 µM TTX) conditions (G-H). Data represents mean ± standard deviation of three independent experiments (individual experiments shown as gray dots; B,G). Dashed lines represent mean values of single data points (C,H). Asterisks represent *p*-values obtained by Student's t-test (B), Mann Whitney U test (E) or Tukey's test post-hoc to one-way ANOVA analysis (G) (**$p < 0.01$, ***$p < 0.001$). Data was obtained from 40 µm dendritic segments at a minimal distance of 20 µm from the cell body. At least 10 dendrites/condition/experiment (A-C, G-H) or 12 neurons/condition (D-F) from 3 independent biological replicates were analyzed. Total number of dendrites (n_d), events (n_e) and synapses (n) analyzed per condition are indicated.

undocking event of either *MS2 only* or *MS2+Rgs4* reporter mRNAs at ~ 34 % *vs* ~ 21% of dendritic synapses, respectively (**Supplementary Fig. 2.4E**). This represents a ~30% significant reduction in the frequency of these events for the *MS2+Rgs4* 3´-UTR reporter mRNA ($p < 0.0001$; **Supplementary Fig. 2.4F,M**). We found that the number of these events showed a moderate correlation (R ~ 0.5) with the estimated mRNA copy number within PSD-95−RFP positive synapses (**Supplementary Fig. 2.4G**). This suggests that the number of docking/undocking events are related with the total number of mRNA particles at synapses. Analysis of the postsynaptic sites revealed that mRNA positive synapses were both larger (*data not shown*) and brighter in their mean PSD-95 signal intensity than mRNA negative synapses ($p < 0.0001$; **Supplementary Fig. 2.4H**). We found that the fraction of *MS2+Rgs4* 3´-UTR positive synapses in dendrites was significantly lower than that of *MS2 only* (57.1 % *vs* 73.9 %; $p < 0.0001$; **Fig. 2.4D**). However, when we focused on mRNA reporter positive synapses, we found a significant difference between the frequency of total docking/undocking events of *MS2 only* and *MS2+Rgs4* 3´-UTR reporter mRNAs at synapses ($p = 0.002$; **Fig. 2.4E**).

Subsequently, we analyzed the net directionality of reporter mRNA docking/undocking at postsynaptic densities. We found that the frequency of docking events was significantly higher for the *MS2+Rgs4,* compared to the *MS2 only* reporter (~0.9 min^{-1} *vs* 0.79 min^{-1}, $p = 0.005$), whereas there was no substantial difference in the frequency of undocking events (~0.99 min^{-1} *vs* 0.97 min^{-1} in *MS2 only* RNA positive synapses). In agreement with these results, we found a net influx ($p = 0.009$, $\alpha = 0.01$) of *MS2+Rgs4* into mRNA positive synapses, in contrast to the *MS2 only* reporter mRNA (**Fig. 2.4F, Supplementary Fig. 2.4I**), which was not significantly different from zero ($p = 0.043$, $\alpha = 0.01$). In general, synapses contained mRNA both at the beginning and during the experiment regardless of their location and reporter mRNA (**Supplementary Fig. 2.4J-L**).

In summary, this data demonstrates that the *MS2+Rgs4* 3´-UTR mediated docking in closer proximity to synapses, compared to the *MS2 only 3´-UTR*. Furthermore, although the *MS2+Rgs4* reporter interacted with fewer synapses, it displayed a net increase at synapses, while the *MS2 only* reporter did not. These findings suggest that dendritically localized *MS2+Rgs4* mRNA was probably associated with a specific subset of synapses.

2.3.5 Neuronal activity induces the recruitment of *Rgs4* 3´-UTR mRNA to synapses

Next, we investigated whether inhibition of neuronal activity affected recruitment of *Rgs4* 3´-UTR mRNA to synapses in addition to its effect on transport directionality. Therefore, we chemically inhibited neuronal activity in mature rat hippocampal neurons transiently co-transfected with either the *MS2 only* or the *MS2+Rgs4* 3´-UTR mRNA, tdMCP-GFP and the synaptic marker PSD-95−RFP. Neither synaptic density nor the ratio of docking to undocking events was altered when silenced cells were compared with vehicle or untreated controls (**Supplementary Fig. 2.4P-Q**). Additionally, *MS2 only* mRNA granules did not exhibit any significant change in their distance to PSD-95−RFP synapses upon inhibition of neuronal activity when compared to vehicle or untreated cells (**Supplementary Fig. 2.4R-S**). However, the inhibition of neuronal activity increased the docking/undocking distance of *MS2+Rgs4* mRNA close to synapses, to values comparable to that of *MS2 only* mRNA ($F_{2,6}$ = 0.001, p = 0.004 for silencing *vs* vehicle, p = 0.001 for silencing *vs* untreated, **Fig. 2.4G-H**; $F_{2,6}$ = 0.001, p = 0.003 for silencing *vs* vehicle, p = 0.00162 for silencing *vs* untreated, **Supplementary Fig. 2.4T-U**). Next, we performed local two-photon glutamate uncaging at individual dendritic spines to evaluate whether the stimulation of single spines would be sufficient to recruit mRNA granules. Either the *MS2 only* or the *MS2+Rgs4* reporter mRNAs were co-transfected together with tdMCP-GFP and tandem Tomato (tdTomato). Upon glutamate uncaging adjacent to individual spines, we observed an increase in spine size by the volume marker (tdTomato) (**Supplementary Fig. 2.5A**). The mRNA granule number before and after uncaging was quantified within a 5µm radius along dendrites centered at the stimulated spine. We observed an average increase of ~ 3 RNA granules for the *MS2+Rgs4* reporter mRNA, while there was no increase of *MS2 only* reporter granules (**Fig. 2.5A-B, Supplementary Fig. 2.5B, movie 2.11**). Together, this data demonstrates that neuronal activity is not only necessary to mediate the *Rgs4* 3´-UTR dependent mRNA transport bias, but is also required to recruit its mRNA to activated synapses. Furthermore, we provide further experimental evidence that it is the *Rgs4* 3´-UTR that has a direct influence on the activity-dependent mRNA docking/undocking, as the *MS2 only* reporter mRNA remained unaffected by neuronal inhibition or local stimulation of dendritic spines.

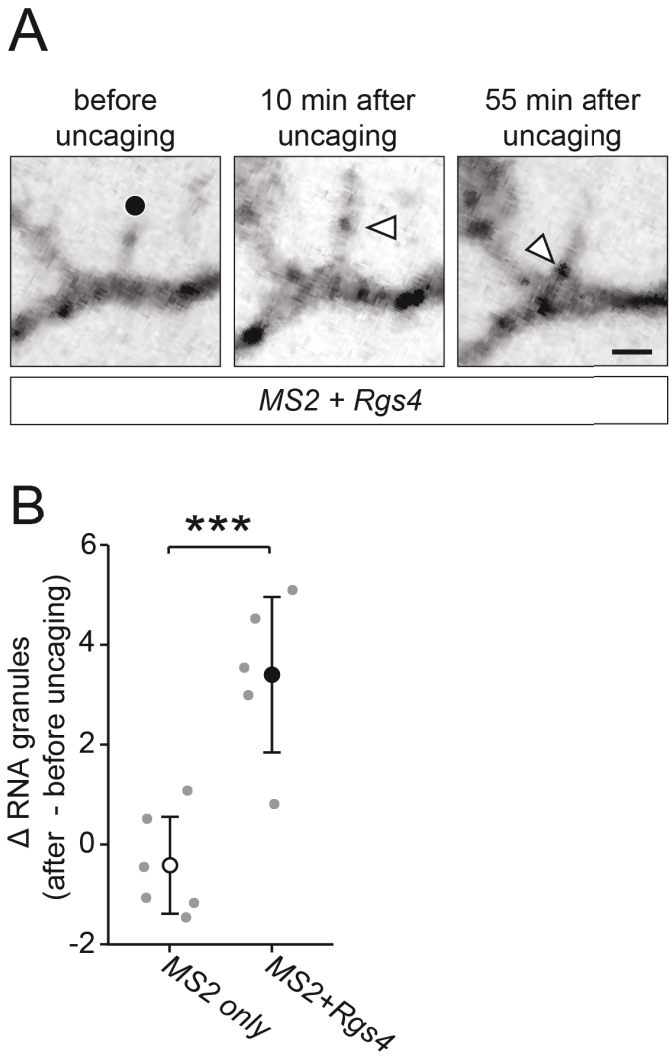

Figure 2.5: Local glutamate uncaging at individual dendritic spines triggers *Rgs4* 3´-UTR dependent mRNA recruitment. (**A**) Representative GFP fluorescence of a hippocampal neuron co-transfected with the *MS2+Rgs4* 3´-UTR reporter and tdMCP-GFP constructs before (left panel) and after (middle, right panels) local glutamate uncaging. Black dot denotes the uncaging spot at dendritic spine. Arrowheads indicate GFP positive *MS2* reporter mRNA granules. Scale bar 2 µm. (**B**) Dot plot displaying the change in RNA granule number 40-45 min after uncaging compared to the RNA granule number before uncaging within 5 µm of the stimulated spine. Data represents mean ± standard deviation (individual neurons shown as gray dots). Asterisks represent *p*-values obtained by Student's t-test (***$p < 0.001$). Data was obtained from 6 dendrites (5 neurons of 4 biological replicates) and 5 dendrites (5 neurons of 5 biological replicates) for *MS2 only* and *MS2+Rgs4* reporter mRNAs, respectively.

2.3.6 Stau2 regulates the transport of *Rgs4* 3´-UTR mRNA in dendrites

Finally, we investigated whether the RBP Stau2, which is known to bind *Rgs4* mRNA (Heraud-Farlow et al., 2013; Sharangdhar et al., 2017), was required for the transport of *MS2+Rgs4* granules. To investigate whether mRNA is co-transported with Stau2, we co-transfected the *MS2+Rgs4* reporter together with tdMCP-GFP and TagRFPt tagged Stau2 (RFP-Stau2). We observed multiple instances, where the *MS2+Rgs4* reporter mRNA granules were co-transported with Stau2 (**Fig. 2.6A, movies 12-13**). Moreover, overexpression of Stau2 resulted in an increase of dendritic *MS2+Rgs4* reporter density, while the *MS2 only* mRNA was unaffected (**Supplementary Fig. 2.6A**). Additionally, we performed a pilot experiment involving *MS2* RNA-mediated tethering of Stau2 to the *MS2 only* reporter mRNA. When we co-transfected both tdMCP-Stau2 and tdMCP-GFP together with the *MS2 only* reporter, we observed that the tethering of Stau2 tended to recruit the control mRNA closer to the synaptic marker vesicular glutamate transporter 1 (VGLUT1) (**Supplementary Fig. 2.6B**). Together, our data suggest that Stau2 might indeed regulate *Rgs4* 3´-UTR dependent recruitment to synapses. However, further work is clearly necessary to substantiate these findings in the future.

To further investigate the involvement of Stau2 in dendritic mRNA transport, we transduced neurons with lentiviral particles expressing either a short hairpin non-targeting control (shNTC) or a short hairpin specific for *Stau2* (shStau2-2) (Goetze et al., 2006) 4 days prior to co-transfection with tdMCP-GFP and *MS2 only* or *MS2+Rgs4* 3´-UTR reporter mRNAs. Time-lapse imaging revealed that the *MS2 only* reporter mRNA remained unaffected by *Stau2* knock-down (**Fig. 2.6B-C, Supplementary Fig. 2.6C-D**). In contrast, *Stau2* knock-down abolished the anterograde transport bias of *MS2+Rgs4* 3´-UTR mRNA granules in distal dendrites (p = 0.012, **Fig. 6D-E**). Total anterograde displacement remained unaffected for *MS2 only* mRNA, but showed a non-significant reduction for the *MS2+Rgs4* 3´-UTR reporter in Stau2 deficient neurons (**Supplementary Fig. 2.6E-F**). Different types of *MS2+Rgs4* 3´-UTR mRNA granule mobility, categorized as stationary, unidirectional, interrupted and multidirectional, as well as speed and displacement length were unaffected by Stau2 knock-down (**Supplementary Fig. 2.6G** and *data not shown*). The reduction of Stau2 expression was verified in the imaged samples by immunostaining (**Supplementary Fig. 2.6H**). In conclusion, this data provides direct

experimental evidence that Stau2, which is co-transported together with *Rgs4* reporter mRNA in distinct RNA granules, is responsible for the observed 3´-UTR-dependent transport bias.

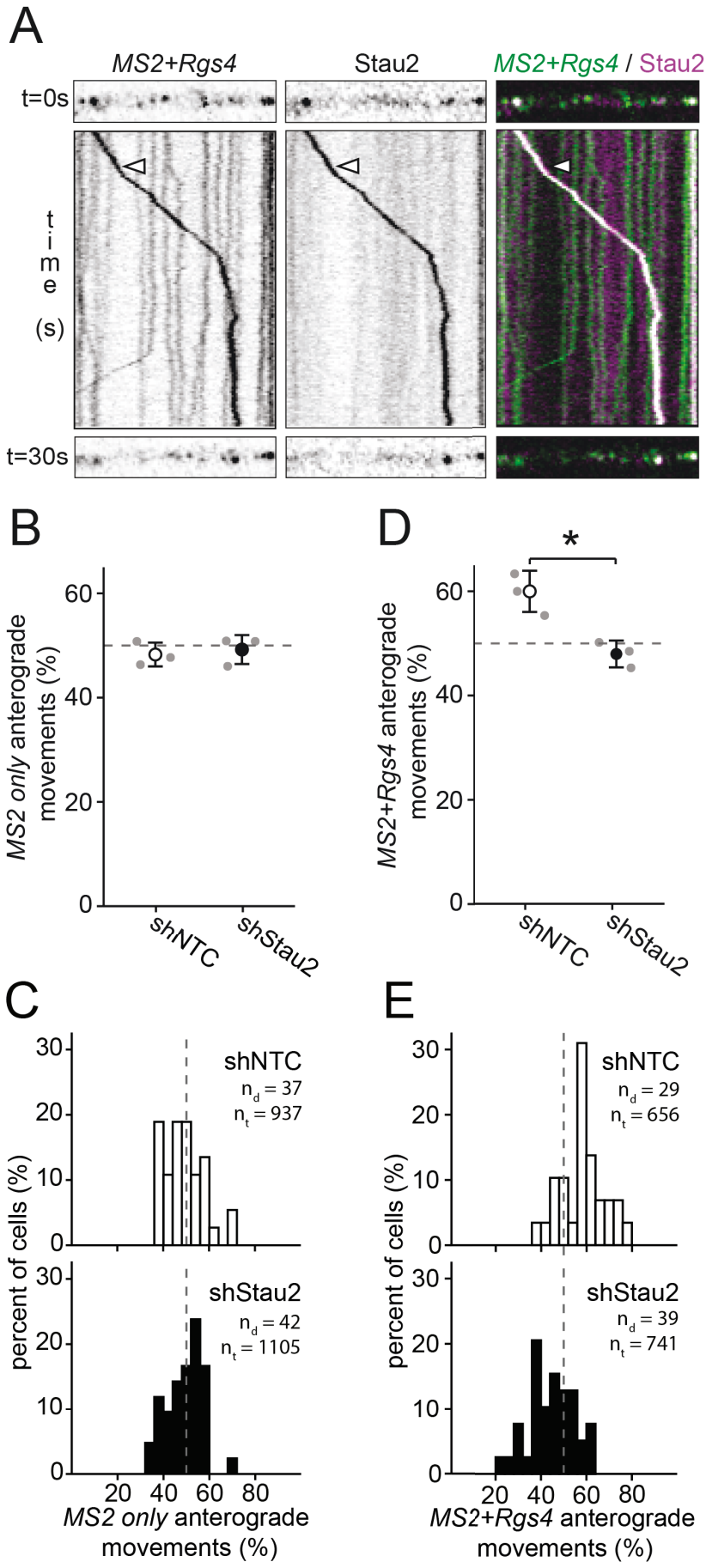
A
MS2+Rgs4
Stau2
MS2+Rgs4 / Stau2
t=0s
time (s)
t=30s
B
MS2 only anterograde movements (%)
shNTC
shStau2
D
MS2+Rgs4 anterograde movements (%)
*
C
shNTC
n_d = 37
n_t = 937
shStau2
n_d = 42
n_t = 1105
percent of cells (%)
MS2 only anterograde movements (%)
E
shNTC
n_d = 29
n_t = 656
shStau2
n_d = 39
n_t = 741
MS2+Rgs4 anterograde movements (%)

←

Figure 2.6: Stau2 regulates *Rgs4* 3´-UTR dependent transport. (**A**) Representative dual-color kymograph showing *MS2+Rgs4* 3´-UTR reporter mRNA (green) and tagRFPt-tagged Stau2 (magenta) from a dendrite of a rat hippocampal neuron. First and last frames are shown at top and bottom. Arrowheads indicate an *MS2+Rgs4* reporter and Stau2 positive RNA granule undergoing co-transport. (**B-E**) Dot plots (**B,D**) and histograms (**C,E**) displaying percentage of anterograde moving *MS2 only* or *MS2+Rgs4* 3´-UTR reporter mRNA granules in shNTC and shStau2 transduced hippocampal neurons. Abbreviation: NTC = non-targeting control. Data represents mean ± standard deviation of three independent experiments (individual experiments shown as gray dots). Asterisks represent *p*-values obtained by Student's t-test (*$p < 0.05$). Data was obtained from 40 µm dendritic segments at a minimal distance of 20 µm from the cell body. Total number of dendrites (n_d) and tracks (n_t) analyzed per condition are indicated. Only displacements ≥ 1.5 µm were considered for analysis.

2.4 Discussion

Here, we show that mRNAs travel along dendrites in a dynamic and multidirectional fashion, a process that does not exclusively require a specific 3´-UTR sequence for this dendritic localization. The presence of the *Rgs4* 3´-UTR, however, conveyed key properties to the reporter mRNA, which fine-tune transport as (i) it introduced a transport bias directed towards distal dendrites, and (ii) regulated the spatio-temporal association to synapses. These effects were dependent on neuronal activity and the RBP Stau2. Together, our data not only provide experimental support for the *sushi-belt* model of dendritic mRNA transport (Doyle and Kiebler, 2011), in which mRNAs dynamically patrol synapses, but also allow us to substantially advance this model by the introduction of a regulated transport bias giving mechanistic insight into global RNA sorting processes including recruitment by individual, stimulated synapses in polarized neurons.

2.4.1 Localized mRNAs traverse the dendrite in a *sushi-belt*-like fashion

We present evidence that mRNA granules traverse distal dendrites in a directed manner, independently of the presence of a specific 3´-UTR. All *MS2 only*, *MS2+Rgs4* and *MS2+histone-3.3* 3´-UTR mRNA reporters formed dendritic mRNA granules, suggesting that additional factors other than 3´-UTR sequences contribute to dendritic localization. For instance, the poly-A-tail or other mRNAs contained in the same granule (Palacios and St Johnston, 2001) might be involved. However, independently of the 3´-UTR sequence, a proportion of the observed RNA granules remained stationary, while others showed variability in speed, displacement length and directionality of transport. In addition to both simple anterograde and retrograde transport, some mRNA granules displayed more complex dynamics. Indeed, some granules interrupted and subsequently reinitiated transport or even switched direction without interruption. This interrupted transport has recently been investigated and computationally modeled, providing a basis for future functional studies (Song et al., 2018). Additionally, we show here that longer observation time revealed an increase in interrupted movements and a decrease in unidirectional or stationary phases, demonstrating that a majority of mRNA granules may undergo multiple transport

phases in different directions. This observation expands our current understanding of mRNA sorting beyond local recruitment, as it experimentally proves that mRNA granules are not irreversibly anchored, but are dynamic, can be targeted to specific sites upon demand, and be released from them later on. Together, we provide experimental evidence that the *sushi-belt* model indeed accurately describes dendritic mRNA transport in live neurons. However, we do not exclude that other factors/mechanisms might contribute as well. Interestingly, a recent computational study provided evidence that the *sushi-belt* model can achieve complex spatial distribution of cargo in neurons (Williams et al., 2016).

2.4.2 The *Rgs4* 3´-UTR mediates an anterograde transport bias dependent on neuronal activity and the Stau2 protein

A key finding of this study is that the 3´-UTR of *Rgs4* mRNA mediated an anterograde transport bias in dendrites, *i.e*. a preferential transport directionality towards distal regions. In contrast, neither the *MS2 only* nor the *MS2+histone-3.3* reporter mRNAs displayed this bias (**Fig. 2.2D** and *data not shown*). Previous studies have observed both anterograde and retrograde mRNA transport. Moreover, a directional bias in transport has not been so frequently reported. It has been shown for *oskar* mRNA in the *Drosophila* oocyte, and for *ß-actin* and *Arc* mRNAs in mouse hippocampal neurons (Das et al., 2018; Dynes and Steward, 2007; Park et al., 2014; Zimyanin et al., 2008). It is worth mentioning that these studies observed a bias of similar magnitude as we report here (~ 60% towards distal regions), indicating that the dendritic bias of the *MS2+Rgs4* 3´-UTR reporter is within a physiological range.

Interestingly, silencing of neuronal activity abolished the *MS2+Rgs4* 3´-UTR specific transport bias, while the transport of the *MS2 only* reporter remained unaffected. Endogenous neuronal signaling in culture restored the bias, demonstrating its physiological pertinence. In contrast with our observations, *Arc* mRNA transport bias was not affected by neuronal activity (Das et al., 2018). This suggests that anterograde transport is differentially regulated depending on mRNA sequence and that distinct RNA granules may be differently regulated by neuronal activity. Furthermore, we show that knock-down of Stau2 abolished the *Rgs4* 3´-UTR dependent anterograde transport bias as well. As the *MS2 only* reporter mRNA remained unaffected by Stau2 knock-down, the loss of the anterograde transport bias

is specific to the *Rgs4* 3´-UTR and might be caused by the absence of Stau2 in *Rgs4* containing mRNA granules. Therefore, we hypothesize that Stau2 might be recruited in conjunction with neuronal activity to modulate dendritic *Rgs4* mRNA transport. Similarly, previous research has shown how Staufen and other RBPs are not necessary for general transport, but can facilitate or modulate it (Brendza et al., 2000; Yoon and Mowry, 2004). Along this line, Staufen has been implicated in kinesin-1 dependent posterior localization of *oskar* mRNA in *Drosophila* and has been found in a complex with kinesin-1 in *Xenopus* (Brendza et al., 2000; Yoon and Mowry, 2004). In line with this finding, we observed directed co-transport of *MS2+Rgs4* granules together with Stau2 in neurons. Importantly, Stau2 depletion results in both morphological and physiological synaptic phenotypes (Goetze et al., 2006; Lebeau et al., 2011). Therefore, it is tempting to speculate that Stau2 might not only regulate the expression of proteins relevant at synapses as previously shown (Heraud-Farlow et al., 2013), but also the transport and recruitment of their mRNAs. In turn, deregulation of synaptic proteins, resulting in aberrant synaptic remodeling, might render a synapse incapable of proper recruiting of relevant transcripts. Together, our data gives functional insight into the regulation of 3´-UTR dependent mRNA transport. We show that it is the *Rgs4* 3´-UTR that facilitates dendritic localization via the anterograde transport bias. Although dendritic sorting might be affected by other factors such as regulated mRNA degradation, this transport bias might enable fast and efficient mRNA recruitment to specific regions such as synapses as needed. Future studies will have to unravel the detailed molecular mechanisms of how Stau2, neuronal activity and 3´-UTR sequences cooperate to mediate this anterograde bias in neurons.

2.4.3 *Rgs4* mRNA is recruited to synapses dependent on its specific 3´-UTR and neuronal activity

We observed that the *MS2+Rgs4* 3´-UTR facilitated mRNA docking and undocking in closer proximity to synapses compared to the *MS2 only*. Upon silencing of endogenous neuronal activity, the distance of docking/undocking was increased for the *MS2+Rgs4* 3´-UTR, while the *MS2 only* reporter remained unaffected. Conversely, local stimulation of individual dendritic spines by glutamate uncaging resulted in increased recruitment of *MS2+Rgs4* granules, but not *MS2 only* mRNAs.

Furthermore, the *MS2+Rgs4* 3´-UTR reporter interacted with fewer synapses and displayed more docking events at dendritic synapses than the *MS2 only* reporter. This led to a slower turnover of *MS2+Rgs4* mRNA content at synapses compared to *MS2 only*, indicating *MS2+Rgs4* is more stably associated and might remain longer at synapses. We propose that the presence of *MS2 only* mRNA at synapses might represent a state of non-specific, default localization. These effects, along with the observed differences in the brightness of PSD-95 clusters could reflect differences in either synaptic activity or in the subtype of the synapse. As the Rgs4 protein is a negative regulator of synaptic activity, we speculate that its mRNA is transported to a subtype of synapses, where it might be regulated *in situ*. Here, the mRNA could be unpacked and locally translated by polysomes localized close to PSD-95 clusters (Ostroff et al., 2002), where the newly synthesized Rgs4 protein would modulate G protein-coupled receptor mediated neuronal signaling. Our findings are in agreement with a study by the Singer lab that showed that endogenous *ß-actin* mRNA is recruited to glutamate-stimulated dendritic spines, where it is locally translated (Yoon et al., 2016). Using a similar approach, we now show that glutamate stimulation of individual spines results in 3´-UTR dependent recruitment of *Rgs4* mRNA, as the *MS2 only* reporter displayed no variation in recruitment.

Taking together, we hypothesize that the observed anterograde transport bias contributes to synaptic recruitment of mRNAs. As both the transport bias and synaptic recruitment are modulated by the 3´-UTR and neuronal activity, anterograde transport might indeed facilitate synaptic recruitment, especially under endogenous mRNA expression levels. Future work will aim to understand how neuronal activity affects the organization of key cytoskeletal components to mediate *Rgs4* mRNA recruitment and whether it affects their capture on ribosomes at synapses.

2.4.4 A model of dynamic dendritic *Rgs4* mRNA sorting and synaptic recruitment

Based on our findings, we propose a model of *Rgs4* trafficking in neuronal Stau2 mRNA granules, in which its 3´-UTR specifically mediates sorting to distal dendrites. The *Rgs4* mRNA might patrol the dendrite in a dynamic fashion in accordance with the *sushi-belt* model (Doyle and Kiebler, 2011). Neuronal activity can result in the docking of this mRNA at specific postsynaptic sites and is thought to cause unpacking of the mRNA from transport granules. There, the mRNA may be

subjected to local translation, making the encoded Rgs4 protein available in a spatially and temporally restricted manner. After the mRNA has fulfilled its function at the synapse, it may undock and reinitiate transport until it is degraded or recruited for a new round of translation. Such processes are the basis of cellular mechanisms in polarized cells involved in, *e.g.* dendritic arborization, long-term potentiation and synaptic plasticity and are indispensable for neuronal development, learning and memory formation.

2.5 Methods

2.5.1 Neuronal Cell Culture, Transfection and Transduction

Primary rat hippocampal neuronal cell cultures were generated as previously described (Goetze et al., 2003). In short, hippocampi of embryonic day 17 (E17) embryos of timed pregnant Sprague-Dawley rats (Charles River Laboratories) were isolated, cells dissociated and plated on poly-L-lysine coated cover slips or glass bottom dishes (WillCo Wells) and cultured in NMEM+B27 medium (Invitrogen). Experiments were performed with cultured neurons between 10-16 days *in vitro* (DIV). Neurons were transiently transfected by calcium phosphate co-precipitation at 10-15 DIV as previously described (Goetze et al., 2004) and imaged at 11-16 DIV. For experiments involving glutamate uncaging, neurons were plated on poly-L-lysine and laminin (Invitrogen) coated 12-mm diameter glass coverslips, at a density of 600 cells/mm^2. Cells were transfected at 15-17 DIV by calcium phosphate co-precipitation and imaged the following day. To knock-down Stau2 expression, 10-11 DIV neurons were transduced overnight with lentiviral suspension, transfected with MCP-GFP and MS2 mRNA reporter constructs at 14-15 DIV and imaged at 15-16 DIV. All animals were used according to the German Welfare for Experimental Animals (LMU-Munich, *Regierung von Oberbayern*).

2.5.2 Plasmids

RNA reporter constructs were placed under the control of an RSV promoter, contained *LacZ* as open reading frame, a stop codon, and an array of either 32 unique MS2 hairpins or a quadruplication of this array, *i.e.* 128 MS2 hairpins (Pichon et al., 2016). The 3´-UTR was either omitted (pRSV-LacZ-MS2) or included (pRSV-LacZ-MS2-*Rgs4* 3´-UTR or pRSV-LacZ-MS2-*H3.3* 3´-UTR) prior to the polyA signal. The sequences of the 3´-UTRs correspond to the positions 728-2919 nt of rat *Rgs4* mRNA (NM_017214.1) or 537-1087 nt of rat *Histone3.3* mRNA (X73683.1). To generate the pUBC-NLS-ha-tdMCP-GFP plasmid, the nls-HA-tdMCP-gfp sequence from the phage-ubc-nls-ha-tdMCP-gfp construct (Addgene #40649) (Wu et al., 2012) was cloned into the pEGFP-C1 vector (Clontech). The pUBC-ha-tdMCP-GFP

plasmid was generated by removing the NLS from the original vector. The pUBC-NLS-ha-tdMCP and pUBC-NLS-ha-tdMCP-Stau2 vectors were generated by extracting the UBC-NLS-ha-tdMCP sequence from the original vector and cloning the 62kD isoform of mouse Stau2 in frame in the pEGFP-C1 vector (Clontech) in place of the EGFP. The CMV-PSD95-tagRFPt vector was generated by cloning the PSD-95 open reading frame into the ptagRFPt-N1 vector (Robert H. Singer, USA). The pCMV-tagRFPt-Stau2 vector was generated by cloning the open reading frame of the 62kD isoform of mouse Stau2 into the ptagRFPt-C1 vector (Robert H. Singer, USA). The pCMV-tdTomato vector was generated by cloning the open reading frame of tdTomato (Dieter Edbauer) into the ptagRFPt-C1 vector (Robert H. Singer, USA) in place of tagRFPt. The lentiviral packaging plasmids psPAX2 and pcDNA3.1-VSV-G have previously been reported (Heraud-Farlow et al., 2013). Lentiviral plasmids pFu3a-H1-sh-NTC-pCaMKIIα-tagRFP and pFu3a-H1-sh-Stau2-2-pCaMKIIα-tagRFP were generated by exchanging the UBC promoter for the CaMKIIα promoter from the previously published FUW based vectors (Heraud-Farlow et al., 2013).

2.5.3 Lentivirus production

Control sh-NTC and sh-Stau2-2 lentiviral particles were obtained from HEK293 cells co-transfected with the plasmids psPAX2, pcDNA3.1-VSV-G and either pFu3a-H1-sh-NTC-pCaMKIIα-tagRFP or pFu3a-H1-sh-Stau2-2-pCaMKIIα-tagRFP, respectively, using calcium phosphate co-precipitation. Supernatants were filtered (0.45 µm RVDF Millex-HV; Millipore), concentrated by ultracentrifugation (23,000 rpm, 140 min, SW 32 Ti rotor; Beckman Coulter) and resuspended in Opti-MEM™ (Life Technologies) (Heraud-Farlow et al., 2013).

2.5.4 Single molecule fluorescent in situ hybridization

Single molecule fluorescent *in situ* hybridization (smFISH) was performed as previously described (Fusco et al., 2003), with slight modifications. Briefly, cells were fixed in 4% PFA for 20 min and permeabilized in 70% ethanol overnight at 4°C, followed by two rounds of DNase treatment for 1 hour each at 37°C to remove plasmid DNA. Hybridization of 10 unique Cy3-labelled antisense-MS2 probes was

performed overnight at 37°C. Coverslips were mounted using Prolong Gold anti-fade mounting medium (Invitrogen). Sequences of probes are available upon request.

2.5.5 Immunostaining

Neurons were immunostained as previously described (Goetze et al., 2006). The following antibodies were used: (i) polyclonal antibodies, *i.e.* selfmade rabbit anti-Stau2 (Fritzsche et al., 2013), guinea pig anti-VGLUT1 (Synaptic Systems, 419005); (ii) secondary antibodies, *i.e.* donkey anti-rabbit and goat anti-guinea pig Alexa 555 or Alexa647 conjugated (Life Technologies, A31570, A31573, A21450).

2.5.6 Chemical treatments

To inhibit neuronal activity, cells were pre-incubated with 100 µM 6-cyano-7-nitroquinoxaline-2,3-dione (CNQX; Sigma, #C127), 50 µM 2-amino-5-phosponopentanoic acid (AP5; Sigma, #A8054) and 1 µM tetrodotoxin (TTX; Abcam, #ab120055) in NMEM+B27 for 1 hour at 37°C. Media was exchanged for HBSS supplemented with 20 mM HEPES pH=7.3, 100 µM CNQX, 50 µM AP5 and 1 µM TTX prior to imaging at the microscope. Vehicle treated cells were incubated with equivalent amount of DMSO.

2.5.7 Microscopy

Live cell imaging was performed on a Zeiss Cell Observer spinning disk system. The setup consisted of a Zeiss Z1 Axio Observer microscope including a Plan-Apochromat 63x objective, a Yokogawa CSU-X1 spinning disk unit with 4 laser lines (405 nm 20 mW; 488 nm 50 mW, 561 nm 75 mW and 638 nm 75 mW) and an Evolve 512 Delta EMCCD Camera. For temperature control, a custom made EMBL environmental chamber (EMBLEM) was constructed for this setup. A 523/610 HC dual-band filter AHF was applied to reduce acquisition delay between channels during dual-color imaging. Hippocampal neurons were imaged at 36°C in HBSS (Life Technologies) supplemented with 20 mM HEPES buffer pH=7.3 (Sigma Aldrich). Time-lapse images were acquired for the duration of 1, 3.5 or 10 minutes, with an

approximate frame rate of ~ 15.3 fps for single channel acquisitions and ~ 4.7 fps for two-channel acquisitions with a 80 ms delay between channels. Cells were selected for proper expression of plasmids as well as for cell morphology and cell viability.

Imaging of fixed cells was performed on a Zeiss Z1 Axio Observer microscope including a Plan-Apochromat 63x objective, a COLIBRI.2 LED or a HXP 120 C light source and the Axiocam 506 mono camera.

Two-Photon Imaging and Glutamate Uncaging were carried out as described previously (Meyer et al., 2014; Scheuss and Bonhoeffer, 2014) except that a single laser (Mai Tai HP; Newport-Spectra Physics, Santa Clara, CA, USA) was used and tuned to 930 nm excitation wavelength for 2-photon imaging and 720 nm for uncaging. In brief, recordings were performed at 35°C in ACSF (in mM: 127 NaCl, 2.5 KCl, 25 $NaHCO_3$, 1.25 NaH_2PO_4, 4 $CaCl_2$, 25 D-glucose; in µM: 1 TTX, 10 D-serine; pH 7.4; saturated with carbogen) on a custom two-photon laser-scanning microscope (objective: 60x, 0.9 numerical aperture; Olympus, Tokyo, Japan). In some experiments the ACSF contained 2 mM $CaCl_2$, 1 mM $MgCl_2$ and no TTX and D-serine. The data obtained under these conditions was similar and pooled. MNI-caged L-glutamate was applied in the bath solution at 1.25 or 2.5 mM. Uncaging protocol: 30 pulses at 0.5 Hz, 4 ms pulse duration, wavelength 720 nm, 20 mW at the objective back aperture). At least 6 baseline image stacks (256 x 256 pixel, pixel size 0.105 or 0.125 µm) were recorded every 30 s on two channels (GFP, tdTomato) before glutamate uncaging was performed close to the spine to be stimulated. 120 s or 150 s after stimulation, time-lapse imaging was resumed every 30 s until 5 min after stimulation, then every 60 s until 30 min and continued every 5 min until 60 min after stimulation.

2.5.8 Image Data Analysis

Time-series image data of reporter mRNAs was analyzed by kymographs. Dendritic 40 µm segments at ≥ 20 µm from the cell body were selected and straightened in ImageJ. The KymographTracker plugin of the ICY Bioimaging software (Chenouard, 2010; de Chaumont et al., 2012) was used to generate kymographs and to trace and extract single tracks. Only movements longer than 1.5 µm were considered for analysis. Tracks were terminated when a particle stopped,

changed direction or left the region of interest. Average speed and displacement were obtained by calculating the mean. Anterograde and retrograde tracks were counted to calculate the percent of anterograde transport. The sum of anterograde and retrograde displacement lengths were used to calculate the percent of total anterograde displacement. Dual-color kymographs were generated by overlaying kymographs of the identical region of interest from two separate channels. Events in dual-color kymographs were manually selected and distances were manually measured in ImageJ, aided by a custom written ImageJ macro script (available upon request). Data was processed and subjected to statistical analyses in R (R-Core-Team, 2016).

The RNA signal intensity of PSD-95 labelled postsynaptic densities was analyzed within the synaptic masks generated by the xsParticle Tracker ImageJ plugin (Gaspar and Ephrussi, 2017; Gaspar et al., 2014).The time series of the measured, background corrected reporter RNA signal was fitted with a series of constants using the rpart package of R (Therneau, 2018). The minimum duration of a single constant fit was set to 5 frames (~ 1 s). The 5^{th} percentile of the RNA signal intensity distribution measured in every 100 frames (for correction of photobleaching, **Supplementary Fig. 2.4N-O**) was used as the signal corresponding to a single reporter RNA molecule. Changes between two adjacent fitted constants whose absolute value exceeded this threshold were quantified as docking and undocking events, depending on the sign of the change.

For deconvolution, z-stacks with 25 images at an interval of 0.26 µm were acquired, covering a total distance of 6.24 µm. Z-stacks were subjected to deconvolution using the constrained iterative quantitative restoration method of the Zeiss ZEN software deconvolution module.

For analysis of time-lapse series with glutamate uncaging, individual frames from image stacks were median filtered (5 x 5 pixel window) and maximum intensity projections generated. Spine size (tdTomato fluorescence) was determined as integrated fluorescence within a region of interest (ROI) containing the spine and subtracting integrated background signal from a ROI of the same size placed outside of any structure. To control for stimulus specific changes in spine size, the size of neighboring unstimulated spines or of an adjacent dendritic region was determined in the same way. Data were analyzed with custom routines written in MATLAB (version

R2018b, MathWorks, Natick, MA, USA). mRNA granules were manually quantified in a 5 µm dendritic radius centered at the stimulated spine. To compensate for fluctuations due to ongoing transport two time points before (~ 7-4 and ~ 2 min) and after (40 and 45 min) uncaging were averaged respectively.

2.5.9 Statistical Analysis

The R software was used for all data processing, plotting and statistical analysis (R-Core-Team, 2016; Wickham, 2009; Wickham, 2011; Wickham, 2016). Figures represent mean ± standard deviation of at least 3 independent biological replicates, unless otherwise stated. Asterisks represent *p*-values obtained by either Student's t-test, Tukey's test post-hoc to one-way ANOVA analysis using the average values per experiment or pairwise Mann Whitney U tests (*$p < 0.05$, **$p < 0.01$, ***$p < 0.001$), as indicated. The *F*-value evaluates whether the variance between the means of populations is significantly different (Fisher-Snedecor's F distribution). The degrees of freedom are indicated as subscript. Significant levels (α) are provided for Fig. 4F and Supplementary Fig.4I.

2.6 Acknowledgments

We thank Sabine Thomas and Jessica Olberz for primary neuron culture preparation; Renate Dombi, Ulrike Kring and Ilaria Brentari for assistance; Dieter Edbauer for the tdTomato plasmid, Daniela Rieger for antibody purification; Tobias Straub and Florian Müller for assistance in image analysis and statistics; Teja Sharangdhar, Marco Tolino and Georgia Vendra for initial experiments; Robert H Singer an Magdalena Götz for general support and Peter Scheiffele, Andre Fischer, Jernej Ule, Walter Neupert and Rico Schieweck for critical comments on the manuscript. This work was supported by grants from the DFG (Großgeräteantrag INST86/1581-1FUGG, SPP1738, FOR2333, SFB870) and the FWF (I 590-B09, F4314-B09 SFB RNA-seq) (all to MAK), SFB870 to VS, ANR-10-BLAN-1222 (to EB) and the Friedrich-Baur-Stiftung (to IS).

Competing Interests

The authors declare no competing interest.

Data availability statement

All datasets that were generated during the current study are found in the source file or will be available upon request.

Author contributions

MAK conceived the project together with EdB. KEB, IS, IG, VS, CI, GA, SH, EuB, SFM and JE performed experiments and all authors were involved in data analysis. KEB, IS and MAK wrote the manuscript, which was approved by all authors before submission.

2.7 Supplementary Materials

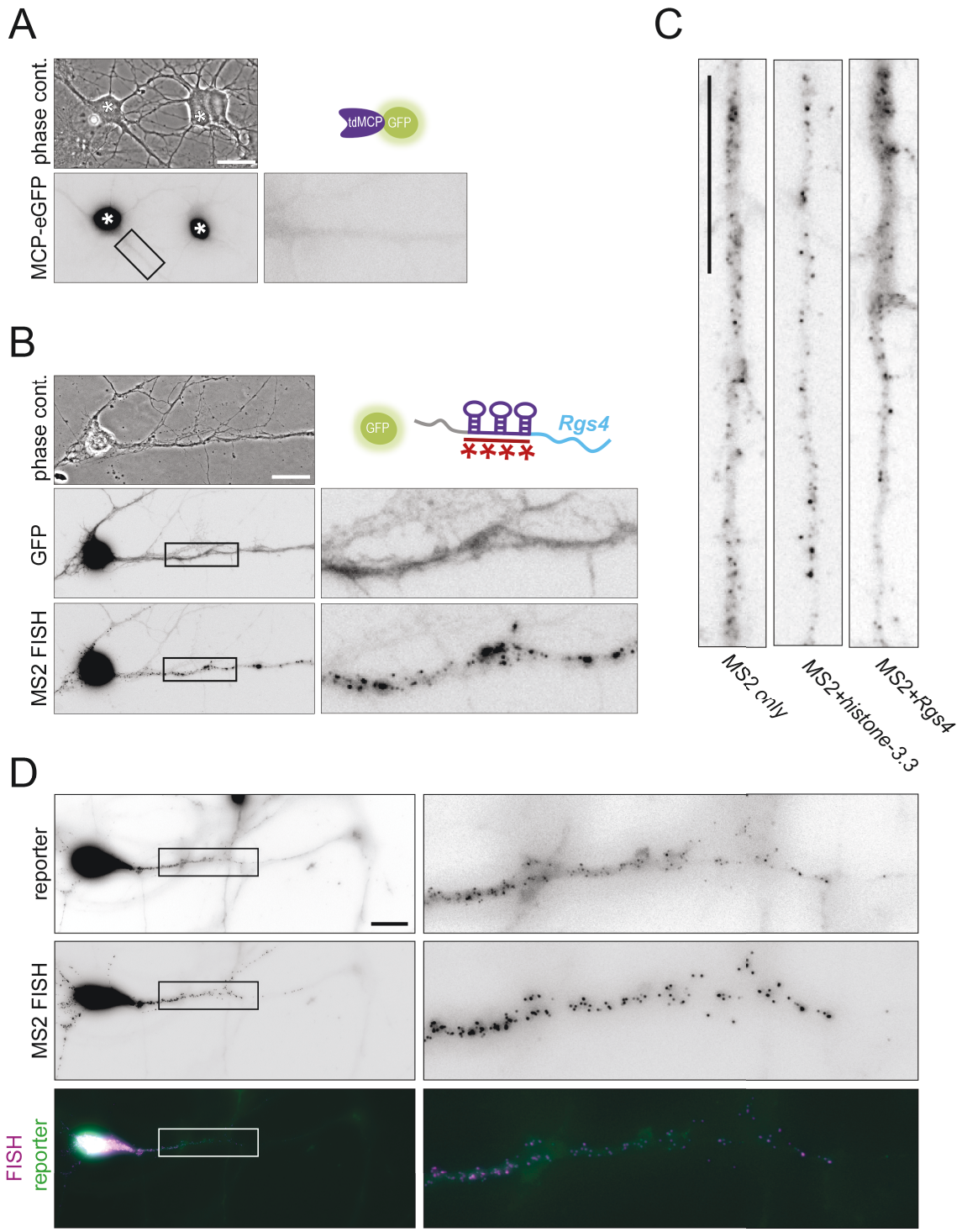

←

Supplementary Figure 2.1: tdMCP-GFP positive granules contain MS2 reporter mRNA and localize to dendrites. (**A**) Phase contrast and GFP fluorescence of rat hippocampal neurons expressing tdMCP-GFP (scheme top right). Asterisks denote transfected cells. (**B**) Phase contrast, GFP fluorescence and MS2 single molecule FISH of rat hippocampal neurons co-expressing control GFP (not fused to MCP) and the *MS2+Rgs4* reporter mRNA (scheme top right). (**C**) Straightened dendritic segments, 60 µm from soma expressing tdMCP-GFP and either *MS2 only*, *MS2+histone-3.3* or *MS2+Rgs4* 3´-UTR reporter mRNAs. (**D**) GFP fluorescence, MS2 single molecule FISH and overlay in a rat hippocampal neuron co-transfected with tdMCP-GFP and *MS2+Rgs4* reporter mRNA. Unprocessed image of deconvolved data shown in Fig. 1B. Scale bars 20 µm. Related to Figure 1.

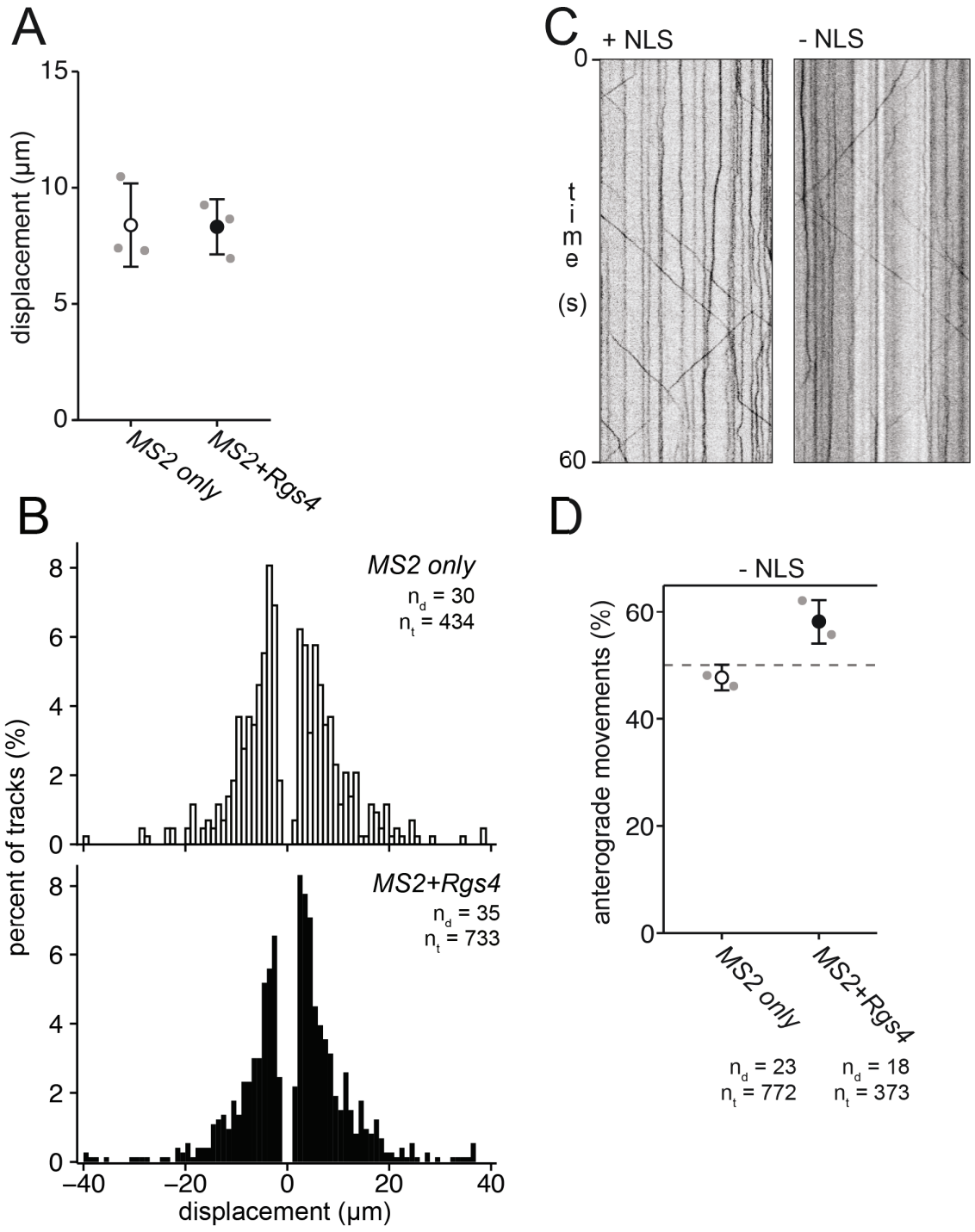
A
displacement (µm)
15
10
5
0
MS2 only
MS2+Rgs4
B
percent of tracks (%)
MS2 only
n_d = 30
n_t = 434
MS2+Rgs4
n_d = 35
n_t = 733
displacement (µm)
C
+ NLS
- NLS
time (s)
0
60
D
- NLS
anterograde movements (%)
MS2 only
MS2+Rgs4
n_d = 23
n_t = 772
n_d = 18
n_t = 373

←

Supplementary Figure 2.2: Displacement of mRNA granules. (**A-B**) Dot plot (**A**) and histogram (**B**) showing transport displacement of *MS2 only* or *MS2+Rgs4* 3´-UTR reporter mRNAs, detected by tdMCP-GFP in co-transfected rat hippocampal neurons. (**C**) Representative kymographs of GFP fluorescence of hippocampal neuronal culture co-transfected with the *MS2+Rgs4* 3´-UTR reporter and tdMCP-GFP constructs either with (+NLS) or without (-NLS) a nuclear localization signal (NLS). (**D**) Dot plot displaying percentage of anterograde moving granules for *MS2 only* or *MS2+Rgs4* 3´-UTR reporter mRNAs, detected by tdMCP-GFP. Data represents mean ± standard deviation of independent experiments (individual experiments shown as gray dots). Data was obtained from 40 µm dendritic segments at a minimal distance of 20 µm from the cell body. Total number of dendrites (n_d) and tracks (n_t) analyzed per condition are indicated. Only displacements ≥ 1.5 µm were considered for analysis. Related to Figure 2.

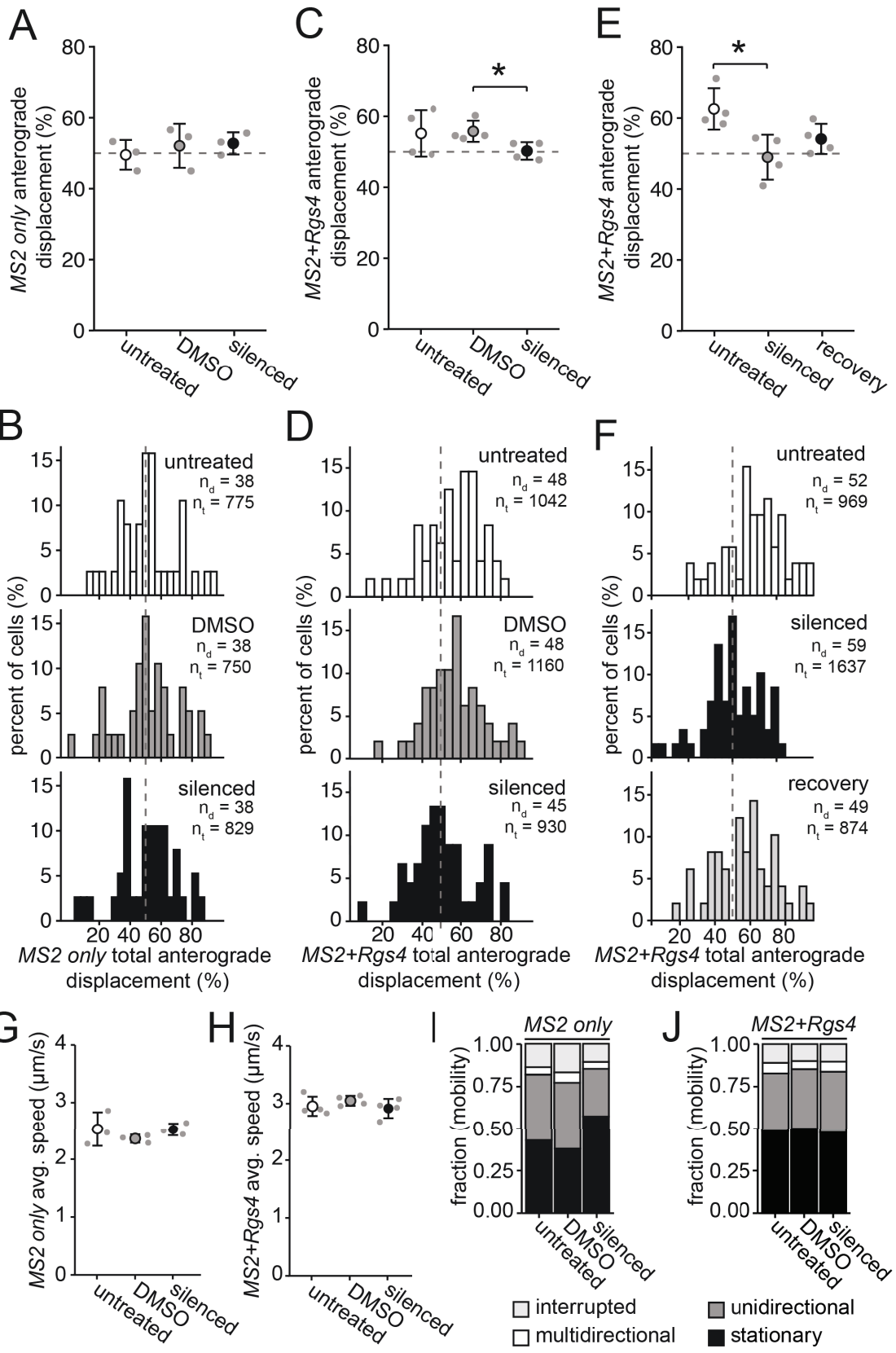
A
C
E
MS2 only anterograde displacement (%)
MS2+Rgs4 anterograde displacement (%)
untreated
DMSO
silenced
recovery
*
B
D
F
percent of cells (%)
n_d = 38
n_t = 775
n_d = 38
n_t = 750
n_d = 38
n_t = 829
n_d = 48
n_t = 1042
n_d = 48
n_t = 1160
n_d = 45
n_t = 930
n_d = 52
n_t = 969
n_d = 59
n_t = 1637
n_d = 49
n_t = 874
MS2 only total anterograde displacement (%)
MS2+Rgs4 total anterograde displacement (%)
G
H
I
J
MS2 only avg. speed (µm/s)
MS2+Rgs4 avg. speed (µm/s)
fraction (mobility)
MS2 only
MS2+Rgs4
interrupted
multidirectional
unidirectional
stationary

←

Supplementary Figure 2.3: Chemical inhibition of neuronal activity affects *Rgs4* 3´-UTR dependent total anterograde travel distance. (**A-H**) Dot plots (**A,C,E, G, H**) and histograms (**B,D,F**) displaying the percentage of total anterograde travel distance (A-F) and average speed (G,H) of *MS2 only* (A,B,G) or *MS2+Rgs4* 3´-UTR (C-F, H) reporter mRNAs in rat hippocampal neurons, under untreated, vehicle (DMSO) or silenced (100 µM CNQX, 50 µM AP5, 1 µM TTX) conditions and after recovery for 1 hour. Data represents mean ± standard deviation of 3-4 independent experiments (individual experiments shown as gray dots). Asterisks represent *p*-values assessed by Student's t-test (C) or Tukey's test post-hoc to one-way ANOVA analysis (E) (* $p < 0.05$). Data was obtained from 40 µm dendritic segments at a minimal distance of 20 µm from the cell body. At least 10 dendrites/condition/experiment were analyzed. Total number of dendrites (n_d) and tracks (n_t) analyzed per condition are indicated. Only displacements ≥ 1.5 µm were considered for analysis. (**I-J**) Quantification of relative transport dynamics of *MS2 only* (I, 9-10 dendrites per condition) and *MS2+Rgs4* 3´-UTR (J, 35-38 dendrites per condition) reporter mRNA under untreated, vehicle (DMSO) or silenced (100 µM CNQX, 50 µM AP5, 1 µM TTX) conditions in 1 minute time-series acquisitions. Related to Figure 3.

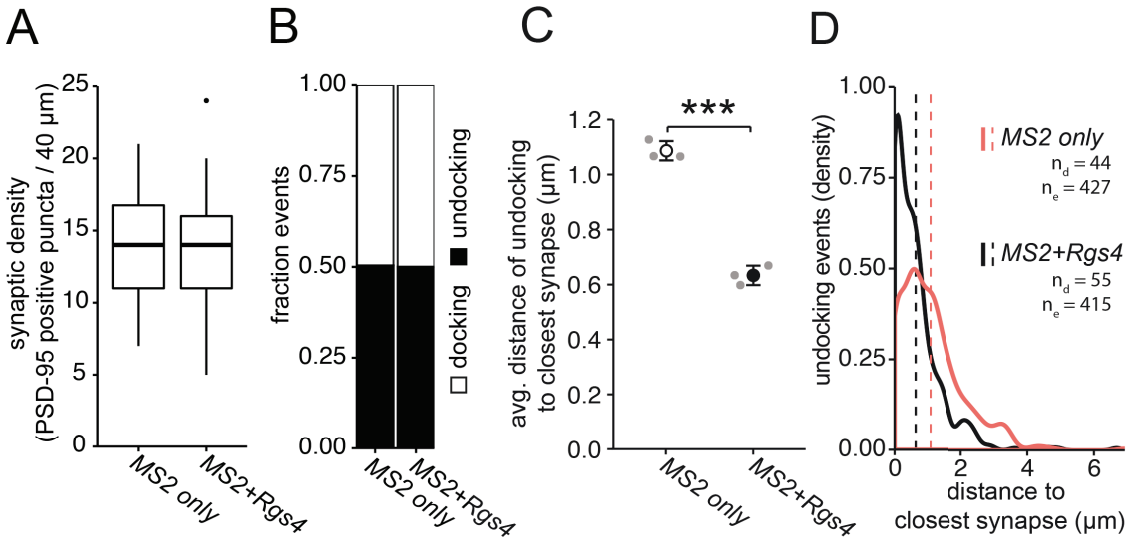

E

	somatic synapses		dendritic synapses	
	dynamic	non-dynamic	dynamic	non-dynamic
MS2 only	112 (76.1%)	35	440 (34.5%)	835
MS2+Rgs4	60 (76.1%), $p = 1$	18	252 (21.2%), $p < 0.0001$	932

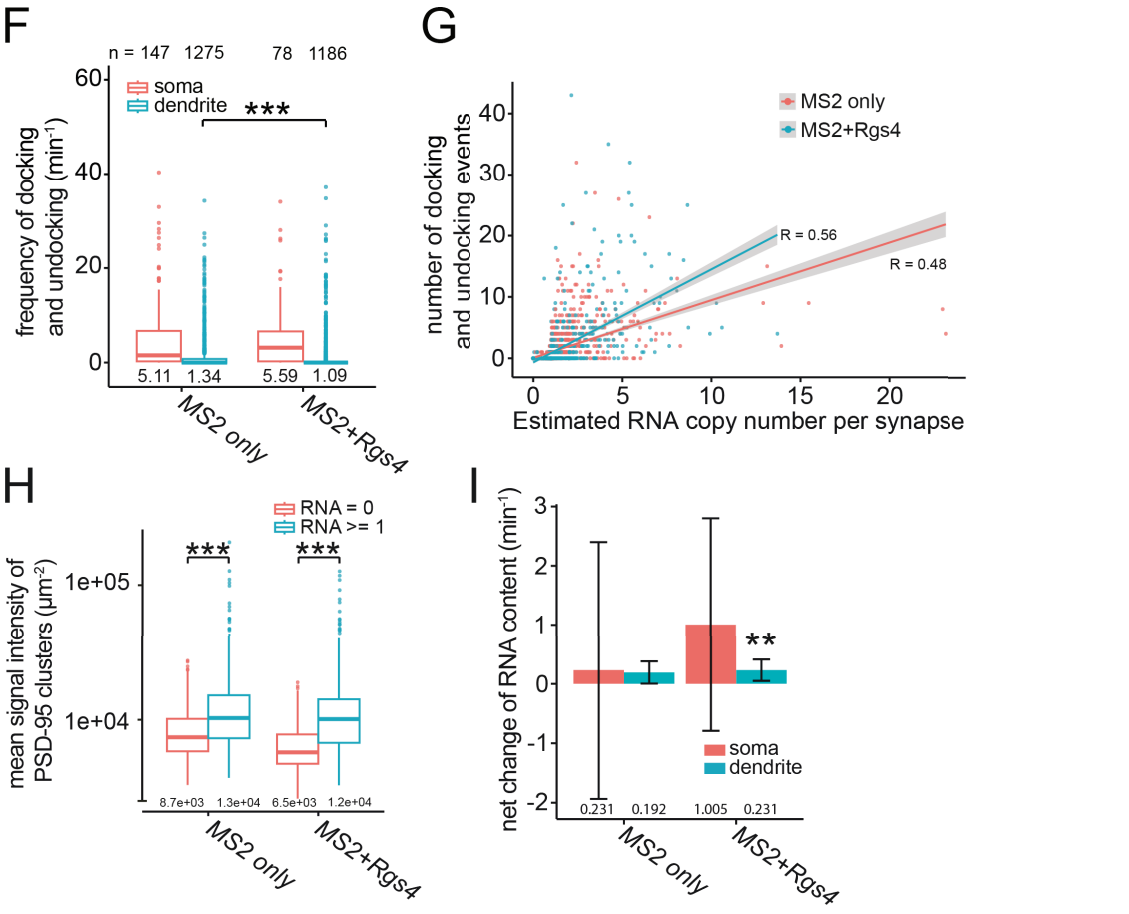

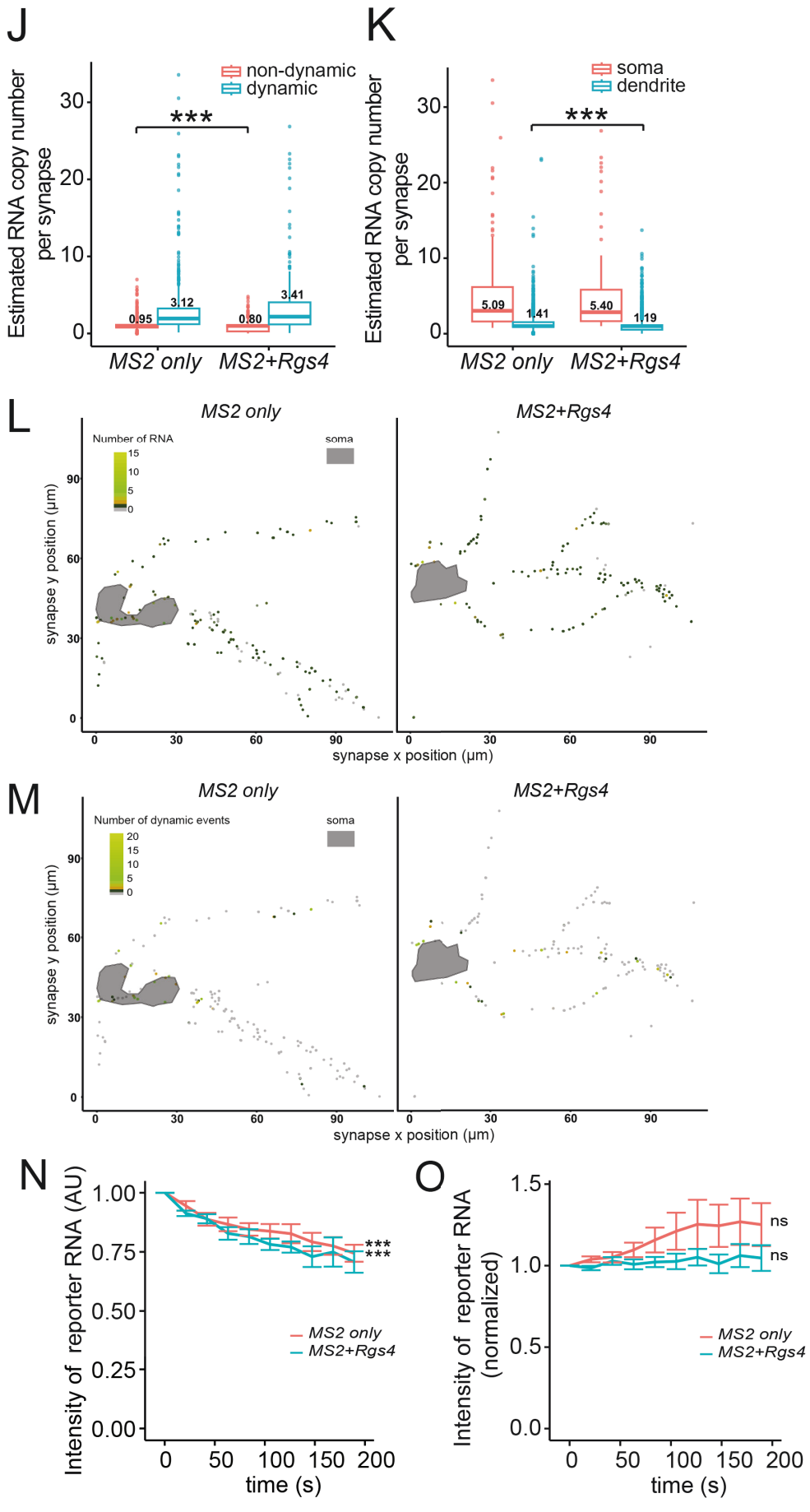
J
non-dynamic
dynamic
Estimated RNA copy number per synapse
***
0.95
3.12
0.80
3.41
MS2 only
MS2+Rgs4
K
soma
dendrite
Estimated RNA copy number per synapse
***
5.09
1.41
5.40
1.19
MS2 only
MS2+Rgs4
L
MS2 only
MS2+Rgs4
Number of RNA
soma
synapse y position (μm)
synapse x position (μm)
M
MS2 only
MS2+Rgs4
Number of dynamic events
soma
synapse y position (μm)
synapse x position (μm)
N
Intensity of reporter RNA (AU)
***
***
MS2 only
MS2+Rgs4
time (s)
O
Intensity of reporter RNA (normalized)
ns
ns
MS2 only
MS2+Rgs4
time (s)

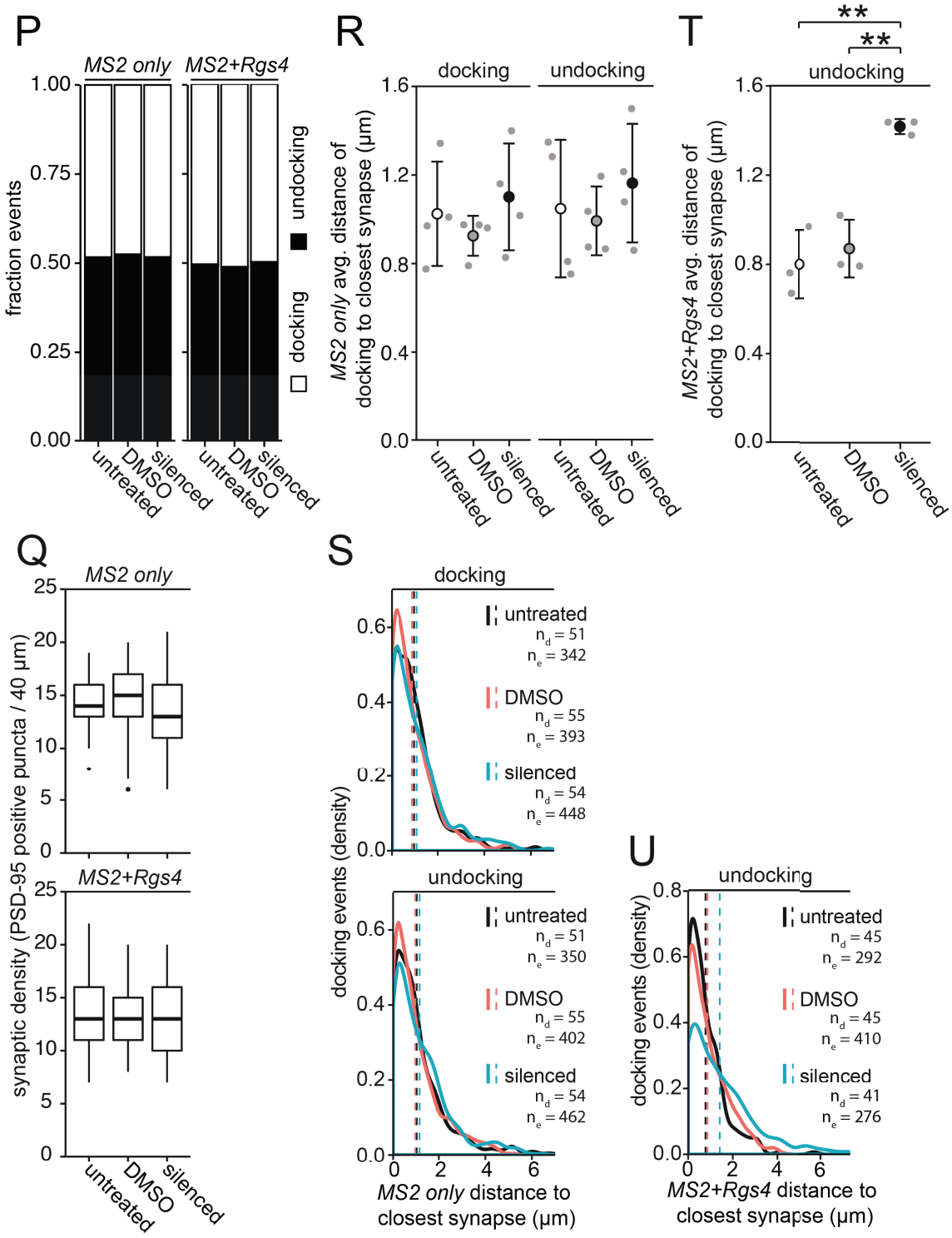
P
MS2 only
MS2+Rgs4
fraction events
1.00
0.75
0.50
0.25
0.00
undocking
docking
untreated
DMSO
silenced
R
docking
undocking
MS2 only avg. distance of docking to closest synapse (µm)
1.6
1.2
0.8
0.4
0.0
T
**
**
undocking
MS2+Rgs4 avg. distance of docking to closest synapse (µm)
Q
MS2 only
MS2+Rgs4
synaptic density (PSD-95 positive puncta / 40 µm)
25
20
15
10
5
0
S
docking
undocking
docking events (density)
untreated
n_d = 51
n_e = 342
DMSO
n_d = 55
n_e = 393
silenced
n_d = 54
n_e = 448
n_d = 51
n_e = 350
n_d = 55
n_e = 402
n_d = 54
n_e = 462
MS2 only distance to closest synapse (µm)
U
undocking
n_d = 45
n_e = 292
n_d = 45
n_e = 410
n_d = 41
n_e = 276
MS2+Rgs4 distance to closest synapse (µm)

←

Supplementary Figure 2.4: *Rgs4* 3´-UTR mRNA undergoes docking and undocking in the proximity of synapses, dependent on neuronal activity. (**A**) Boxplot displaying synaptic density measured as number of PSD-95 positive clusters per 40 µm dendritic segment in hippocampal neurons co-transfected with either *MS2 only* or *MS2+Rgs4* 3´-UTR reporters and PSD-95-TagRFPt. (**B**) Bar plot showing the fraction of docking to undocking events in *MS2 only* or *MS2+Rgs4* 3´-UTR reporter transfected hippocampal neurons. (**C,D**) Dot plot (**C**) and density plot (**D**) displaying the distance between undocking events and the closest PSD-95 positive cluster in co-transfected rat hippocampal neurons. Data displays both *MS2 only* and *MS2+Rgs4* 3´-UTR reporter mRNAs. (**E**) Distribution of dynamic (at least one docking and/or undocking event of the reporter RNA) and non-dynamic PSD-95-tagRFPt positive structures in the soma and in the dendrites. *P*-values of Chi^2 tests against the control are indicated. (**F**) Integrated frequency of the reporter docking and undocking events in somatic and dendritic synapses within one minute. Number of observations and the population mean are indicated above boxplots, respectively. (**G**) Integrated number of docking and undocking events as a function of estimated RNA copy number per synapse. Fitted lines and goodness of fit (R) are indicated. (**H**) PSD-95-TagRFPt signal intensity over synaptic area in presence or absence of RNA. (**I**) Average net change of *MS2 only* or *MS2+Rgs4* mRNA content in somatic and dendritic synapses. Numbers indicate the mean value of net RNA level change. Error bars represent the 95% confidence intervals. (**$p < 0.01$; difference compared to zero (no net flux, null hypothesis)). (**J-K**) Estimated *MS2 only* and *MS2+Rgs4* reporter mRNA copy number in dynamic or non-dynamic (**J**) and somatic or dendritic (**K**) synapses. Numbers indicate the mean value of estimated RNA levels. (**L-M**) Representative detection masks of PSD-95-RFP clusters, color-code indicating estimated mRNA content (**L**) or number of docking/undocking events (**M**) with *MS2 only* or *MS2+Rgs4* reporter mRNA. Gray areas indicate cell soma. (**N-O**) Intensity of reporter RNA (red – *MS2 only*, blue – *MS2+Rgs4*) at synapses normalized to the first frame to correct the effects of photobleaching (N). (***$p < 0.0001$) difference between the first and last data points of corresponding experiments (*MS2 only* or *MS2+Rgs4*). Photobleaching was compensated by adjusting the unit threshold in

100 frame increments (O, see also *Methods*). ns indicates non-significant ($p > 0.05$) between the first and last data points of corresponding experiments. (**P**) Bar plot showing the fraction of docking to undocking events in *MS2 only* or *MS2+Rgs4* 3´-UTR reporter transfected hippocampal neurons under untreated, vehicle (DMSO) or silenced (100 µM CNQX, 50 µM AP5, 1 µM TTX) conditions. (**Q**) Boxplots displaying synaptic density measured as number of PSD-95-RFP positive clusters per 40µm dendritic segment in hippocampal neurons co-transfected with either *MS2 only* (top) or *MS2+Rgs4* 3´-UTR (down) reporters and PSD-95-TagRFPt. (**R-U**) Dot plots (**R,T**) and density plots (**S,U**) displaying the distance between docking (R,S) or undocking (R-U) events to the closest PSD-95 positive cluster in co-transfected rat hippocampal neurons with *MS2+Rgs4* 3´-UTR reporter and PSD-95-TagRFPt, under untreated, vehicle (DMSO) and silenced (100 µM CNQX, 50 µM AP5, 1 µM TTX) conditions. Data represents mean ± standard deviation of 3-4 independent experiments in dot plots (C,R,T; individual experiments shown as gray dots). Dashed lines represent mean of individual data points (D,S,U). Asterisks represent *p*-values obtained by Student's t-test (C), Mann Whitney U (F,H, K, L, I,), or Tukey's test post-hoc to one-way ANOVA analysis (T) (** $p < 0.01$, *** $p < 0.001$). Data was obtained from 40 µm dendritic segments at a minimal distance of 20 µm from the cell body. At least 10 dendrites/condition/experiment (A-D, P-U) or 12 neurons/condition (E-O) from 3 independent biological replicates were analyzed. Total number of dendrites (n_d), events (n_e) and synapses (n) analyzed per condition are indicated.
Related to Figure 4.

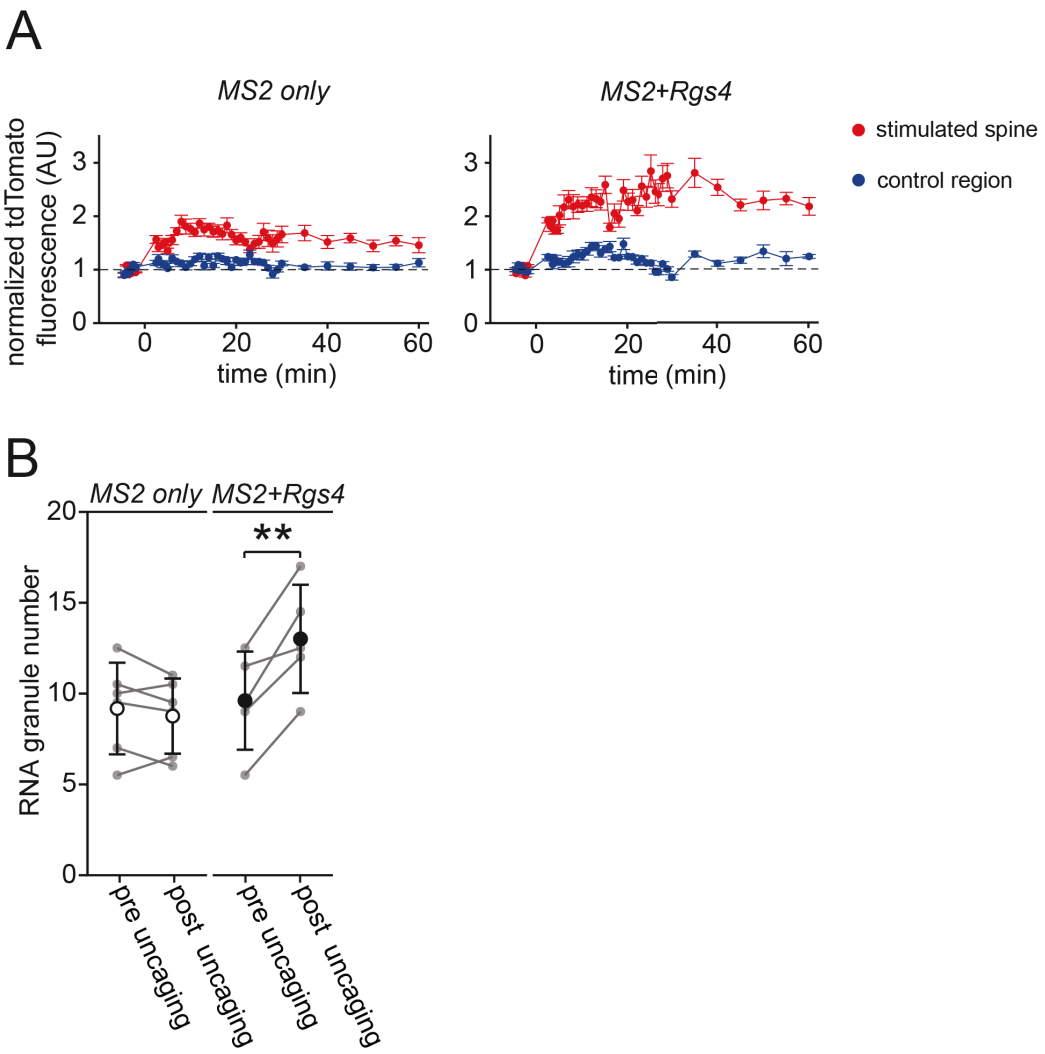

Supplementary Figure 2.5: Local Glutamate uncaging at individual dendritic spines triggers *Rgs4* 3´-UTR dependent mRNA recruitment. (**A**) Fluorescent intensity of volume marker (tdTomato) in stimulated dendritic spines (red) or control regions (adjacent to unstimulated spine or dendritic segment, blue) over time, normalized to first measurement, in neurons transfected with tdTomato, tdMCP-GFP and either *MS2 only* or *MS2+Rgs4* reporter mRNA. Data represents mean ± standard error of the mean (**B**) Dot plot displaying the number of RNA granules of *MS2 only* or *MS2+Rgs4* 3´-UTR reporter mRNAs pre (2-7 min before) and post (40-45 min after) uncaging in rat hippocampal neurons within 5 µm of the stimulated spine. Data represents mean ± standard deviation (individual neurons shown as gray dots linked by gray lines). Data was obtained from 6 dendrites (from 5 neurons of 4 biological replicates) and 5 dendrites (from 5 neurons of 5 biological replicates) for *MS2 only* and *MS2+Rgs4* reporter mRNAs respectively. Asterisks represent *p*-values obtained by paired Student's t-test (** $p < 0.01$).

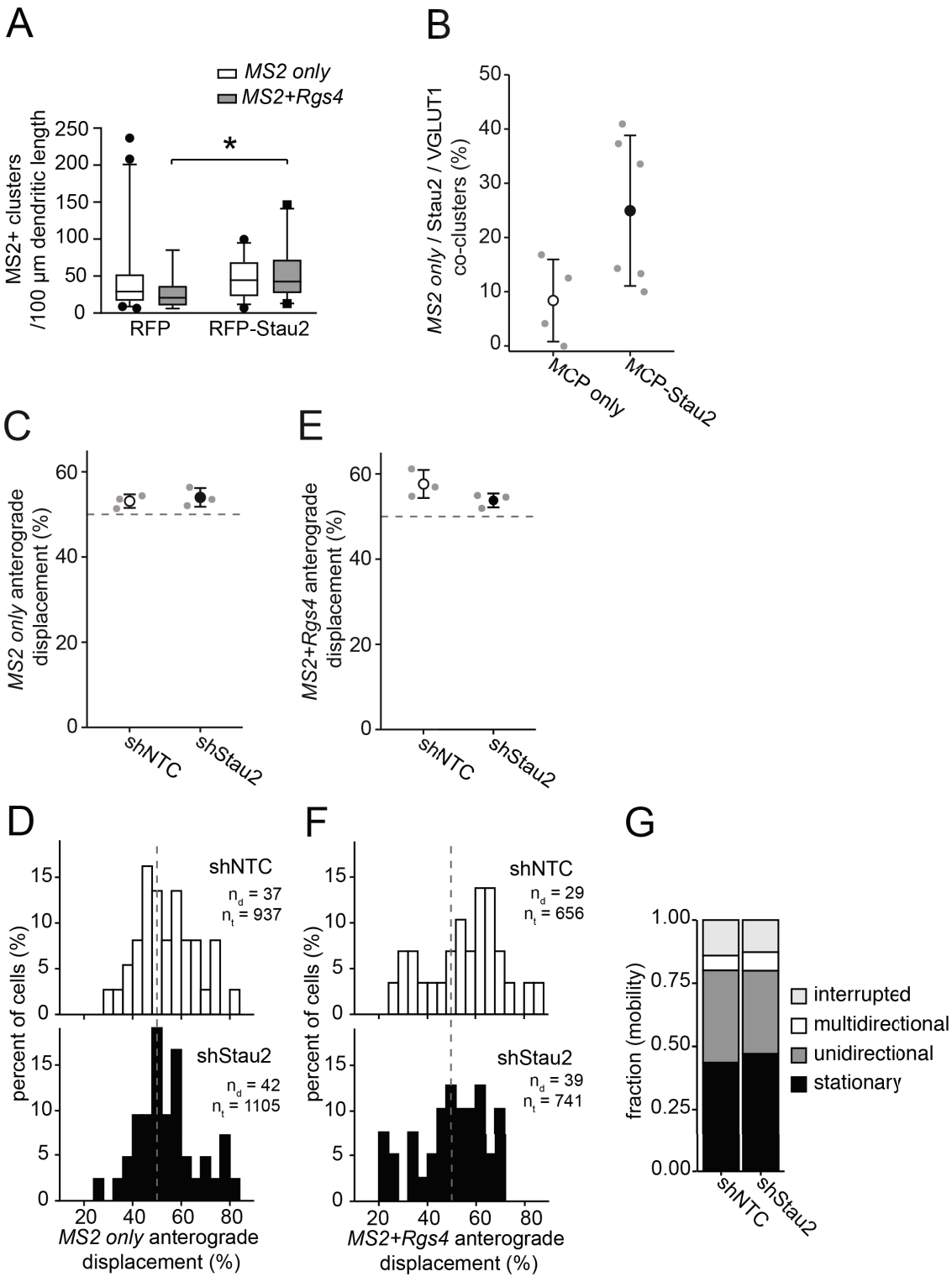
A
MS2 only
MS2+Rgs4
MS2+ clusters /100 µm dendritic length
250
200
150
100
50
0
*
RFP
RFP-Stau2
B
MS2 only / Stau2 / VGLUT1 co-clusters (%)
50
40
30
20
10
0
MCP only
MCP-Stau2
C
MS2 only anterograde displacement (%)
60
40
20
0
shNTC
shStau2
E
MS2+Rgs4 anterograde displacement (%)
60
40
20
0
shNTC
shStau2
D
percent of cells (%)
shNTC
n_d = 37
n_t = 937
shStau2
n_d = 42
n_t = 1105
15
10
5
0
20
40
60
80
MS2 only anterograde displacement (%)
F
percent of cells (%)
shNTC
n_d = 29
n_t = 656
shStau2
n_d = 39
n_t = 741
15
10
5
0
20
40
60
80
MS2+Rgs4 anterograde displacement (%)
G
fraction (mobility)
1.00
0.75
0.50
0.25
0.00
interrupted
multidirectional
unidirectional
stationary
shNTC
shStau2

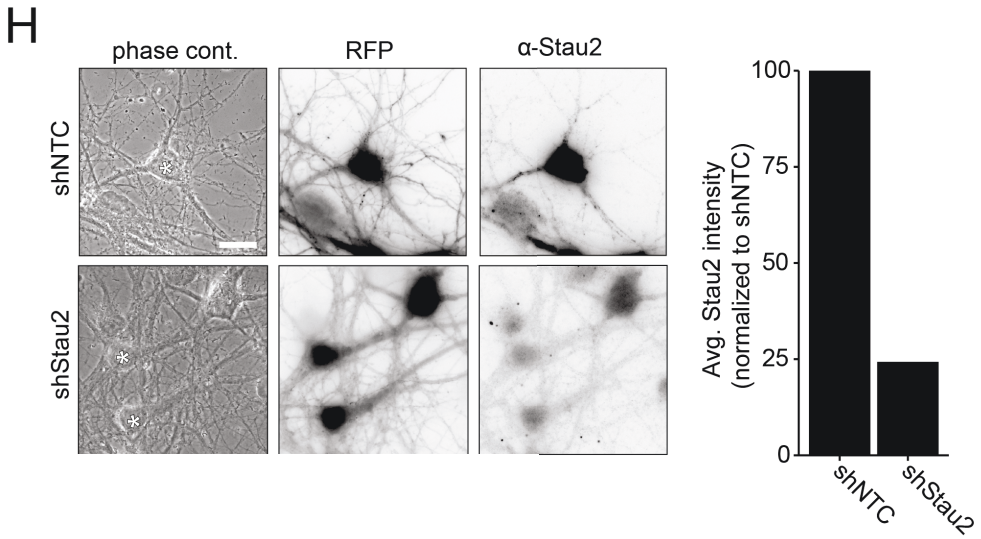

Supplementary Figure 2.6: Effects of Stau2 on *Rgs4* 3´-UTR dependent mRNA localization and transport. (**A**) Boxplot displaying number of dendritic *MS2 only* or *MS2+Rgs4* 3´-UTR reporter mRNA granules co-transfected with either RFP or RFP-Stau2. Asterisks represent *p*-values obtained by Student's t-test (* $p < 0.05$). (**B**) Dot plot displaying percent of dendritic *MS2 only* reporter mRNA granules in co-clusters with Stau2 and vesicular glutamate transporter 1 (VGLUT 1), in hippocampal neurons co-transfected with *MS2 only* mRNA, tdMCP-GFP and either tdMCP only or tdMCP-Stau2 and stained with anti-Stau2 and anti-VGLUT 1 antibodies. Data represents mean ± standard deviation (individual neurons shown as gray dots). (**C-F**) Dot plots (**C,E**) and histograms (**D,F**) displaying the percentage of total anterograde travel distance of *MS2 only* or *MS2+Rgs4* 3´-UTR reporter mRNA granules in shNTC and shStau2 transduced hippocampal neurons. NTC = non-targeting control. Data represents mean ± standard deviation of three independent experiments (individual experiments shown as gray dots). Data was obtained from 40 µm dendritic segments at a minimal distance of 20 µm from the cell body. Only displacements ≥ 1.5 µm were considered for analysis. (**G**) Quantification of relative transport dynamics of *MS2+Rgs4* 3´-UTR reporter mRNA in shNTC and shStau2 transduced neurons, in 1 minute time-series acquisitions. (**H**) Representative neurons transduced with either shNTC or shStau2 lentiviral particles and transfected with *MS2+Rgs4* 3´-UTR reporter and MCP-GFP, were fixed after imaging and stained with anti-Stau2 antibodies (left). Relative Stau2 intensity quantification (right) in rat hippocampal neurons 5 days after viral transduction with either shNTC or shStau2 lentiviral particles. Asterisks denote MCP-GFP positive cells. Scale bar 10 µm. Related to Figure 5.

Movie 2.1: Representative time-lapse movie of *MS2+Rgs4* 3´-UTR reporter mRNA granules moving at different speed (arrowheads) in a dendrite of a 15 DIV hippocampal neuron. Green arrowheads indicate anterograde movement. Playback speed 2x real time. Scale bar 10 µm. Related to Fig. 1C.

Movie 2.2: Representative time-lapse movie of *MS2+Rgs4* 3´-UTR reporter mRNA granules moving different displacement lengths (arrowheads) in a dendrite of a 14 DIV hippocampal neuron. Red arrowheads indicate retrograde movement. Playback speed 2x real time. Scale bar 10 µm. Related to Fig. 1D.

Movie 2.3: Representative time-lapse movie of *MS2+Rgs4* 3´-UTR reporter mRNA granules moving in different directions (arrowheads) in a dendrite of a 15 DIV hippocampal neuron. Green arrowhead indicates anterograde movement, red arrowhead indicates retrograde movement. Playback speed 2x real time. Scale bar 10 µm. Related to Fig. 1E.

Movie 2.4: Representative time-lapse movie of an *MS2+Rgs4* 3´-UTR reporter mRNA granule interrupting movement (arrowhead) in a dendrite of a 15 DIV hippocampal neuron. Playback speed 2x real time. Scale bar 10 µm. Related to Fig. 1F.

Movie 2.5: Representative time-lapse movie of an *MS2+Rgs4* 3´-UTR reporter mRNA granule moving in an uninterrupted multidirectional fashion (arrowhead) in a dendrite of a 14 DIV hippocampal neuron. Playback speed 2x real time. Scale bar 10 µm. Related to Fig. 1G.

Movie 2.6: Representative time-lapse movie of an *MS2+Rgs4* 3´-UTR reporter mRNA granule moving in an uninterrupted multidirectional fashion (arrowhead) in a dendrite of a 14 DIV hippocampal neuron. Playback speed 4x real time. Scale bar 10 µm. Related to Fig. 1.

Movie 2.7: Representative time-lapse movie of an *MS2+Rgs4* 3´-UTR reporter mRNA granule moving in a multidirectional fashion between dendrites at a branching point (arrowhead) in a 12 DIV hippocampal neuron. Playback speed 2x real time. Scale bar 10 µm. Related to Fig. 1.

Movie 2.8: Representative time-lapse movie of *MS2+Rgs4* 3´-UTR reporter mRNA granules moving in different directions (arrowheads) in a dendrite of a 14 DIV hippocampal neuron. Green arrowhead indicates anterograde movement, red arrowheads indicate retrograde movement. Playback speed 2x real time. Scale bar 10 µm. Related to Fig. 2A-C.

Movie 2.9: Representative time-lapse movie of an *MS2+Rgs4* 3´-UTR reporter mRNA granule (green fluorescence and arrowhead) moving to a PSD-95-TagRFPt positive cluster (magenta fluorescence and arrowhead) in a dendrite of a 15 DIV hippocampal neuron. Playback speed 2x real time. Scale bar 10 µm. Related to Fig. 4A.

Movie 2.10: Representative time-lapse movie of an *MS2+Rgs4* 3´-UTR reporter mRNA granule (green fluorescence and arrowhead) moving to a PSD-95-TagRFPt positive cluster (magenta fluorescence and arrowhead) in a dendrite of a 15 DIV hippocampal neuron. Playback speed 2x real time. Scale bar 10 µm. Related to Fig. 4.

Movie 2.11: Representative time-lapse movie of *MS2+Rgs4* 3´-UTR reporter mRNA granules in a dendrite of an 18 DIV hippocampal neuron upon glutamate uncaging. Green arrowheads indicate examples of GFP positive *MS2+Rgs4* 3´-UTR reporter mRNA granules, red dot indicates uncaging spot. Playback pre uncaging indicated by negative time, playback post uncaging indicated by positive time. Playback speed variable (increased over time). Scale bar 5 µm. Related to Fig. 5.

Movie 2.12: Representative time-lapse movie of an *MS2+Rgs4* 3´-UTR reporter mRNA (green fluorescence and arrowhead) and TagRFPt-Stau2 (magenta fluorescence and arrowhead) positive RNA granule undergoing co-transport in a dendrite of a 15 DIV hippocampal neuron. Playback speed 2x real time. Scale bar 10 µm. Related to Fig. 6A.

Movie 2.13: Representative time-lapse movie of an *MS2+Rgs4* 3´-UTR reporter mRNA (green fluorescence and arrowhead) and TagRFPt-Stau2 (magenta fluorescence and arrowhead) positive RNA granule undergoing co-transport in a dendrite of a 15 DIV hippocampal neuron. Playback speed 2x real time. Scale bar 10 µm. Related to Fig. 6.

3. Manuscript 2:

Neuronal activity governs Rck granule size during maturation of hippocampal neurons in culture

Karl E Bauer[1], Inmaculada Segura[1], Saskia Hutten[1], and Michael A Kiebler[1]*

[1] BioMedical Center, Dept. Cell Biology and Anatomy, Medical Faculty, Ludwig Maximilians University, Großhaderner Str. 9, 82152 Planegg-Martinsried, Germany

* Correspondence: mkiebler@lmu.de (MAK)

No. of Figures: **5 Figures**
4 Supplementary Figures

Running title: Localization of Rck in maturing neurons

Key words: Rck, DDX6, p54, p-body, protein localization, neuronal activity, protein assembly, RNA-binding, RNA-degradation

Author contribution: Dr. Inmaculada Segura performed experiments relevant to Supplementary Fig. 3.1B and Supplementry Fig. 3.3A. Dr. Saskia Hutten provided independent analysis of experiments relevant to Figure 3.1B.

3.1 Abstract

The assembly and disassembly of RNA granules is suggested to be a key mechanism by which various cellular processes are regulated, including the morphology and function of neurons. Here we showed that neuronal P-bodies, containing the RNA-helicase Rck, changed in morphology during neuronal maturation in culture. Rck granules in the soma of hippocampal neurons were prominent in early stages of development (8 day *in vitro*, DIV), but disassembled and reduced in size during maturation (22-29 DIV). This change in granule morphology was dependent on synaptic activity, as neuronal inhibition led to the formation of prominent P-body structures, while N-Methyl-D-Aspartate (NMDA) receptor activation resulted in their quick dispersal. However, the dispersal of P-bodies induced by the stalling of ribosomes with cycloheximide was not affected by neuronal signaling, suggesting that neuronal maturation and ribosome stalling induce P-body dispersal by different mechanisms. Moreover, the depletion of the RNA-binding protein Staufen2, which localizes with Rck-containing RNA granules, had no effect on P-body morphology. Finally, the expression of a dominant negative RNA-helicase Rck mutant (E247Q) had a diffuse cytoplasmic localization, but did not result in the complete disassembly of P-bodies, suggesting that either Rck or its helicase activity were not required for morphological P-body maintenance. This diffuse localization pattern could not be rescued by neuronal inhibition, indicating that helicase activity acts upstream of neuronal signaling. Taken together, this data provides a unique insight into the mechanisms of neuronal P-body assembly, dependent on cellular maturation, synaptic activity and Rck helicase activity. Moreover, this study provides the basis for further research into the assembly of different types of neuronal RNA granules. The data presented here suggests that P-bodies might be uniquely regulated in neurons, which would have significant impact on synaptic plasticity and the processes of learning and memory formation.

3.2 Introduction

The subcellular localization of RNA-binding proteins (RBPs) is a key factor in the spatial regulation of mRNA translation. By binding to specific *cis*-acting elements within the 3´-UTR of mRNAs, RBPs form ribonucleoprotein particles (RNPs), also termed neuronal RNA granules (Kiebler and Bassell, 2006). These RNPs can exert various functions and show distinct localization patterns. Moreover, RNPs are dynamic in their composition and can assemble or disassemble, dependent on specific cellular cues, such as neuronal activity or stress. Thereby, they govern mRNA metabolism through the regulation of post-transcriptional gene expression, *e.g*. mRNA splicing, nuclear export, transport, translation and degradation (Fernandez-Moya et al., 2014; Hentze et al., 2018; Hutten et al., 2014).

One well-studied subtype of a cytoplasmic RNP is the processing body (P-body), also referred to as GW- (Glycine-Tryptophan) or DCP- (mRNA decapping enzyme) body. P-bodies appear as large, distinct, cytoplasmic granules and are sites of mRNA storage, degradation and translation control (Cougot et al., 2004; Hubstenberger et al., 2017; Liu et al., 2005; Sheth and Parker, 2003). Moreover, they have been implicated in mRNA degradation by the regulation of microRNAs (Jakymiw et al., 2007; Lian et al., 2006; Parker and Sheth, 2007). They contain (i) components of the mRNA decay machinery, (ii) translational regulators and (iii) components of the RNA-induced silencing complex (RISC) (Behm-Ansmant et al., 2006; Chu and Rana, 2006; Ding et al., 2005; Liu et al., 2005; Parker and Sheth, 2007). Therefore, P-bodies have a key role in regulating the degradation and translational activity of mRNAs. In neurons, these functions are crucial for neuronal development and synaptic plasticity (Ashraf et al., 2006; Schratt et al., 2006). Indeed, the P-body component Rck (also known as Dead box helicase 6 or DDX6) is required for translationally regulated dendrite morphogenesis in *Drosophila* (Barbee et al., 2006). Previous research has shown that P-bodies are localized in dendrites of rat hippocampal neurons and that chemical stimulation of neuronal activity results in a reduction in dendritically localized P-bodies (Vessey et al., 2006; Zeitelhofer et al., 2008). These dendritic P-bodies are distinct from transport mRNPs and are not co-transported with them. However, the frequent observation of docking events between the P-body marker Decapping mRNA 1 (DCP1) and the mRNP marker Staufen2

(Stau2) suggest an interaction between these two subtypes of RNA-carrying granules. Moreover, the dendritic P-bodies marked Rck have been shown to associate with ribosomes (Elvira et al., 2006).

We have recently identified Rck, a core P-body protein, as a component of neuronal Stau2 transport granules (Fritzsche et al., 2013), indicating a function for Rck outside of P-bodies. Additionally, the 3´-UTR of *Rck* mRNA contains *in vivo* cross-linking sites for Stau2 (Sharangdhar et al., 2017). Rck is an ATP-dependent RNA helicase involved in mRNA decapping during mRNA decay, as well as in translational control (Fenger-Gron et al., 2005; Ladomery et al., 1997). This helicase has a key function in the formation of P-bodies, by binding to Protein Associated with Topoisomerase II Homolog 1 (Pat1b) (Ozgur and Stoecklin, 2013; Serman et al., 2007), and by the recruitment of RNA degradation factors (Andrei et al., 2005). Other neuronal RNPs, such as Staufen and FMRP granules in *Drosophila* have been shown to contain P-body components as well (Barbee et al., 2006). Moreover, Stau2 has been implicated in multiple aspects of mRNA metabolism, including the regulation of mRNA transport, stability and translation, raising the possibility that neuronal transport granules work in conjunction with P-body components to achieve translational control (Heraud-Farlow et al., 2013; Sharangdhar et al., 2017).

In the current study, we investigated the subcellular localization of Rck in maturing neurons, and addressed the question, which cellular processes can lead to alterations in its localization and disassembly from P-bodies.

3.3 Results

3.3.1 Somatic Rck granules partially disassemble during hippocampal neuronal maturation in culture

To investigate whether the subcellular sorting of Rck changes during neuronal maturation, we evaluated Rck localization in rat primary hippocampal neurons that were isolated from E17 rat brains and were kept in culture up to 29 days. Neurons were allowed to mature in culture, fixed at different time points during maturation (8, 14, 22 and 29 days *in vitro*, DIV) and immunostained for Rck (**Fig. 3.1A**). We were able to detect Rck expression at all time points analyzed, however, the pattern of Rck localization varied between the different developmental stages. A striking observation was that both neurons with large or small somatic Rck granules were present during maturation. These somatic Rck granules, which resemble P-bodies were reduced in size, but appeared in higher number in more mature neurons (22 and 29 DIV). This observation was quantified by assessing the percentage of neurons that contained large or small Rck granules in the total population. We found that in young neurons (8 DIV) nearly the entire population contained large Rck granules in the soma (**Fig. 3.1B**). However, in mature neurons (29 DIV) the large majority of the population lacked these large granules, in favor of smaller clusters (Student's t-test, p = 6.113e-05). Interestingly, intermediate time points during maturation (14 DIV and 22 DIV) contained more mixed P-body populations with both neurons containing large or small Rck granules in the soma (**Supplementary Fig. 3.1A**; $F_{3,8}$ = 0.0044), suggesting a gradual transition from neurons with large to small somatic Rck granules during maturation. To assess whether the observed phenotype might be associated with a change in Rck protein levels during maturation, we collected neuronal protein lysates at different time points during maturation in culture and analyzed these samples by Western blot. Overall, Rck protein levels showed a modest decline in cortical neurons during maturation (**Supplementary Fig. 3.1B**). Therefore, it cannot be excluded that the change in Rck granules size might be exaggerated by a reduction in intracellular protein concentration, in addition to a change in localization. To confirm that the observed Rck granules belonged to the

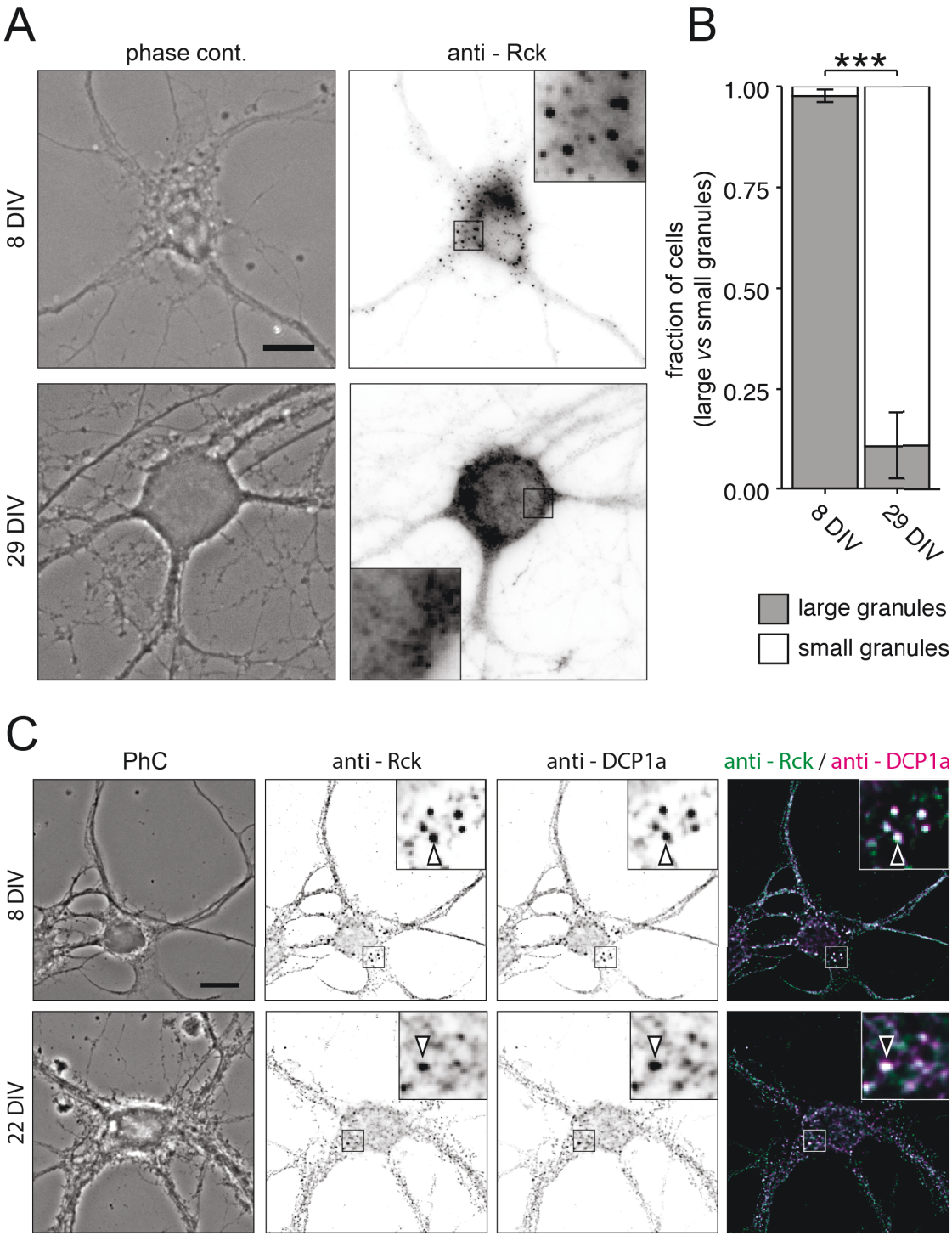
A
phase cont.
anti - Rck
8 DIV
29 DIV
B
***
1.00
0.75
0.50
0.25
0.00
fraction of cells
(large vs small granules)
8 DIV
29 DIV
large granules
small granules
C
PhC
anti - Rck
anti - DCP1a
anti - Rck / anti - DCP1a
8 DIV
22 DIV

←

Figure 3.1: Cytoplasmic Rck granules disassemble during neuronal maturation in culture. **(A)** Representative examples of phase contrast (PC) and Rck immunostaining of 8 days *in vitro* (DIV) and 29 DIV hippocampal neurons in culture. **(B)** Bar plot displaying quantification of cell population by fraction of cells containing either large or small Rck granules as exemplified in (A), at 8 and 29 DIV, respectively. Data represents mean ± standard deviation of three independent experiments. Asterisks represent p-values obtained by Student's t-test (*** $p < 0.001$). At least 100 cells/condition/experiment were quantified. **(C)** Representative examples of phase contrast, Rck and DCP1a immunostaining and overlay of 8 DIV or 22 DIV hippocampal neurons in culture. Fluorescent images in (C) were deconvolved to assess overlap. Boxed regions in images are displayed as magnified insets. Arrowhead indicates colocalization. Scale bars 10 µm (A,C).

population of P-bodies, we performed co-immunostainings with a second P-body marker, such as DCP1a, which has been previously shown to interact with Rck in yeast (Coller et al., 2001). Indeed, DCP1a localized in distinct cytoplasmic granules that overlapped with Rck granules (**Fig. 3.1C**). In contrast, Rck granules only partially overlapped with cytoplasmic Polyadenylate-binding protein 1 (PABP1) granules, a protein reported to be involved in translation initiation as well as mRNA decay (**Supplementary Fig. 3.1C**) (Behm-Ansmant et al., 2007; Derry et al., 2006; Gray et al., 2000).

Taken together, neuronal maturation causes a significant alteration in somatic Rck localization, showing a shift in the ratio of neuronal population from cells with large granules to cells with small granules.

3.3.2 Somatic Rck granules in mature neurons reversibly reassemble after inhibition of neuronal activity

As neuronal maturation progresses together with synaptic development and an increase in neuronal signaling activity, we evaluated whether these processes may lead to the observed reduction in Rck granule size in mature neurons. To test this hypothesis we investigated mature neurons (22 DIV), where a majority of the neuronal population contained small Rck granules in the soma, and silenced neuronal activity by simultaneously inhibiting AMPA receptors, NMDA receptors and sodium channels via combined bath application of CNQX, AP5 and TTX, respectively (Sharangdhar et al., 2017). The inhibition of neuronal activity resulted in the reassembly of large Rck granules in the soma of these neurons, resulting in a shift of approximately 45 percent in the neuronal population (**Fig. 3.2A-B**; Student's t-test, p = 0.0001). P-bodies are known to have overlapping components with stress granules (Decker and Parker, 2012; Youn et al., 2018). Both proteins and mRNAs are dynamically exchanged between P-bodies and stress granules (Kedersha et al., 2005; Mollet et al., 2008). Importantly, the large Rck granules induced by neuronal silencing were not stress granules, as assessed by co-immunostaining with the stress granule marker G3BP (**Supplementary Fig. 3.2A**) and remained associated with DCP1a (*data not shown*). The size of large Rck granules observed in young neurons (8 DIV) was not affected by neuronal inhibition (*data not shown*). Furthermore, the reassembly of large Rck granules in mature neurons (22 DIV) was quickly reversible by 15 min wash off of the CNQX/AP5/TTX mix (p = 0.028) or was even opposed by a short wash off and 15 min stimulation by 100 µM NMDA (p < 0.0000001 for untreated *vs* NMDA, p = 0.00001 for recovery *vs* NMDA) (**Fig. 3.2C**; $F_{2,22}$ = 1.59e-05; $F_{2,22}$ = 2.38e-11). Indeed, stimulation by NMDA induced the disassembly of large Rck granules independent of the prior treatment, resulting in small Rck granules in the large majority of the population, as observed in more mature neurons. These findings suggest that neuronal activity via the activation of NMDA-receptors could regulate the disassembly of Rck granules. Vehicle treatment had no effect in any of the conditions.

Together, these findings suggest that changes in neuronal activity in mature neurons can lead to the accumulation of Rck in large somatic granules, as observed in developing neurons (8 DIV), an effect that is quickly reversible by reinstating endogenous neuronal signaling.

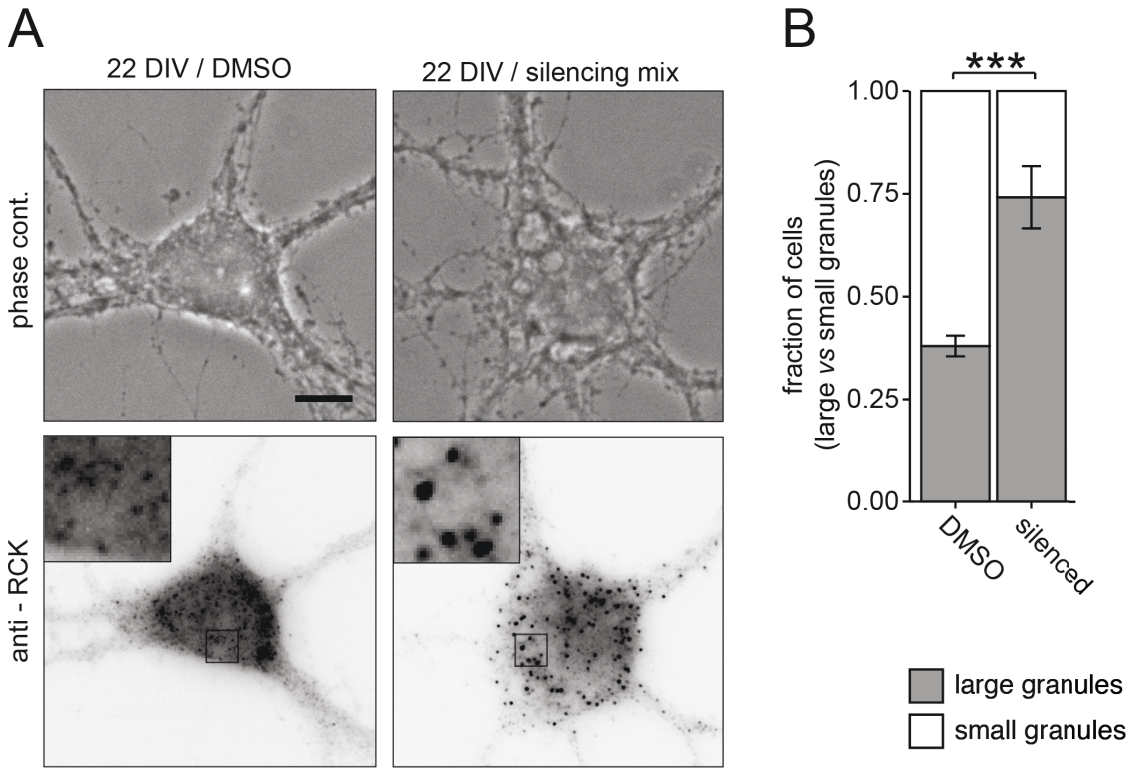
A
22 DIV / DMSO
22 DIV / silencing mix
phase cont.
anti - RCK
B
***
1.00
0.75
0.50
0.25
0.00
fraction of cells
(large vs small granules)
DMSO
silenced
large granules
small granules

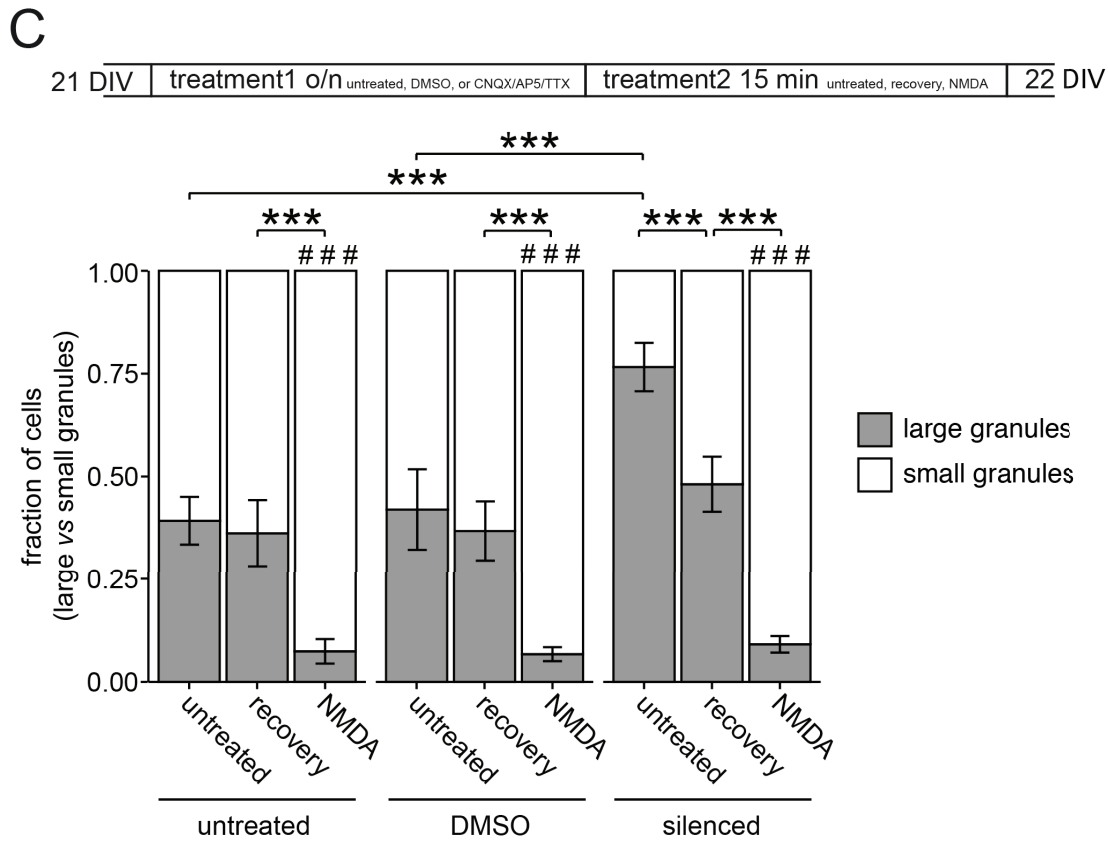
C
21 DIV
treatment1 o/n untreated, DMSO, or CNQX/AP5/TTX
treatment2 15 min untreated, recovery, NMDA
22 DIV
***
***
***
***
***
***
###
###
###
1.00
0.75
0.50
0.25
0.00
fraction of cells
(large vs small granules)
untreated
recovery
NMDA
untreated
recovery
NMDA
untreated
recovery
NMDA
untreated
DMSO
silenced
large granules
small granules

←

Figure 3.2: Chemical inhibition of neuronal activity results in the reassembly of large cytoplasmic Rck granules. **(A)** Representative examples of phase contrast (PC) and Rck immunostaining of 22 DIV hippocampal neurons in culture under vehicle (DMSO) treated or silenced (100µM CNQX, 50µM AP5, 1µM TTX) conditions, immunostained for Rck. Boxed regions in images are displayed as magnified insets. Scale bar 10 µm. **(B-C)** Bar plots displaying quantification of cell population by fraction of cells containing either large or small Rck granules as exemplified in (A) under untreated, vehicle treated or silenced conditions (B-C), followed by recovery or NMDA treatment (C). Data represents mean ± standard deviation of three independent experiments. Asterisks represent *p*-values obtained by Student's t-test (B) or Tukey's test post-hoc to one- or two-way ANOVA analysis (C-D) (*** $p < 0.001$). Hashtags represent *p*-values obtained by Tukey's test compared to untreated conditions (C-D) (### $p < 0.001$). At least 100 cells/condition/experiment were quantified.

3.3.3 Translation activity control Rck granule size upstream of neuronal activity

It has previously been shown that short treatment with the translation inhibitor cycloheximide (CHX) leads to the disassembly of P-bodies (Cougot et al., 2004; Eulalio et al., 2007; Sheth and Parker, 2003), similar to the effect we observed during neuronal maturation for Rck. To evaluate whether CHX treatment was able to induce the disassembly of Rck as well, we incubated mature neurons (22 DIV) with 7 µM CHX for 4 hours. Here, we found a drastic reduction in somatic Rck granules size (*data not shown*). We next tested whether the inhibition of synaptic transmission, which led to the formation of large Rck granules, could inhibit the disassembly of Rck granules in response to CHX in neurons. We inhibited neuronal activity by application of the CNQX/AP5/TTX mix over night and followed up by a 4 h incubation of these

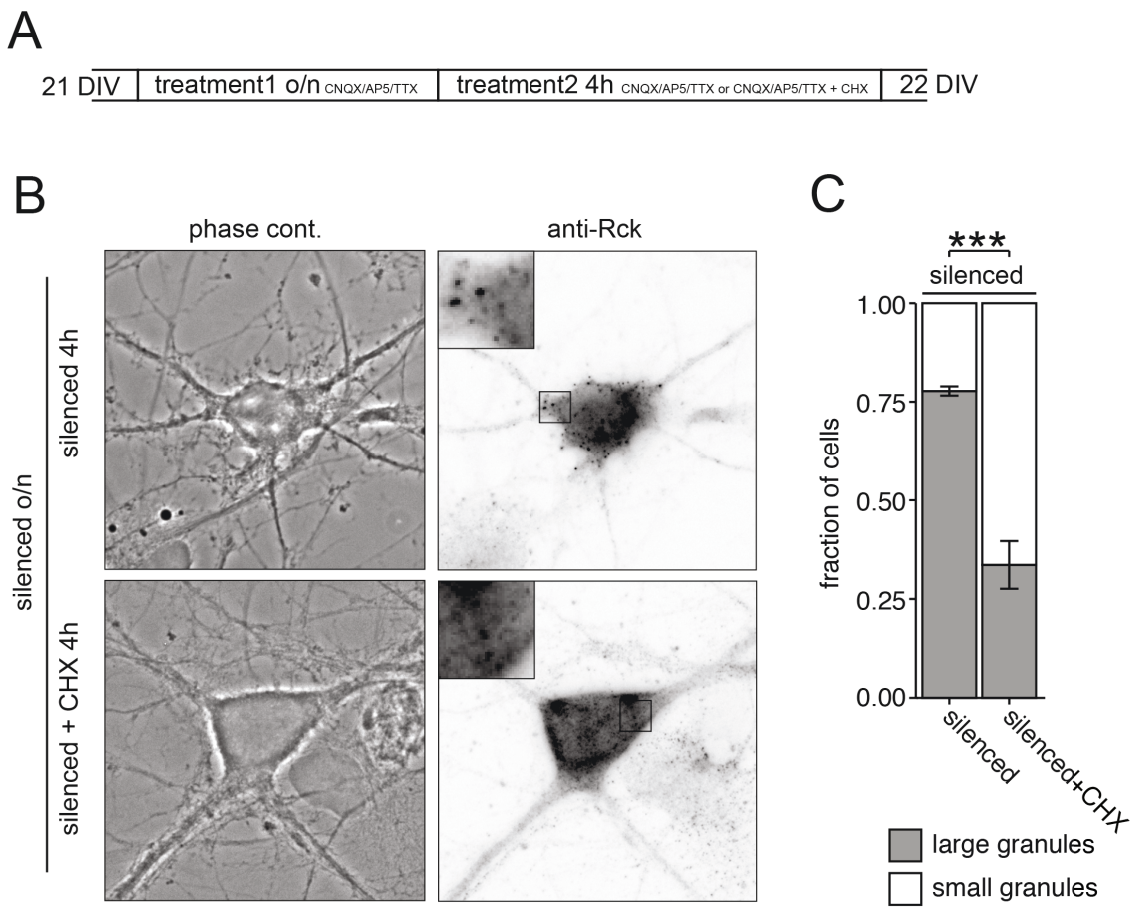

Figure 3.3: Chemical inhibition of neuronal activity does not counteract the disassembly of large cytoplasmic Rck granules upon cycloheximide treatment. **(A)** Experimental outline. **(B)** Representative examples of phase contrast and Rck immunostaining of 22 DIV hippocampal neurons in culture under vehicle treated or silenced (100µM CNQX, 50µM AP5, 1µM TTX) conditions, followed by 4h additional silencing or silencing + CHX. Abbreviations: CHX= cycloheximide. Boxed regions in images are displayed as magnified insets. Scale bars 10 µm. **(C)** Bar plot displaying quantification of cell population by fraction of cells containing either large or small Rck granules as exemplified in (A). Data represents mean ± standard deviation of three independent experiments. Asterisks represent p-values obtained by Student's t-test (B) (*** $p < 0.001$). At least 100 cells/condition/experiment were quantified.

cells with a new batch of the CNQX/AP5/TTX mix and 7 µM CHX (**Fig. 3.3A-C**; $F_{2,5}$ = 0.0002). As previously observed, the inhibition of neuronal activity resulted in the formation of large Rck granules in the soma. However, the prior inhibition of neuronal activity had no effect on the disassembly of Rck granules by CHX (p = 0.0003 for untreated *vs* silenced + CHX, p = 0.0005 for silenced *vs* silenced + CHX).

This data confirms that P-body disassembly by CHX is independent of signaling activity in neurons.

3.3.4 Disassembly of Rck granules in mature neurons is independent of Stau2

Previous research has shown that the knock-down of the RBP Stau2 leads to aberrant dendritic spine morphology and changes in electrophysiology (Berger et al., 2017; Goetze et al., 2006). Additionally, a role in neurogenesis and neuronal maturation has been attributed to Stau2 (Heraud-Farlow et al., 2013). We have previously identified Rck as a component of neuronal Stau2 granules and reported *in vivo* cross-linking sites for Stau2 in the 3´-UTR of *Rck* mRNA (Fritzsche et al., 2013; Sharangdhar et al., 2017). Therefore, we next asked whether depletion of Stau2 might result in a similar phenotype for somatic Rck granules as neuronal inhibition. As Rck displayed an age dependent phenotype during maturation in neuronal cell culture, we made use of a transgenic rat line that expressed a siRNA for Stau2 and the green fluorescent protein (GFP) under the ubiquitous P-CAG promoter (Berger et al., 2017). E17 rat hippocampal cell cultures were prepared from mixed GFP positive and negative embryos, resulting in a mixed culture containing both Stau2 deficient and Stau2 *wild type* neurons. Neurons were allowed to mature in culture, fixed at different time points and immunostained for Rck (**Fig. 3.4A**). We found no differences in Rck granule size when comparing *wild type* to knock-down neurons at any of the time points. In addition, Rck localization was not significantly altered in cryosections of 3-month-old Stau2 deficient rats, compared to *wild type* littermates (**Supplementary Fig. 3.3A**).

This data indicates that Stau2 levels do not affect Rck granule size during neuronal maturation, or the general Rck distribution throughout the brain.

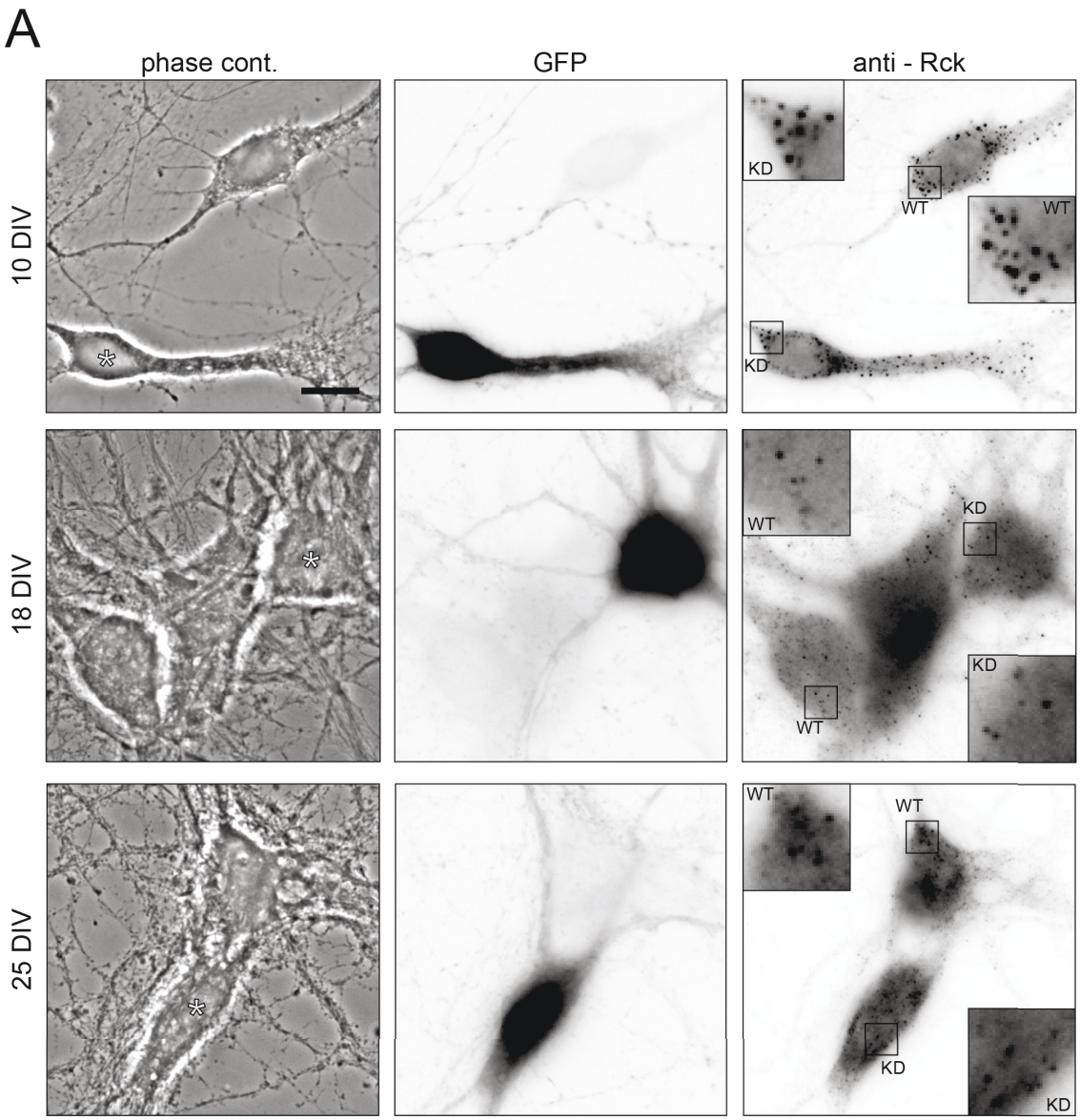

Figure 3.4: Knock-down of Stau2 does not affect the assembly of Rck granules. (**A**) Representative examples of phase contrast, GFP fluorescence (labeling Stau2-knock-down cells) and Rck immunostaining of 10 DIV, 18 DIV and 25 DIV hippocampal neurons in mixed culture from wild type and Stau2 knock-down E17 rat embryos. Neurons from Stau2 knock-down embryos are reported by GFP (denoted by asterisks in PC). Boxed regions in images are displayed as magnified insets. WT indicates wild type, KD indicates Stau2 knock-down neurons. Scale bar 10 µm.

3.3.5 The expression of a helicase deficient Rck mutant disrupts endogenous Rck granules independent of neuronal inhibition in mature neurons

The Rck protein is an ATP-dependent RNA helicase (Akao et al., 2003). A previous publication has shown that the introduction of a point mutation causing a change in the amino acid sequence from glutamic acid to glutamine (E247Q), which leads to a loss of helicase activity, results in diffuse mislocalization of the protein in FT3-7 cells, a clonal derivate of the Huh-7 cell line (Jangra et al., 2010). As this diffuse localization may give insight into the disassembly of Rck from larger granules, we generated expression vectors with C-terminally GFP-tagged Rck carrying the point mutation (termed Rck-E247Q) or *wild type* Rck (Rck-wt) as control. These vectors were transiently transfected in hippocampal neurons and expressed overnight. Rck-wt localized in large granules in the soma and proximal dendrites, comparable to the localization of the endogenous protein (**Fig. 3.5A**, top panels). Live imaging of these granules demonstrated that they moved in a restricted diffusive manner over short distances in the cell's soma, and were able to fuse or split (**movie 3.1**). In contrast, Rck-E247Q did not localize in granules, but was diffuse and present throughout the cell (**Fig. 3.5A**, bottom panels). In addition, the expression of Rck-E247Q had a dominant effect on the endogenous Rck protein, leading to a diffuse mislocalization of endogenous Rck as well. Inhibiting neuronal activity, did not affect the localization of either this mutant or endogenous Rck in neurons co-expressing Rck-E247Q (**Supplementary Fig. 3.4A**). Next, we asked the question whether this mislocalization of Rck caused by the expression of Rck-E247Q might have an effect on other P-body components. Therefore, we tested the localization of DCP1a and PABP under these conditions. We found that Rck-wt localized with DCP1a in cytoplasmic granules (**Fig. 3.5B**, top panel). Importantly, upon expression of Rck-E247Q, DCP1a retained its granular structure (**Fig. 3.5B**, bottom panel), as did PABP (**Supplementary Fig. 3.4B**).

Interestingly, the mutation in the helicase domain of Rck affects the localization pattern of endogenous Rck, but not endogenous DCP1a, indicating it does not disrupt P-bodies entirely. Together, these findings confirmed that the Rck-E247Q mutant displayed the same diffuse localization in neurons as previously show in the FT3-7 cell line.

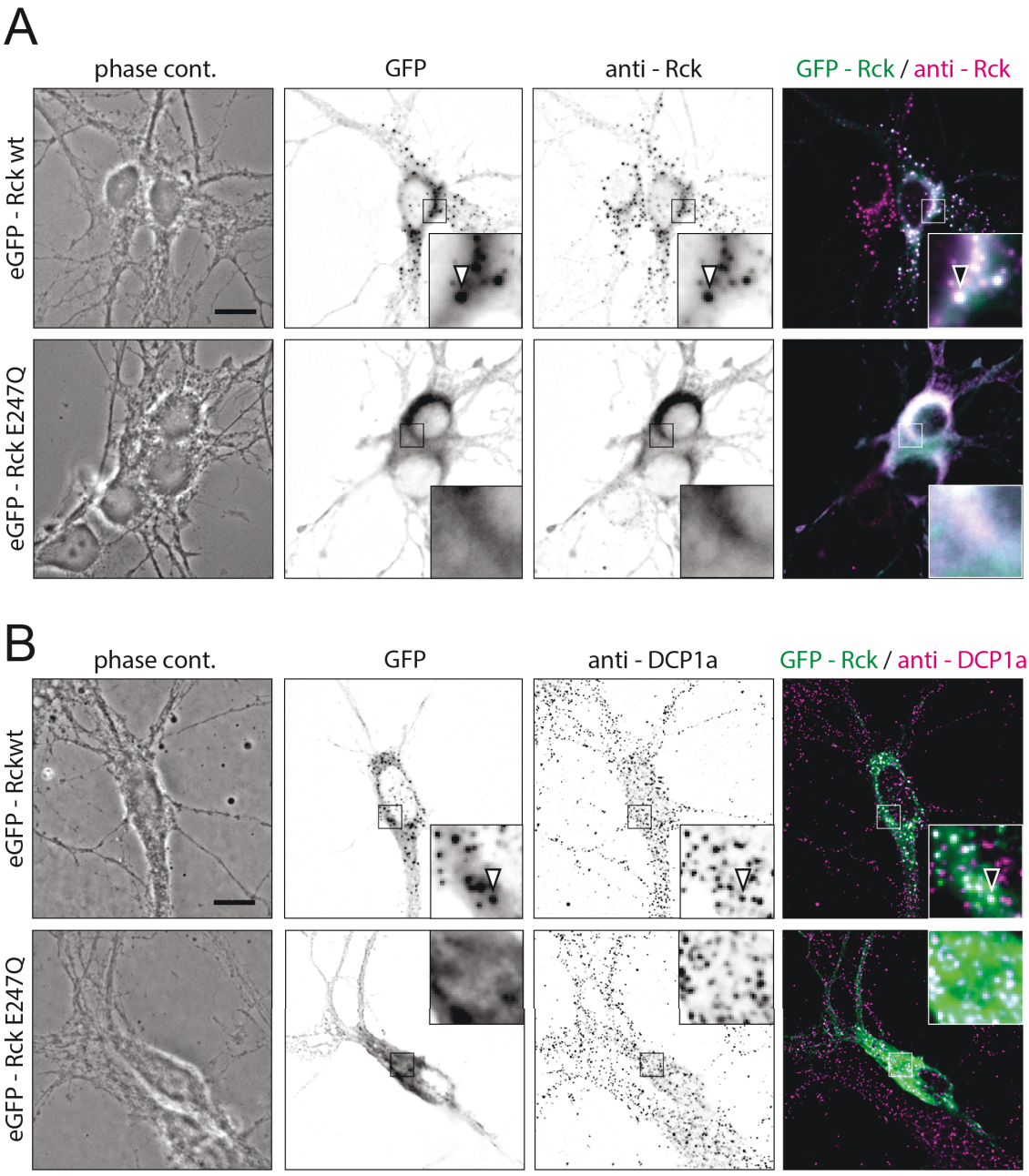

Figure 3.5: Disruption of helicase activity leads to mislocalization of cytoplasmic Rck. **(A-B)** Representative examples of phase contrast (PC), GFP fluorescence, Rck (A) or DCP1a (B) immunostaining and overlay of 11 DIV hippocampal neurons in culture transfected with either GFP-Rck-wt or GFP-Rck-E247Q. Boxed regions in images are displayed as magnified insets. Fluorescent images were deconvolved to assess overlap. Arrowheads indicate colocalization. Scale bars 10 µm.

3.4 Discussion

In the current study, we show that large Rck granules in the cell body disassemble during the maturation of hippocampal neurons in culture. These granules are very likely P-bodies, as they contain DCP1a, and therefore have an essential function in the regulation of mRNA decay and storage. A similar disassembly of DCP1a granules can be observed during *in vitro* meiotic maturation of the mouse oocyte (Swetloff et al., 2009). P-bodies marked by EGFP-hDCP1a are present in the germinal vesicle stage (arrested prophase I) and disassemble completely during maturation to metaphase II arrested secondary oocytes. However, in this case the authors found only a modest degree of colocalization (29%) between small EGFP-hDCP1a granules and endogenous Rck, and no colocalization with large EGFP-hDCP1a granules. A study in somatic cells show that P-bodies disassemble during mitosis and reassemble in the G1 phase (Yang et al., 2004). Together with our data, these observations suggest P-bodies might be comprised differently, dependent on cell type, cell cycle stage or intracellular subpopulations of granules, inferring that these granules can be highly dynamic in their composition. As neuronal maturation goes hand in hand with the development of synapses, we inquired whether an increase in signaling activity might be responsible for the disassembly of Rck granules that we observed. We showed that this is the case, by inhibiting neuronal activity in mature (22 DIV) neurons, which caused the reassembly of Rck granules in the cell body. This reassembly was dependent on maturation, as large Rck granules present at 8 DIV did not further increase in size. Importantly, the effect was quickly reversible by reinstating endogenous signaling activity or by stimulation of the NMDA receptor. Together, these findings are in line with previous research, which shows that stimulation by glutamate, NMDA or BDNF leads to a decrease of dendritic granules identified by P-body markers (Zeitelhofer et al., 2008). The same publication of our lab, however, did not identify any change in the localization of dendritic P-bodies upon neuronal silencing. As we show that large Rck granules in the cell soma of mature neurons reliably reassemble upon neuronal silencing, we propose that P-bodies may be differently regulated in different cellular compartments, such as the soma and dendrites in mature neurons. Additionally, different size or protein compositions of these P-bodies in the soma or dendrites may also impose a

different mode of regulation by neuronal activity. A recent publication showed that NMDA receptor activation leads to Ago2 phosphorylation and an increased interaction between Ago2 and Rck (Rajgor et al., 2018). It is possible that synaptic activity regulates P-bodies by a similar mechanism, as we show that NMDA receptor activation quickly disassembles somatic Rck granules.

As P-bodies are sites of storage for translationally repressed mRNAs, their disassembly during maturation or neuronal activity might also reflect a state of translational control (Brengues et al., 2005). It is noteworthy to mention that translational regulation as well as mRNA degradation does not depend on the presence of detectable P-bodies, as shown by the disruption of P-bodies in yeast (Decker et al., 2007; Tritschler et al., 2007). The disassembly of P-bodies upon CHX treatment was unaffected in silenced neurons, indicating that neurons cannot counteract this effect, by modulating activity and therefore act as other cell types in this context. Another explanation for the observed effect might be that the stalling of ribosomes by CHX block mRNAs, which are required for the formation of P-bodies (Brengues et al., 2005; Teixeira et al., 2005). Taken together, this data points to a unique regulation of P-bodies by neuronal activity, which is absent in other cell types. In addition to the regulation already present in developing neurons or neuronal precursors, mature neurons appear to regulate P-bodies by neuronal activity.

Previous research indicates that the neuronal RBP Stau2 might interact with P-bodies and that it regulates the *Rck* mRNA (Sharangdhar et al., 2017; Zeitelhofer et al., 2008). However, in the current study we found no evidence that the assembly or localization of Rck granules depends on the RBP Stau2. Conversely, the disassembly of Rck from granules by the introduction of a point mutation disrupting its helicase activity (E247Q) did not alter Stau2 localization (*data not shown*). These observations indicate that distinct neuronal granules can function independently. However, interactions such as the docking of DCP1 granules with Stau2 granules in dendrites, as previously observed (Zeitelhofer et al., 2008) would be hindered and possibly disrupt various aspects of mRNA regulation. Moreover, Stau2 might regulate P-bodies and Rck on other levels. For instance, Stau2 might regulate *Rck* translation, via the binding to its 3´-UTR (Sharangdhar et al., 2017). Future research will need to investigate whether this is indeed the case.

Finally, we show that the introduction of a point mutation disrupting helicase activity (E247Q) leads to diffuse mislocalization of Rck in neurons. This phenotype is comparable to the previously observed localization in FT3-7 cells (Jangra et al., 2010). This suggests that the helicase activity is required for the localization of Rck in P-bodies or smaller granules. Importantly, DCP1a remained clustered in P-body like granules in the presence of the diffusely localized Rck mutant, while endogenous Rck was mislocalized, suggesting proper Rck localization and its helicase activity might not be required for the formation and maintenance of P-bodies. A study in HeLa cells demonstrated that Rck, eIF4E-T, LSm1 and Ccr4, but not Dcp2, require one another to accumulate in P-bodies (Andrei et al., 2005). As the absence of Dcp2 did not disrupt the assembly of other proteins in P-bodies, and we show that DCP1a is unaffected by Rck mislocalization, it is tempting to speculate that these RNA-decapping enzymes are distinctly regulated in P-bodies, possibly linked to their function in 5´ to 3´ degradation.

In conclusion we show that the assembly of Rck into P-bodies is uniquely regulated in neurons. The process depends on neuronal maturation, neuronal signaling activity and the helicase activity of Rck itself. It is likely that these mechanisms affect the manner by which Rck interacts with other RNP components, both RNA and protein. The regulation of RNAs by P-bodies is proposed to play an essential role in the regulation of protein expression. This process is particularly important in neurons, where *de novo* protein synthesis is required for lasting synaptic strengthening by long-term potentiation, the basis of learning and memory. Therefore, regulation by P-bodies can have a significant impact on the modification of higher order synaptic networks. Future research needs to determine the effects of P-body assembly and disassembly on synaptic plasticity, learning and memory formation.

3.5 Materials and Methods

3.5.1 Neuronal Cell Culture, Transfection and Transduction

Primary rat hippocampal neuronal cell cultures were generated as previously described (Goetze et al., 2003). In short, hippocampi of embryonic day 17 (E17) embryos of timed pregnant Sprague-Dawley rats (Charles River Laboratories) or Stau2 deficient rats (Berger et al., 2017) were isolated, cells dissociated and plated on Poly-L-Lysine coated cover slips or glass bottom dishes (WillCo Wells) and cultured in NMEM+B27 medium (Invitrogen). Experiments were performed with cultured neurons between 8-29 days *in vitro* (DIV). All animals were used according to the German Welfare for Experimental Animals (LMU-Munich, Regierung von Oberbayern).

3.5.2 Cryosections

Adult rats (3 months old) were perfused intracranially with 4% PFA. Brains were removed and postfixed in 4% PFA o/n, and then placed in 30% sucrose till they sunk down. Samples were embedded in OCT (Tissue-Tek) and cryopreserved. Sagittal cryosections (20 µm thick) were permeabilized with PBS-0.1% Triton X-100 (PBT) and then blocked with 5% BSA in PBT. Primary antibody rabbit-anti-RCK (MBL; #PD009) was incubated o/n at 4ºC. Secondary antibody donkey-anti-rabbit A657-conjugated (Molecular Probes) was incubated for 2h at RT, and then counter stained with DAPI (4',6-Diamidine-2'-phenylindole dihydrochloride). Slides were mounted with Prolong-Diamond (Invitrogen).

3.5.3 Plasmids

The Rck sequence was obtained by PCR amplification from rat cDNA. The Rck E247Q mutant was generated by primer mutagenesis. These sequences were

cloned without a functional stop codon and placed in frame with GFP in the pEGFP-C1 vector (Clontech).

3.5.4 Chemical treatments

To inhibit neuronal activity, cells were incubated with 100 µM 6-cyano-7-nitroquinoxaline-2,3-dione (CNQX; Sigma, #C127), 50 µM 2-amino-5-phosponopentanoic acid (AP5; Sigma, #A8054) and 1 µM tetrodotoxin (TTX; Abcam, #ab120055) in NMEM+B27 over night at 37°C, unless otherwise stated. Vehicle treated cells were incubated with equivalent amount of DMSO. Wash off experiments were performed by a short wash in pre-warmed HBSS and subsequent 15 min recovery in NMEM+B27 at 37°C. Stimulation by NMDA was done by a quick wash pre-warmed HBSS and 15 min incubation with 100 µM NMDA in NMEM+B27. Cycloheximide (CHX, 7 µM, Roth) was incubated for 4 h in NMEM+B27 before fixation.

3.5.5 Immunostaining

Neurons were fixed for 10 min with 4% paraformaldehyde (PFA) and immunostained as previously described (Goetze et al., 2006). The following antibodies were used in this study: polyclonal rabbit anti-Rck (MBL), polyclonal goat anti-DDX6 (Abnova), polyclonal mouse anti-DCP1a (Abnova), polyclonal rabbit anti-PABP1 (Cell Signaling) and polyclonal rabbit anti-G3BP (Proteintech) antibodies together with the following secondary antibodies: donkey anti-rabbit or donkey anti-mouse Alexa488, Alexa555 or Alexa647 conjugated antibodies (Life Technologies).

3.5.6 Microscopy

Imaging of fixed cells was performed on a Zeiss Z1 Axio Observer microscope including a Plan-Apochromat 63x objective, a COLIBRI.2 LED light source and the Axiocam 506 mono camera.

Live cell imaging was performed on a Zeiss Cell Observer spinning disk system. The setup consisted of a Zeiss Z1 Axio Observer microscope including a Plan-Apochromat 63x objective, a Yokogawa CSU-X1 spinning disk unit with 4 laser lines (405 nm 20 mW; 488 nm 50 mW, 561 nm 75 mW and 638 nm 75 mW) and an Evolve 512 Delta EMCCD Camera. For temperature control, a custom made EMBL environmental chamber (EMBLEM) was constructed for this setup. Hippocampal neurons were imaged at 36°C in HBSS (Life Technologies) supplemented with 20 mM HEPES buffer pH=7.3 (Sigma Aldrich). Time-lapse images were acquired for the duration of 120 minutes, with an approximate frame interval of 30 sec. Cells were selected for proper expression of plasmids as well as for cell morphology and cell viability.

3.5.7 Image Data Analysis

Assessments of neuronal population with the observed phenotypes was done by manually scoring >100 cells/condition/experiment.

For deconvolution, z-stacks with 50 images at an interval of 0.26 µm were acquired, covering a total distance of 13 µm. Z-stacks were subjected to deconvolution using the constrained iterative quantitative restoration method of the Zeiss ZEN software deconvolution module.

3.5.8 Statistical Analysis

The R software was used for all data processing, plotting and statistical analysis (R-Core-Team, 2016; Wickham, 2009; Wickham, 2011; Wickham, 2016). Figures represent mean ± standard deviation of at least 3 independent experiments, unless otherwise stated. Asterisks represent *p*-values obtained by either Student's t-test or Tukey's test post-hock to one-way ANOVA analysis (* $p < 0.05$, ** $p < 0.01$, *** $p < 0.001$), as indicated. The subscript of F values denotes the degrees of freedom.

3.6 Acknowledgments

We thank Sabine Thomas Christin Illig, and Jessica Olberz for primary neuron culture preparation; Renate Dombi for assistance in cloning; Daniela Rieger for antibody purification; Marco Tolino for initial experiments; Sandra M Fernández-Moya and Rico Schieweck for critical comments on the manuscript. This work was supported by grants from the DFG (Großgeräteantrag INST86/1581-1FUGG, SPP1738, FOR2333, SFB870) and the FWF (I 590-B09, F4314-B09 SFB RNA-seq) (all to MAK) and the Friedrich-Baur-Stiftung (to IS).

Competing Interests

The authors declare no competing interest.

Data availability statement

All datasets that were generated during the current study are found in the source file or are be available upon request.

Author contributions

MAK conceived the project. KEB, IS, SH, performed experiments and all authors were involved in data analysis. KEB, IS and MAK wrote the manuscript.

3.7 Supplementary Materials

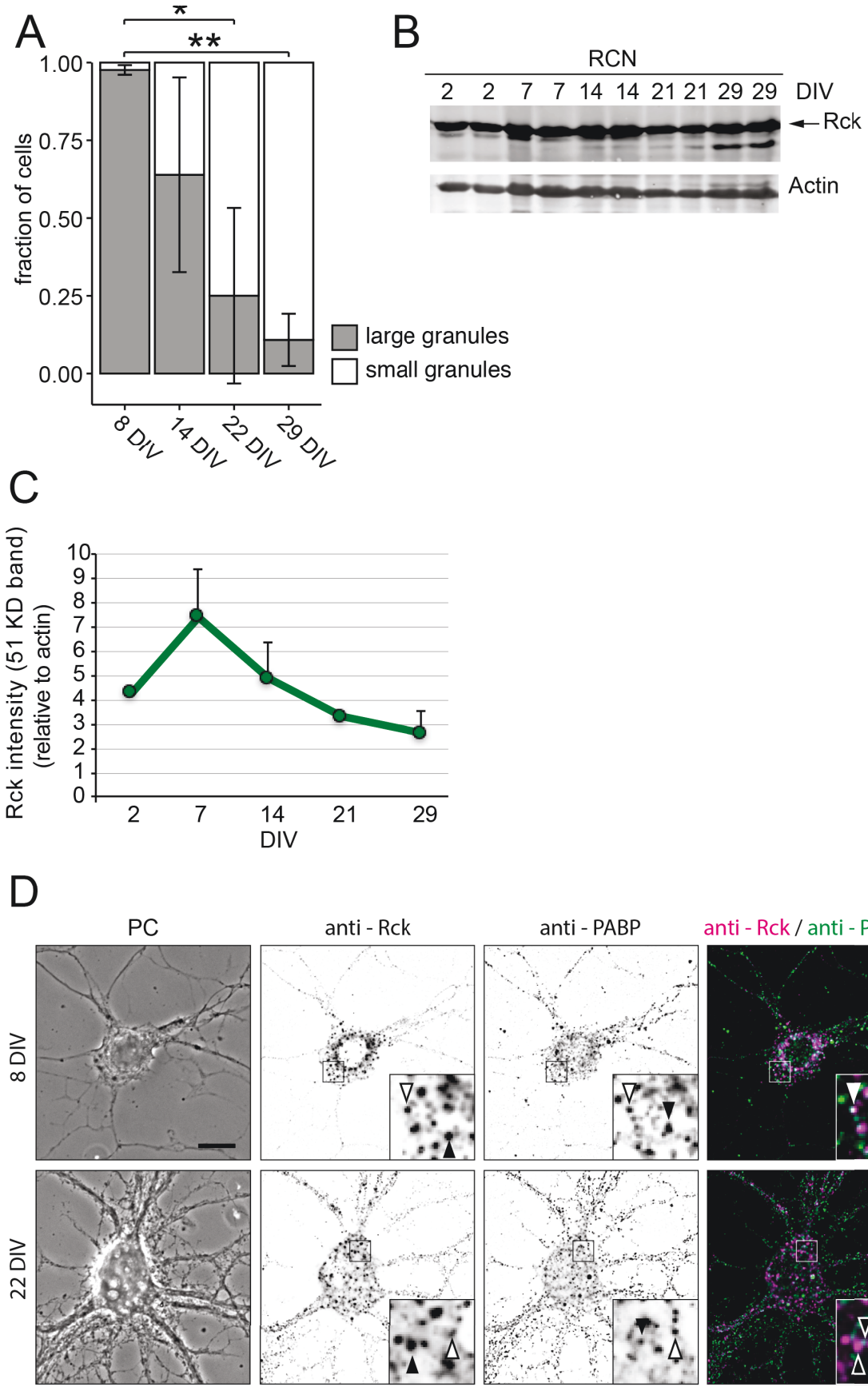

←

Supplementary Figure 3.1: Cytoplasmic Rck granules during neuronal maturation in culture. **(A)** Bar plot displaying quantification of cell population by fraction of cells containing either large or small Rck granules, at 8, 14, 22 and 29 DIV. Data represents mean ± standard deviation of three independent experiments. Asterisks represent p-values obtained by Tukey's test post-hoc to one-way ANOVA analysis (* $p < 0.05$, ** $p < 0.01$). At least 100 cells/condition/experiment were quantified. **(B-C)** Representative western blot (B) and quantification (C) of Rck protein levels and actin (loading control) in 2, 7, 14, 21 and 29 DIV rat cortical neurons in culture. Data represents mean ± standard deviation of two independent experiments with two technical replicates each. Hashtag (#) indicates uncharacterized small band. **(D)** Representative examples of phase contrast (PC), Rck and PABP immunostaining and overlay of 8 DIV and 22 DIV hippocampal neurons in culture. Boxed regions in images are displayed as magnified insets. Fluorescent images were deconvolved to assess overlap. White arrowheads indicate colocalization, black arrowheads indicate no colocalization. Scale bars 10 μm. Related to Figure 1.

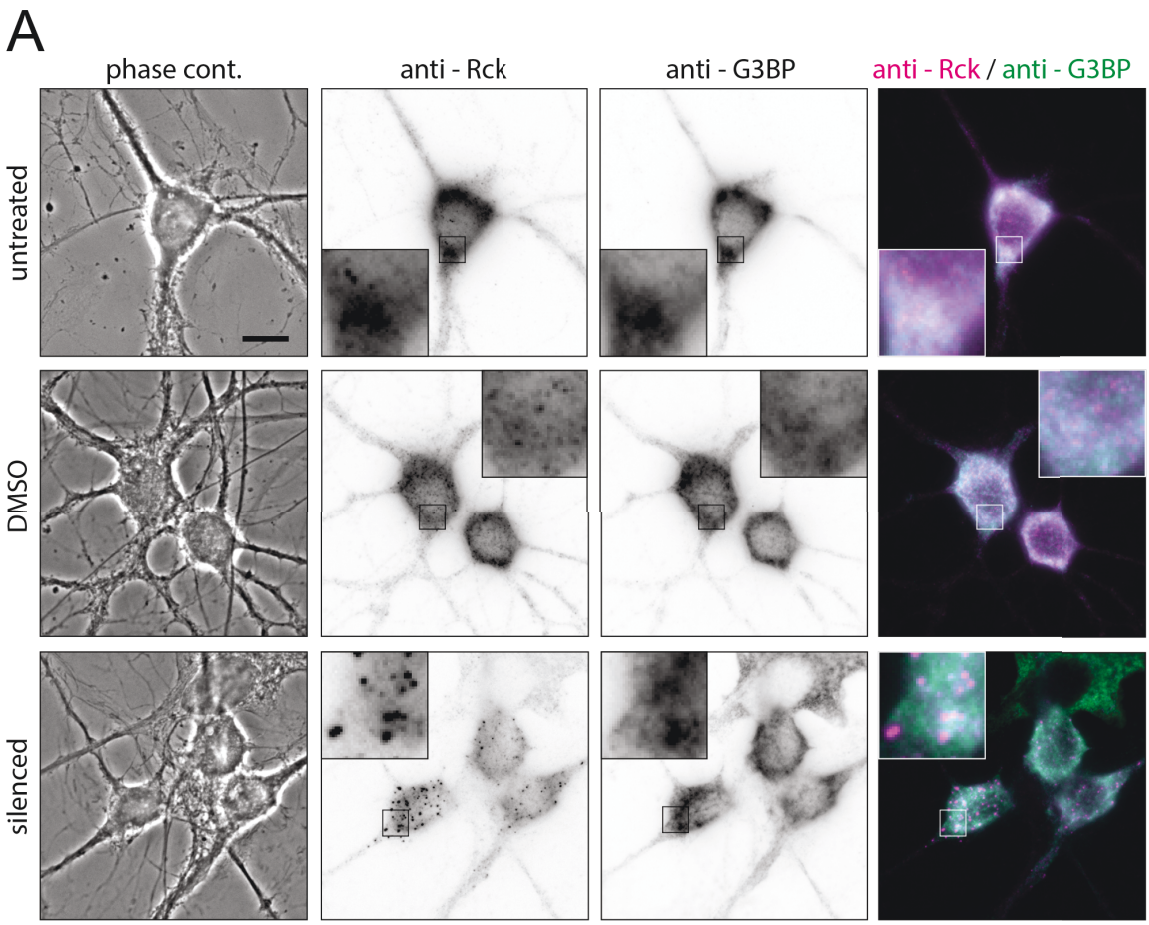

Supplementary Figure 3.2: Large Rck granules induced by chemical inhibition of neuronal activity are not stress granules. **(A)** Representative examples of phase contrast, Rck and G3BP immunostaining of 22 DIV hippocampal neurons in culture under untreated, vehicle treated or silenced (100µM CNQX, 50µM AP5, 1µM TTX) conditions. Boxed regions in images are displayed as magnified insets. Scale bars 10 µm. Related to Figure 2.

A

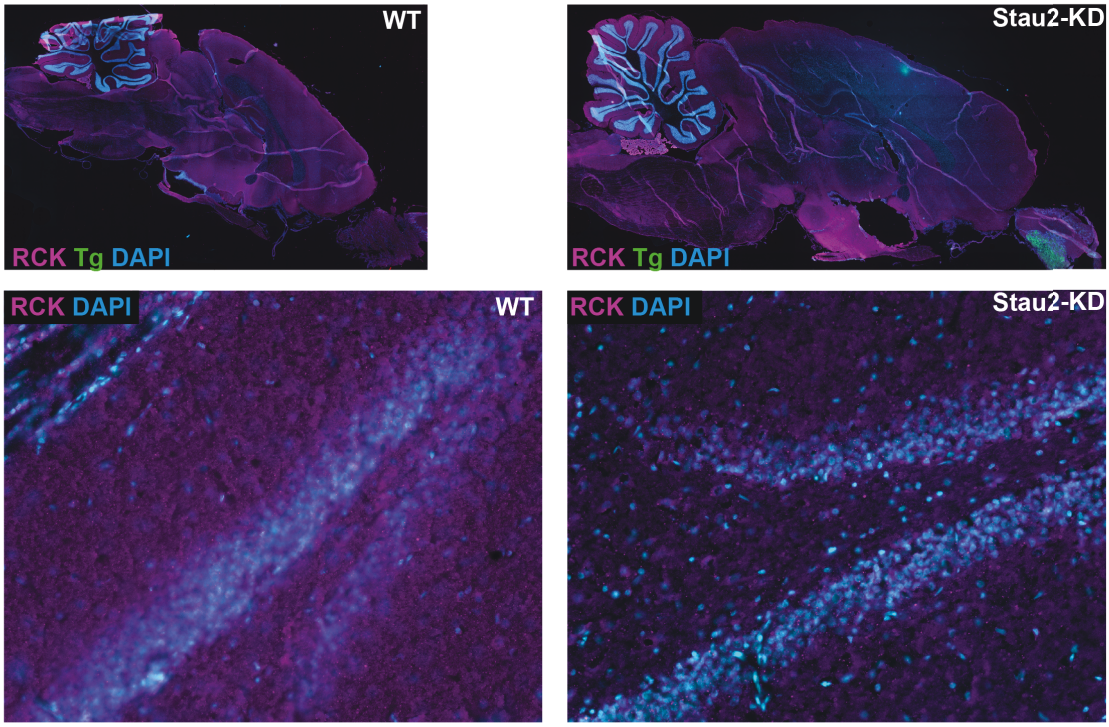

Supplementary Figure 3.3: Localization of Rck in the dentate gyrus upon Stau2 knock-down. **(A)** Representative examples of Rck immunostaining, GFP (transgenic) and DAPI in whole brain sagittal cryosections of 3-month-old *wild type* or Stau2 knock-down rats. Region of the dentate gyrus magnified in lower panels. Abbreviations: WT = *wild type*, KD = knock-down, Tg = transgenic.
Related to Figure 3.

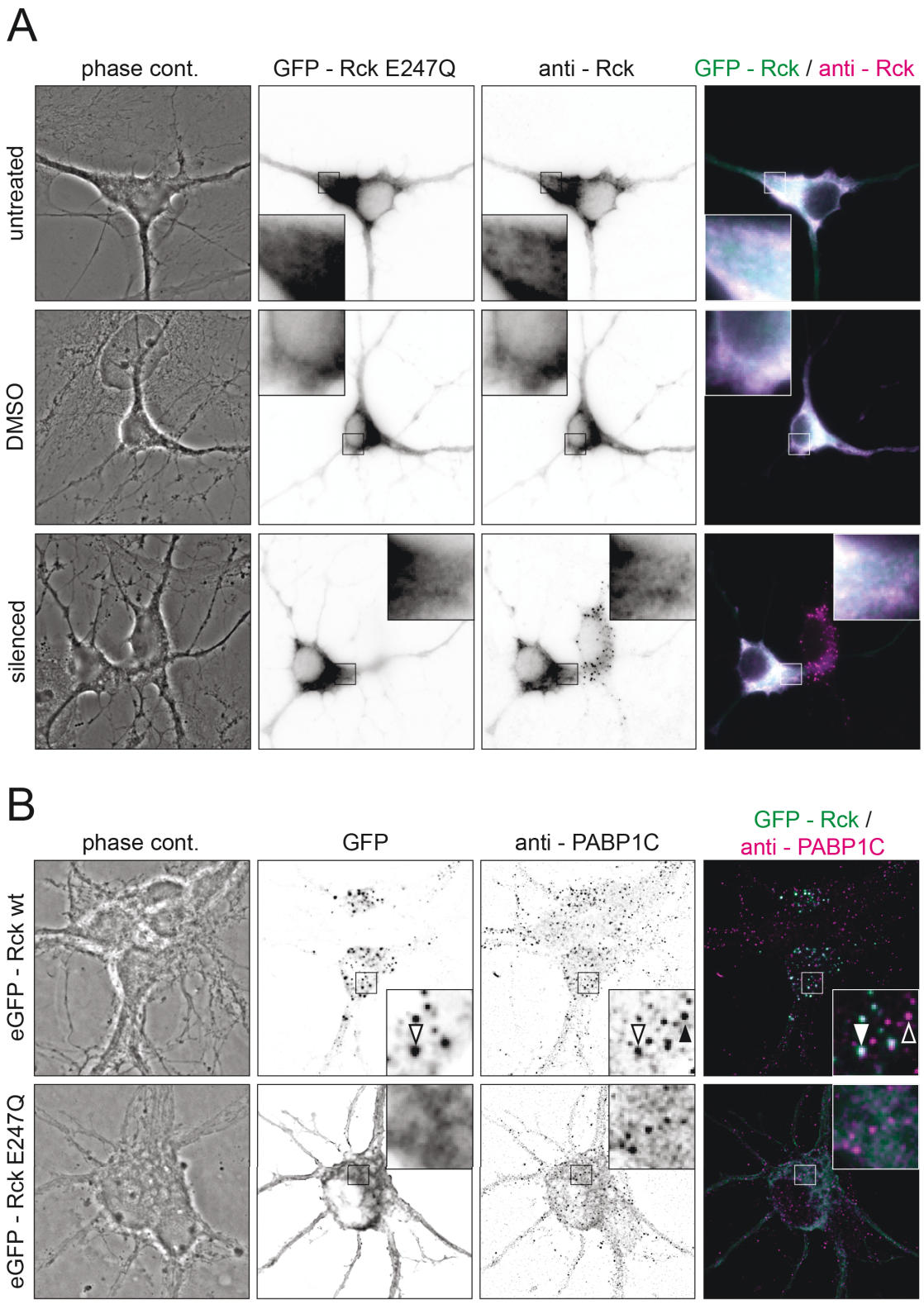
A
phase cont.
GFP - Rck E247Q
anti - Rck
GFP - Rck / anti - Rck
untreated
DMSO
silenced
B
phase cont.
GFP
anti - PABP1C
GFP - Rck /
anti - PABP1C
eGFP - Rck wt
eGFP - Rck E247Q

←

Supplementary Figure 3.4: Mislocalization of the Rck-E247Q helicase mutant is not affected by neuronal inhibition and does not affect cytoplasmic PABP. **(A)** Representative examples of phase contrast (PC), GFP fluorescence, Rck immunostaining and overlay of 15 DIV hippocampal neurons in culture transfected with GFP-Rck-E247Q under untreated, vehicle treated or silenced (100µM CNQX, 50µM AP5, 1µM TTX) conditions. Boxed regions in images are displayed as magnified insets. Fluorescent images were deconvolved to assess overlap. White arrowheads indicate colocalization, black arrowheads indicate no colocalization. Scale bar 10 µm. **(B)** Representative examples of phase contrast (PC), GFP fluorescence, PABP immunostaining and overlay of 11 DIV hippocampal neurons in culture transfected with either GFP-Rck-wt or GFP-Rck-E247Q.
Related to Figure 4.

Movie 3.1: Representative time-lapse movie of GFP-Rck in the soma of a 11 DIV hippocampal neuron. Boxed region magnified in right panel. Green arrowheads indicate fusing and red arrowheads splitting GFP-Rck granules. Time indicates hours:minutes. Scale bar 10 µm. Related to Figure 3.5.

4. Discussion

The individual findings of the two studies presented here are discussed separately in previous chapters (see chapters 2.4 and 3.4). This section aims to provide a more general and comprehensive discussion together with an outlook for future research in the field, on the basis of the results reported in this dissertation.

4.1 Summary

The two studies presented here address the intracellular sorting of mRNAs together with their RBPs and its regulation in hippocampal neurons in culture. The aims outlined in the introduction (chapter 1.7) were addressed from multiple angels by fluorescent microscopy, both in fixed and living neurons.

The first study investigated dendritic mRNA transport and sorting to synapses. Time-lapse live-cell imaging in combination with the MS2 RNA imaging system revealed that a majority of mRNA was dynamically transported in a multidirectional manner in accordance with the previously proposed *sushi-belt* model (**Aim 1.1)** (Doyle and Kiebler, 2011). Furthermore, the 3´-UTR of *Rgs4* was sufficient to mediate an anterograde transport bias (**Aim 1.2**). This anterograde transport bias was not only dependent on the *Rgs4* 3´-UTR, but also on neuronal activity and the dsRBP Stau2 (**Aims 1.3** and **1.4**). In addition, the recruitment of *Rgs4* mRNA to synapses was dependent on its 3´-UTR and synaptic activity, which resulted in a dynamic but sustainable association of the mRNA at synapses (**Aims 1.2** and **1.3**).

The second study addressed the sorting of RBPs, using the dissociation of the ATP-dependent helicase Rck from P-bodies as a model. Immunolabeling of Rck demonstrated, that P-bodies disassembled in the cell body of hippocampal neurons during neuronal maturation in culture (**Aim 2.1**). This effect was reversed in mature neurons by the inhibition of neuronal activity, while it was potentiated by neuronal stimulation of the NMDA receptor (**Aim 2.2**). The translation inhibitor cycloheximide disassembled P-bodies, hence Rck clusters, independent of neuronal activity, while Stau2 knock-down had no effect on the age-dependent disassembly of Rck. However, the overexpression of a helicase deficient Rck mutant resulted in the

mislocalization of endogenous Rck protein and in the loss of large Rck granules in the soma (**Aim 2.3**).

Together, these studies provide new insight into how intracellular sorting of mRNA and RBPs can be achieved, and highlight how hippocampal neurons regulate these processes by synaptic activity.

4.2 Advancement of the MS2 system

Multiple improvements have been made to the MS2 system, with the ultimate goal to provide a better signal-to-noise ratio for the live imaging of RNA. Some of these improvements have already been presented in the introduction, including the generation of the MS2 coat protein tandem dimer tdMCP and the sequence optimization of the MS2 stem-loop array (Pichon et al., 2016; Wu et al., 2012; Wu et al., 2015) (see chapter 1.6.3). Initially, an increase in binding stability was considered favorable, as it would result in a higher specificity and reduced fluorescence background. However, in yeast under metabolic stress conditions it has been reported that MS2-MCP binding might stall RNA degradation, resulting in 3´- or 5´-degradation fragments (Garcia and Parker, 2015; Garcia and Parker, 2016; Haimovich et al., 2016; Heinrich et al., 2017). Although this effect has not been observed in mammalian cells, it might be a drawback of the system, as degradation fragments would therefore still be fluorescently marked by MCP-FP and indistinguishable from non-degraded mRNA at the microscope. It is especially important to consider this possibility for the binding of MCP to the mutated stem-loop optimized for increased affinity. Moreover, if we consider that several studies, including this dissertation, have reported differences between 3´-UTRs containing only MS2 stem-loops or containing additional 3´-UTR sequences (Fusco et al., 2003), it would suggest that if degradation occurs in mammalian cells, it would either not or only marginally affect the biological readout of mRNA transport *in vivo*. Indeed, the analysis of mRNA degradation would be faulty with such a system. Therefore, the Singer lab recently generated yet another version of an MS2 array with stem-loops of reduced binding affinity to the MCP, separated by longer linkers (Tutucci et al., 2018a; Tutucci et al., 2018b). In addition, the expression levels of the MCP-FP were optimized to decrease an excess of coat-protein. This allows a more dynamic

interaction of the reporter mRNA with endogenous factors, enabling the degradation machinery to displace bound MCP and properly degrade the reporter mRNAs. These examples demonstrate nicely how the MS2-system can be flexibly adapted, depending on the biological inquiry. It will be interesting if this new MS2-system will hold up to previous version in terms of RNA detectability, or if other workarounds can be developed to circumvent aberrant processing of reporter mRNA *in vivo*.

4.3 How is anterograde transport regulated via the 3´-UTR?

One of the key findings presented in this dissertation is that the *Rgs4* 3´-UTR mediated an anterograde transport bias in dendrites of hippocampal neurons. Furthermore, this transport bias was dependent on neuronal activity and on the dsRBP Stau2. An anterograde transport bias of similar magnitude (~ 60 *vs.* 40 %) has previously been reported for other mRNAs and in different model systems (Konig et al., 2009; Park et al., 2014; Zimyanin et al., 2008). Similarly, a recent publication reports an anterograde speed bias, where *ß-actin* mRNA travels faster in the anterograde direction along growing axons of *Xenopus* retinal ganglion cells (Turner-Bridger et al., 2018). These examples point to a global mechanism across cell types and species, by which the directionality of mRNA transport is regulated to achieve correct subcellular sorting and localization. However, detailed mechanistic insight into this regulation is currently not available. To unravel the process of directional transport, it will be essential to investigate the involved motor proteins and their movement along cytoskeletal structures. A recent publication compared the transport of kinesin-1 (KIF5) and kinesin-3 (KIF1A) membrane associated protein cargo in dendrites and axons of rat hippocampal neurons (Karasmanis et al., 2018). The authors report that the kinesin-3 motor domain and kinesin-3 cargo display an anterograde transport bias and higher mobility in the initial segment of dendrites, while the kinesin-1 motor domain displays a stronger anterograde transport and more mobility than the kinesin-3 motor domain in axons. This study demonstrates that different motor proteins can act differently, dependent on the cellular compartment. In addition, dendritic anterograde transport is promoted by the microtubule-associated protein (MAP) Septin 9 (SEPT9). The authors suggest that SEPT9 distinguishes between kinesin-1 and kinesin-3, imparting the directional bias during entry into

dendrites. This data provides a new viewpoint on dendritic cargo sorting, via the differential regulation of motor proteins by a MAP.

If such a transport model would hold true for mRNPs as well, distinct mRNA cargoes enriched in different cellular compartments should be found in mRNPs associated with different motor proteins. The direct imaging of fluorescently-labeled motor proteins or their chemical inhibition during the imaging of MS2 mRNA reporters should provide additional insights into mRNA cargo specific transport and a putative involvement in a directional bias. However, additional articles report that different motor proteins can be associated with the same mRNP (Messitt et al., 2008; Vershinin et al., 2007). Here it will be essential to define the necessary components of a functional mRNP and how mRNAs are differentially packaged in different granules. Interestingly, a recent publication attempted to define the minimal components of an mRNA transport granule for *Drosophila in vitro* (McClintock et al., 2018), reporting that the adaptor protein Bicaudal-D (BicD), the RBP Egalitarian (Egl), dynein and dynactin are sufficient to form a functional transport mRNP that is transported along microtubules towards the minus end *in vitro*. The presence of mRNA strongly promotes this transport. Furthermore, the interaction of BicD and Egl is triggered by an RNA localization signal, which would result in the subsequent recruitment of dynein and dynactin. This data suggests that mRNPs might be assembled by initial protein interactions dependent on specific RNA localization sequences or structures, which is followed by the association of specific motor proteins. As data presented in this study suggest that the lack of Stau2 results in the loss of a 3´-UTR dependent anterograde transport bias in dendrites, Stau2 might be involved in mediating the assembly of its target mRNAs with specific factors necessary to promote anterograde transport. This would allow these mRNAs to predefine their subcellular localization via the 3´-UTR. However, the assembled mRNPs might not be finite, and able to adapt their composition on the go as required, *e.g*. in response to a change in synaptic activity. The association of a *cis*-acting zipcode element and an RBP has been demonstrated by multiple examples (Jambhekar and Derisi, 2007; Mayr, 2017; Sharangdhar et al., 2017). In the case of Stau2, which is involved not only in mRNA transport, but also in mRNA stability and translational control, it will be interesting to identify specific structural RNA-binding sites, and investigate if and how they promote different Stau2 functions and how external factors might regulate these functions. Previous publications demonstrate

how competitive or cooperative mRNA binding can regulate different aspects of RNA metabolism (Gong and Maquat, 2011; Liu et al., 2006). If Stau2 can regulate its target mRNAs, and its subcellular sorting via such mechanisms, will be a key question for future research.

4.4 What are the molecular mechanisms governing mRNA localization and local translation?

Data reported in this dissertation show that mRNA is actively recruited to subcellular locations, specifically the synapses of hippocampal neurons. This process depends on both the 3´-UTR of the transcript and on synaptic activity. In addition, the influx/efflux of mRNA at the synapse was 3´-UTR dependent as well. As discussed above, a specific 3´-UTR might be responsible for recruiting factors to the mRNA, which conveys key properties for transport and regulation via *cis*-acting elements. The 3´-UTR dependent recruitment to synapses reported here suggest that such factors might be involved in mediating synaptic localization as well. It will be interesting to see whether a specific mRNA localization element can be identified that would regulate this process by the binding of *trans*-acting factors such as Stau2. However, it will be more challenging to pinpoint how mRNPs are ultimately anchored and released at synapses. This could be achieved via the stalling of motor proteins or possibly even via changes to the cytoskeleton and/or its associated proteins. In this respect it is of note that MAPs have been proposed to act as “speed-bumps” at microtubules. In addition, it has been reported that microtubules can enter dendritic spines upon neuronal stimulation (Gu et al., 2008; Jaworski et al., 2009) and that local actin filaments can be reorganized via their associated proteins (Goetze et al., 2006; Yoon et al., 2016). A recent study in axons of hippocampal neurons found that GTP-rich microtubule plus ends accumulate at *en passant* synapses and that weak interactions of kinesin-3 with such regions allow the motor protein to readily detach (Guedes-Dias et al., 2019). However, key components at or close to synapses must recognize factors on specific mRNPs to trigger 3´-UTR dependent capture and anchoring. The identification of the molecular mechanism governing mRNP capture, according to the synaptic tagging and capture hypothesis, (Doyle and Kiebler, 2011; Wilhelm and Vale, 1993) would be a significant advance in the field, opening up the

possibility to investigate subcellular mRNA localization in different cellular compartments or cell types and under different conditions in detail.

Once localized, mRNA has been proposed to be unpacked, at least in part, from its associated mRNPs, making the transcripts available for the binding of ribosomes and subsequent translation (Buxbaum et al., 2014). Various methods have been employed to visualize local translation of nascent protein (Halstead et al., 2016; Morisaki and Stasevich, 2018; Pilaz et al., 2016; tom Dieck et al., 2015; Yoon et al., 2016). However, the use of the SunTag- or FLAG- system, as recently proposed in five independent publications (Morisaki et al., 2016; Pichon et al., 2016; Wang et al., 2016; Wu et al., 2016; Yan et al., 2016), has been shown to be highly promising in visualizing live translation with high temporal and spatial sensitivity. In short, multiple repeats of the SunTag-coding sequence are cloned in frame of the ORF in a reporter mRNA. Once translated by ribosomes, the repetitive Suntag epitopes can be recognized intracellularly and bound by a specific nanobody tagged with a fluorescent protein. Thereby, upon translation of the SunTag epitope the nanobody clusters in distinct fluorescent punctae. This reporter mRNA could be eventually combined with the MS2-system, using a second spectrally distinct fluorescent protein to visualize both mRNA and translated protein simultaneously. The publications mentioned above have modified the SunTag-system to, *e.g*. reduce fluorescent background (using an NLS), increase temporal sensitivity (introduction of an auto cleavage site to rapidly degrade nascent protein) or reduce protein mobility for easier tracking (tethering the nascent chain to membrane compartments) (Pichon et al., 2016; Wang et al., 2016; Yan et al., 2016). As this system has been shown to be reliable in the quantification of local translation, it will be interesting to see how future applications will address more distinct questions, such as investigating differences in translation dependent on 3´-UTR sequences, associated factors (*e.g*. Stau2), or subcellular localization (*e.g*. different synaptic types). Although the molecular mechanism of translation itself is well established, the precise processes that result in mRNP unpacking, as well as how translation initiation and termination are locally triggered by synaptic activity are not fully known. In addition, the process of active translation itself may affect mRNA transport, such as the *Rgs4* 3´-UTR dependent anterograde transport bias or its local recruitment. A detailed insight could be achieved by the general chemical inhibition of translation (*i.e*. by cycloheximide or puromycin) during the imaging of MS2-SunTag mRNA dual reporters. Indeed, a

recent publication shows that mRNA granules associated with nascent protein travel slower on average and interact only transiently with stress granules (Moon et al., 2019). Such experiments represent a first important step towards tying mRNA transport to its translation in defined subcellular compartments.

4.5 How does neuronal activity regulate mRNA and protein sorting?

As presented in both studies here, neuronal activity is one key factor controlling both mRNA and RBP sorting in hippocampal neurons in culture. Although other cell types show some form of electrophysiology, electro-chemical transmission and the ability to produce an action potential is the hallmark of neurons that sets them apart from other cell types. It is well established that neurons use this ability to modulate various aspects of cell morphology and function, such as the regulation of branching or local translation, and moreover even require these inputs for survival (Pfisterer and Khodosevich, 2017). Data presented here, provides additional insight and shows how physiological neuronal activity is required for a 3´-UTR dependent anterograde mRNA transport bias, the 3´-UTR dependent sorting of mRNA towards synapses and the disassembly of large Rck granules during neuronal maturation. This data opens the question which specific signal transduction pathways or synaptic types might be involved in each of these processes and how they are regulated and integrated. Indeed, the detailed analysis of mRNA sorting at synapses reported here showed how an *MS2*-tagged *Rgs4* 3´-UTR mRNA reporter interacts with fewer synapses in dendrites than an *MS2 only* reporter, while the number of synapses visited in the somatic area are equal. As a consequence, fewer dendritic synapses contained the *MS2*-tagged *Rgs4* reporter and more contained the *MS2 only* control reporter. This apparently stricter regulation of synaptic mRNA sorting via the *Rgs4* 3´-UTR, suggest a 3´-UTR dependent mechanism linked to neuronal activity. However, this data may also indicate that different 3´-UTRs might regulate the sorting to different synaptic types. This is partially supported by the fact that synapses containing a reporter mRNA had a higher mean signal intensity of tagRFP-tagged PSD-95 fusion protein than synapses lacking any reporter mRNA. Studies on how neuronal signaling through different pathways might impose sorting of mRNA in a 3´-UTR dependent manner would be of great interest. The labeling of synapses by

receptor specific molecular markers combined with the chemical inhibition or activation of specific membrane receptors or channels, would be a first step to address this important question. There are of course indications of how different mRNAs might play a role at specific subcellular locations upon neuronal signaling. For instance, it has been shown that *ß-actin* mRNA is recruited to dendrites of hippocampal neurons and nascent ß-actin is incorporated into the dendritic spine cytoskeleton upon local glutamate uncaging (Yoon et al., 2016). This nicely exemplifies how the recruitment of a specific mRNA has local consequences, which are regulated by synaptic activation. It is known that the Rgs4 protein plays an inhibitory role in receptor mediated neuronal signaling through G-protein coupled receptors (GPCRs) (Abramow-Newerly et al., 2006; Gerber et al., 2016). Therefore, it is to be expected that *Rgs4* mRNA would be recruited to synapses when this signal transmission is activated. As a consequence, changes in signaling through the GPCR pathway itself would regulate the recruitment of *Rgs4*. However, this remains to be proven experimentally. It is possible that more global synaptic signaling events result in the regulation of mRNA transport to dendrites, where individual transcripts can respond to specific cues as proposed by the *sushi-belt* model (Doyle and Kiebler, 2011). Additionally, it would be interesting to see if other mRNAs, encoding proteins of the GPCR pathway, would also be recruited to the same synapses as *Rgs4* and if their recruitment would be mediated by Stau2, as previously proposed (Heraud-Farlow et al., 2013). The idea that the localization and expressions of proteins of the same pathway might be regulated by the same RBP is intriguing. Future research might determine such a role for Stau2 in mRNA transport and recruitment. Indeed, Stau2 depletion results in the dendritic reduction of the *Rgs4*, a *Calm3* intron-containing and a *CaMKIIα* intron-containing mRNAs (Heraud-Farlow et al., 2013; Ortiz et al., 2017; Sharangdhar et al., 2017; **Figure 1.3D**).

Another example of subcellular mRNA targeting is recruitment of mRNA granules to P-bodies. As shown in this dissertation, these mRNA containing granules change their assembly dependent on neuronal signaling. It would be interesting to assess how this flexibility is achieved on a molecular level, and determine a possible involvement of helicase activity, as suggested by the data presented here. Moreover, as it has been shown that neuronal stimulation leads to an increase of local mRNA recruitment and translation at synapses (Yoon et al., 2016), it would be interesting to see how mRNA sorting to P-bodies would be affected by synaptic activity. Would

differently localized mRNAs be sorted to or released from P-bodies upon neuronal inhibition or activation? Or, would mRNAs even be released from P-bodies and recruited to synapses upon a specific stimulus? It is of course tempting to speculate that change in P-body size observed upon neuronal inhibition, might be a direct reflection of translational repression and mRNA degradation, opposing mRNA recruitment and translation at synapses. Therefore, it would be interesting to follow a single mRNA transcript and determine its lifetime at synapses and P-bodies.

4.6 Outlook

The data provided in this dissertation give unique and novel insight into the processes of mRNA and RBP sorting. The experimental techniques applied here, along with further advancements of the past years, demonstrate the importance of fluorescent microscopy and well-constructed image analysis as a tool, to address questions, which cannot be answered by other means. It will be interesting to see further technical advancements to come in this field. The past years have shown that research can greatly benefit from new technologies, such as two-photon or light sheet microscopy, or the development of new fluorescent reporters such as split GFP or photoactivatable proteins. Ultimately it will be the combination of microscopy along with biochemical and molecular biological techniques, which will answer the questions outlined above. The comprehensive understanding of mRNA and RBP sorting and its regulation in the single neuron will be an essential advance in our understanding of many cellular processes, such as neurite outgrowth, regeneration or branching, subcellular proteome regulation and synaptic plasticity. The inclusive viewpoint of these processes will refine our understanding of how individual synapses undergo alterations and how cells modulate their synaptic connections, affecting higher order networks and ultimately enabling learning and the formation of memory.

References

Abramow-Newerly, M., A.A. Roy, C. Nunn, and P. Chidiac. 2006. RGS proteins have a signalling complex: interactions between RGS proteins and GPCRs, effectors, and auxiliary proteins. *Cell Signal*. 18:579-591.

Ainger, K., D. Avossa, F. Morgan, S.J. Hill, C. Barry, E. Barbarese, and J.H. Carson. 1993. Transport and localization of exogenous myelin basic protein mRNA microinjected into oligodendrocytes. *J Cell Biol*. 123:431-441.

Aizer, A., Y. Brody, L.W. Ler, N. Sonenberg, R.H. Singer, and Y. Shav-Tal. 2008. The dynamics of mammalian P body transport, assembly, and disassembly in vivo. *Mol Biol Cell*. 19:4154-4166.

Akao, Y., H. Yoshida, K. Matsumoto, T. Matsui, K. Hogetu, N. Tanaka, and J. Usukura. 2003. A tumour-associated DEAD-box protein, rck/p54 exhibits RNA unwinding activity toward c-myc RNAs in vitro. *Genes Cells*. 8:671-676.

Albright, T.D., T.M. Jessell, E.R. Kandel, and M.I. Posner. 2000. Neural science: a century of progress and the mysteries that remain. *Cell*. 100 Suppl:S1-55.

Allen, N.J., and D.A. Lyons. 2018. Glia as architects of central nervous system formation and function. *Science*. 362:181-185.

Andreassi, C., and A. Riccio. 2009. To localize or not to localize: mRNA fate is in 3'UTR ends. *Trends Cell Biol*. 19:465-474.

Andrei, M.A., D. Ingelfinger, R. Heintzmann, T. Achsel, R. Rivera-Pomar, and R. Luhrmann. 2005. A role for eIF4E and eIF4E-transporter in targeting mRNPs to mammalian processing bodies. *RNA*. 11:717-727.

Ashraf, S.I., A.L. McLoon, S.M. Sclarsic, and S. Kunes. 2006. Synaptic protein synthesis associated with memory is regulated by the RISC pathway in Drosophila. *Cell*. 124:191-205.

Baas, P.W., J.S. Deitch, M.M. Black, and G.A. Banker. 1988. Polarity orientation of microtubules in hippocampal neurons: uniformity in the axon and nonuniformity in the dendrite. *Proc Natl Acad Sci U S A*. 85:8335-8339.

Bailey, C.H., and M. Chen. 1983. Morphological basis of long-term habituation and sensitization in Aplysia. *Science*. 220:91-93.

Bailey, C.H., E.R. Kandel, and K.M. Harris. 2015. Structural Components of Synaptic Plasticity and Memory Consolidation. *Cold Spring Harb Perspect Biol*. 7:a021758.

Balagopal, V., and R. Parker. 2009. Polysomes, P bodies and stress granules: states and fates of eukaryotic mRNAs. *Curr Opin Cell Biol*. 21:403-408.

Barbee, S.A., P.S. Estes, A.M. Cziko, J. Hillebrand, R.A. Luedeman, J.M. Coller, N. Johnson, I.C. Howlett, C. Geng, R. Ueda, A.H. Brand, S.F. Newbury, J.E. Wilhelm, R.B. Levine, A. Nakamura, R. Parker, and M. Ramaswami. 2006. Staufen- and FMRP-containing neuronal RNPs are structurally and functionally related to somatic P bodies. *Neuron*. 52:997-1009.

Bashkirov, V.I., H. Scherthan, J.A. Solinger, J.M. Buerstedde, and W.D. Heyer. 1997. A mouse cytoplasmic exoribonuclease (mXRN1p) with preference for G4 tetraplex substrates. *J Cell Biol*. 136:761-773.

Bauer, K.E., M.A. Kiebler, and I. Segura. 2017. Visualizing RNA granule transport and translation in living neurons. *Methods*. 126:177-185.

Behm-Ansmant, I., D. Gatfield, J. Rehwinkel, V. Hilgers, and E. Izaurralde. 2007. A conserved role for cytoplasmic poly(A)-binding protein 1 (PABPC1) in nonsense-mediated mRNA decay. *EMBO J*. 26:1591-1601.

Behm-Ansmant, I., J. Rehwinkel, T. Doerks, A. Stark, P. Bork, and E. Izaurralde. 2006. mRNA degradation by miRNAs and GW182 requires both CCR4:NOT deadenylase and DCP1:DCP2 decapping complexes. *Genes Dev*. 20:1885-1898.

Berger, S.M., I. Fernandez-Lamo, K. Schonig, S.M. Fernandez Moya, J. Ehses, R. Schieweck, S. Clementi, T. Enkel, S. Grothe, O. von Bohlen Und Halbach, I. Segura, J.M. Delgado-Garcia, A. Gruart, M.A. Kiebler, and D. Bartsch. 2017. Forebrain-specific, conditional silencing of Staufen2 alters synaptic plasticity, learning, and memory in rats. *Genome Biol*. 18:222.

Berman, D.M., T. Kozasa, and A.G. Gilman. 1996. The GTPase-activating protein RGS4 stabilizes the transition state for nucleotide hydrolysis. *J Biol Chem*. 271:27209-27212.

Bertrand, E., P. Chartrand, M. Schaefer, S.M. Shenoy, R.H. Singer, and R.M. Long. 1998. Localization of ASH1 mRNA particles in living yeast. *Mol Cell*. 2:437-445.

Betke, K.M., C.A. Wells, and H.E. Hamm. 2012. GPCR mediated regulation of synaptic transmission. *Prog Neurobiol*. 96:304-321.

Bourne, H.R., D.A. Sanders, and F. McCormick. 1990. The GTPase superfamily: a conserved switch for diverse cell functions. *Nature*. 348:125-132.

Brangwynne, C.P., C.R. Eckmann, D.S. Courson, A. Rybarska, C. Hoege, J. Gharakhani, F. Julicher, and A.A. Hyman. 2009. Germline P granules are liquid droplets that localize by controlled dissolution/condensation. *Science*. 324:1729-1732.

Brendza, R.P., L.R. Serbus, J.B. Duffy, and W.M. Saxton. 2000. A function for kinesin I in the posterior transport of oskar mRNA and Staufen protein. *Science*. 289:2120-2122.

Brengues, M., D. Teixeira, and R. Parker. 2005. Movement of eukaryotic mRNAs between polysomes and cytoplasmic processing bodies. *Science*. 310:486-489.

Broytman, O., P.R. Westmark, Z. Gurel, and J.S. Malter. 2009. Rck/p54 interacts with APP mRNA as part of a multi-protein complex and enhances APP mRNA and protein expression in neuronal cell lines. *Neurobiol Aging*. 30:1962-1974.

Burton, P.R. 1988. Dendrites of mitral cell neurons contain microtubules of opposite polarity. *Brain Res*. 473:107-115.

Buxbaum, A.R., G. Haimovich, and R.H. Singer. 2015a. In the right place at the right time: visualizing and understanding mRNA localization. *Nat Rev Mol Cell Biol*. 16:95-109.

Buxbaum, A.R., B. Wu, and R.H. Singer. 2014. Single beta-actin mRNA detection in neurons reveals a mechanism for regulating its translatability. *Science*. 343:419-422.

Buxbaum, A.R., Y.J. Yoon, R.H. Singer, and H.Y. Park. 2015b. Single-molecule insights into mRNA dynamics in neurons. *Trends Cell Biol*. 25:468-475.

Cajigas, I.J., G. Tushev, T.J. Will, S. tom Dieck, N. Fuerst, and E.M. Schuman. 2012. The local transcriptome in the synaptic neuropil revealed by deep sequencing and high-resolution imaging. *Neuron*. 74:453-466.

Chenouard, N., Buisson, J., Bloch, I., Bastin, P. and Olivo-Marin, J.-C. 2010. Curvelet analysis of kymograph for tracking bi-directional particles in fluorescence microscopy images. *17th IEEE International Conference on Image Processing (ICIP)*.

Chu, C.Y., and T.M. Rana. 2006. Translation repression in human cells by microRNA-induced gene silencing requires RCK/p54. *PLoS Biol*. 4:e210.

Cockburn, D.M., J. Charish, N.G. Tassew, J. Eubanks, R. Bremner, P. Macchi, and P.P. Monnier. 2012. The double-stranded RNA-binding protein Staufen 2 regulates eye size. *Mol Cell Neurosci*. 51:101-111.

Coller, J.M., M. Tucker, U. Sheth, M.A. Valencia-Sanchez, and R. Parker. 2001. The DEAD box helicase, Dhh1p, functions in mRNA decapping and interacts with both the decapping and deadenylase complexes. *RNA*. 7:1717-1727.

Cougot, N., S. Babajko, and B. Seraphin. 2004. Cytoplasmic foci are sites of mRNA decay in human cells. *J Cell Biol*. 165:31-40.

Cougot, N., S.N. Bhattacharyya, L. Tapia-Arancibia, R. Bordonne, W. Filipowicz, E. Bertrand, and F. Rage. 2008. Dendrites of mammalian neurons contain specialized P-body-like structures that respond to neuronal activation. *J Neurosci*. 28:13793-13804.

Das, S., H.C. Moon, R.H. Singer, and H.Y. Park. 2018. A transgenic mouse for imaging activity-dependent dynamics of endogenous Arc mRNA in live neurons. *Sci Adv*. 4:eaar3448.

Dascal, N. 1997. Signalling via the G protein-activated K+ channels. *Cell Signal*. 9:551-573.

de Chaumont, F., S. Dallongeville, N. Chenouard, N. Herve, S. Pop, T. Provoost, V. Meas-Yedid, P. Pankajakshan, T. Lecomte, Y. Le Montagner, T. Lagache, A. Dufour, and J.C. Olivo-Marin. 2012. Icy: an open bioimage informatics platform for extended reproducible research. *Nat Methods*. 9:690-696.

De Vries, L., B. Zheng, T. Fischer, E. Elenko, and M.G. Farquhar. 2000. The regulator of G protein signaling family. *Annu Rev Pharmacol Toxicol*. 40:235-271.

Decker, C.J., and R. Parker. 2012. P-bodies and stress granules: possible roles in the control of translation and mRNA degradation. *Cold Spring Harb Perspect Biol*. 4:a012286.

Decker, C.J., D. Teixeira, and R. Parker. 2007. Edc3p and a glutamine/asparagine-rich domain of Lsm4p function in processing body assembly in Saccharomyces cerevisiae. *J Cell Biol*. 179:437-449.

Derry, M.C., A. Yanagiya, Y. Martineau, and N. Sonenberg. 2006. Regulation of poly(A)-binding protein through PABP-interacting proteins. *Cold Spring Harb Symp Quant Biol*. 71:537-543.

Dictenberg, J.B., S.A. Swanger, L.N. Antar, R.H. Singer, and G.J. Bassell. 2008. A direct role for FMRP in activity-dependent dendritic mRNA transport links filopodial-spine morphogenesis to fragile X syndrome. *Dev Cell*. 14:926-939.

Ding, J., J.N. Guzman, T. Tkatch, S. Chen, J.A. Goldberg, P.J. Ebert, P. Levitt, C.J. Wilson, H.E. Hamm, and D.J. Surmeier. 2006. RGS4-dependent attenuation of M4 autoreceptor function in striatal cholinergic interneurons following dopamine depletion. *Nat Neurosci*. 9:832-842.

Ding, L., A. Spencer, K. Morita, and M. Han. 2005. The developmental timing regulator AIN-1 interacts with miRISCs and may target the argonaute protein ALG-1 to cytoplasmic P bodies in C. elegans. *Mol Cell*. 19:437-447.

Doyle, M., and M.A. Kiebler. 2011. Mechanisms of dendritic mRNA transport and its role in synaptic tagging. *EMBO J*. 30:3540-3552.

Dubnau, J., A.S. Chiang, L. Grady, J. Barditch, S. Gossweiler, J. McNeil, P. Smith, F. Buldoc, R. Scott, U. Certa, C. Broger, and T. Tully. 2003. The staufen/pumilio pathway is involved in Drosophila long-term memory. *Curr Biol*. 13:286-296.

Duchaine, T.F., I. Hemraj, L. Furic, A. Deitinghoff, M.A. Kiebler, and L. DesGroseillers. 2002. Staufen2 isoforms localize to the somatodendritic domain of neurons and interact with different organelles. *J Cell Sci*. 115:3285-3295.

Dynes, J.L., and O. Steward. 2007. Dynamics of bidirectional transport of Arc mRNA in neuronal dendrites. *J Comp Neurol*. 500:433-447.

Dynes, J.L., and O. Steward. 2012. Arc mRNA docks precisely at the base of individual dendritic spines indicating the existence of a specialized microdomain for synapse-specific mRNA translation. *J Comp Neurol*. 520:3105-3119.

Eliscovich, C., S.M. Shenoy, and R.H. Singer. 2017. Imaging mRNA and protein interactions within neurons. *Proc Natl Acad Sci U S A*. 114:E1875-E1884.

Elvira, G., S. Wasiak, V. Blandford, X.K. Tong, A. Serrano, X. Fan, M. del Rayo Sanchez-Carbente, F. Servant, A.W. Bell, D. Boismenu, J.C. Lacaille, P.S. McPherson, L. DesGroseillers, and W.S. Sossin. 2006. Characterization of an RNA granule from developing brain. *Mol Cell Proteomics*. 5:635-651.

Eom, T., L.N. Antar, R.H. Singer, and G.J. Bassell. 2003. Localization of a beta-actin messenger ribonucleoprotein complex with zipcode-binding protein modulates the density of dendritic filopodia and filopodial synapses. *J Neurosci*. 23:10433-10444.

Ephrussi, A., L.K. Dickinson, and R. Lehmann. 1991. Oskar organizes the germ plasm and directs localization of the posterior determinant nanos. *Cell*. 66:37-50.

Erdely, H.A., C.A. Tamminga, R.C. Roberts, and M.W. Vogel. 2006. Regional alterations in RGS4 protein in schizophrenia. *Synapse*. 59:472-479.

Eroglu, C., and B.A. Barres. 2010. Regulation of synaptic connectivity by glia. *Nature*. 468:223-231.

Eulalio, A., I. Behm-Ansmant, D. Schweizer, and E. Izaurralde. 2007. P-body formation is a consequence, not the cause, of RNA-mediated gene silencing. *Mol Cell Biol*. 27:3970-3981.

Fenger-Gron, M., C. Fillman, B. Norrild, and J. Lykke-Andersen. 2005. Multiple processing body factors and the ARE binding protein TTP activate mRNA decapping. *Mol Cell*. 20:905-915.

Fernandez-Moya, S.M., K.E. Bauer, and M.A. Kiebler. 2014. Meet the players: local translation at the synapse. *Front Mol Neurosci*. 7:84.

Ferrandon, D., L. Elphick, C. Nusslein-Volhard, and D. St Johnston. 1994. Staufen protein associates with the 3'UTR of bicoid mRNA to form particles that move in a microtubule-dependent manner. *Cell*. 79:1221-1232.

Fontes, M.M., A. Guvenek, R. Kawaguchi, D. Zheng, A. Huang, V.M. Ho, P.B. Chen, X. Liu, T.J. O'Dell, G. Coppola, B. Tian, and K.C. Martin. 2017. Activity-Dependent Regulation of Alternative Cleavage and Polyadenylation During Hippocampal Long-Term Potentiation. *Sci Rep*. 7:17377.

Frey, U., M. Krug, K.G. Reymann, and H. Matthies. 1988. Anisomycin, an inhibitor of protein synthesis, blocks late phases of LTP phenomena in the hippocampal CA1 region in vitro. *Brain Res*. 452:57-65.

Fritzsche, R., D. Karra, K.L. Bennett, F.Y. Ang, J.E. Heraud-Farlow, M. Tolino, M. Doyle, K.E. Bauer, S. Thomas, M. Planyavsky, E. Arn, A. Bakosova, K. Jungwirth, A. Hormann, Z. Palfi, J. Sandholzer, M. Schwarz, P. Macchi, J. Colinge, G. Superti-Furga, and M.A. Kiebler. 2013. Interactome of two diverse

RNA granules links mRNA localization to translational repression in neurons. *Cell Rep*. 5:1749-1762.

Fusco, D., N. Accornero, B. Lavoie, S.M. Shenoy, J.M. Blanchard, R.H. Singer, and E. Bertrand. 2003. Single mRNA molecules demonstrate probabilistic movement in living mammalian cells. *Curr Biol*. 13:161-167.

Gagnon, J.A., and K.L. Mowry. 2011. Molecular motors: directing traffic during RNA localization. *Crit Rev Biochem Mol Biol*. 46:229-239.

Garcia, J.F., and R. Parker. 2015. MS2 coat proteins bound to yeast mRNAs block 5' to 3' degradation and trap mRNA decay products: implications for the localization of mRNAs by MS2-MCP system. *RNA*. 21:1393-1395.

Garcia, J.F., and R. Parker. 2016. Ubiquitous accumulation of 3' mRNA decay fragments in Saccharomyces cerevisiae mRNAs with chromosomally integrated MS2 arrays. *RNA*. 22:657-659.

Garnier, M., P.F. Zaratin, G. Ficalora, M. Valente, L. Fontanella, M.H. Rhee, K.J. Blumer, and M.A. Scheideler. 2003. Up-regulation of regulator of G protein signaling 4 expression in a model of neuropathic pain and insensitivity to morphine. *J Pharmacol Exp Ther*. 304:1299-1306.

Gaspar, I., and A. Ephrussi. 2017. Ex vivo Ooplasmic Extract from Developing Drosophila Oocytes for Quantitative TIRF Microscopy Analysis. *Bio Protoc*. 7.

Gaspar, I., Y.V. Yu, S.L. Cotton, D.H. Kim, A. Ephrussi, and M.A. Welte. 2014. Klar ensures thermal robustness of oskar localization by restraining RNP motility. *J Cell Biol*. 206:199-215.

Gerber, K.J., K.E. Squires, and J.R. Hepler. 2016. Roles for Regulator of G Protein Signaling Proteins in Synaptic Signaling and Plasticity. *Mol Pharmacol*. 89:273-286.

Goetze, B., B. Grunewald, S. Baldassa, and M. Kiebler. 2004. Chemically controlled formation of a DNA/calcium phosphate coprecipitate: application for transfection of mature hippocampal neurons. *J Neurobiol*. 60:517-525.

Goetze, B., B. Grunewald, M.A. Kiebler, and P. Macchi. 2003. Coupling the iron-responsive element to GFP--an inducible system to study translation in a single living cell. *Sci STKE*. 2003:PL12.

Goetze, B., F. Tuebing, Y. Xie, M.M. Dorostkar, S. Thomas, U. Pehl, S. Boehm, P. Macchi, and M.A. Kiebler. 2006. The brain-specific double-stranded RNA-

binding protein Staufen2 is required for dendritic spine morphogenesis. *J Cell Biol*. 172:221-231.

Gold, S.J., Y.G. Ni, H.G. Dohlman, and E.J. Nestler. 1997. Regulators of G-protein signaling (RGS) proteins: region-specific expression of nine subtypes in rat brain. *J Neurosci*. 17:8024-8037.

Gong, C., and L.E. Maquat. 2011. lncRNAs transactivate STAU1-mediated mRNA decay by duplexing with 3' UTRs via Alu elements. *Nature*. 470:284-288.

Gray, N.K., J.M. Coller, K.S. Dickson, and M. Wickens. 2000. Multiple portions of poly(A)-binding protein stimulate translation in vivo. *EMBO J*. 19:4723-4733.

Gu, J., B.L. Firestein, and J.Q. Zheng. 2008. Microtubules in dendritic spine development. *J Neurosci*. 28:12120-12124.

Gu, Z., Q. Jiang, and Z. Yan. 2007. RGS4 modulates serotonin signaling in prefrontal cortex and links to serotonin dysfunction in a rat model of schizophrenia. *Mol Pharmacol*. 71:1030-1039.

Guedes-Dias, P., J.J. Nirschl, N. Abreu, M.K. Tokito, C. Janke, M.M. Magiera, and E.L.F. Holzbaur. 2019. Kinesin-3 Responds to Local Microtubule Dynamics to Target Synaptic Cargo Delivery to the Presynapse. *Curr Biol*. 29:268-282 e268.

Haimovich, G., D. Zabezhinsky, B. Haas, B. Slobodin, P. Purushothaman, L. Fan, J.Z. Levin, C. Nusbaum, and J.E. Gerst. 2016. Use of the MS2 aptamer and coat protein for RNA localization in yeast: A response to "MS2 coat proteins bound to yeast mRNAs block 5' to 3' degradation and trap mRNA decay products: implications for the localization of mRNAs by MS2-MCP system". *RNA*. 22:660-666.

Halstead, J.M., J.H. Wilbertz, F. Wippich, T. Lionnet, A. Ephrussi, and J.A. Chao. 2016. TRICK: A Single-Molecule Method for Imaging the First Round of Translation in Living Cells and Animals. *Methods Enzymol*. 572:123-157.

Hamm, H.E. 1998. The many faces of G protein signaling. *J Biol Chem*. 273:669-672.

Han, S.P., L.R. Friend, J.H. Carson, G. Korza, E. Barbarese, M. Maggipinto, J.T. Hatfield, J.A. Rothnagel, and R. Smith. 2010. Differential subcellular distributions and trafficking functions of hnRNP A2/B1 spliceoforms. *Traffic*. 11:886-898.

Harrison, P.J., and D.R. Weinberger. 2005. Schizophrenia genes, gene expression, and neuropathology: on the matter of their convergence. *Mol Psychiatry*. 10:40-68; image 45.

Heinrich, S., C.L. Sidler, C.M. Azzalin, and K. Weis. 2017. Stem-loop RNA labeling can affect nuclear and cytoplasmic mRNA processing. *RNA*. 23:134-141.

Hentze, M.W., A. Castello, T. Schwarzl, and T. Preiss. 2018. A brave new world of RNA-binding proteins. *Nat Rev Mol Cell Biol*. 19:327-341.

Hepler, J.R., D.M. Berman, A.G. Gilman, and T. Kozasa. 1997. RGS4 and GAIP are GTPase-activating proteins for Gq alpha and block activation of phospholipase C beta by gamma-thio-GTP-Gq alpha. *Proc Natl Acad Sci U S A*. 94:428-432.

Heraud-Farlow, J.E., and M.A. Kiebler. 2014. The multifunctional Staufen proteins: conserved roles from neurogenesis to synaptic plasticity. *Trends Neurosci*. 37:470-479.

Heraud-Farlow, J.E., T. Sharangdhar, X. Li, P. Pfeifer, S. Tauber, D. Orozco, A. Hormann, S. Thomas, A. Bakosova, A.R. Farlow, D. Edbauer, H.D. Lipshitz, Q.D. Morris, M. Bilban, M. Doyle, and M.A. Kiebler. 2013. Staufen2 regulates neuronal target RNAs. *Cell Rep*. 5:1511-1518.

Holt, C.E., and S.L. Bullock. 2009. Subcellular mRNA localization in animal cells and why it matters. *Science*. 326:1212-1216.

Horn, W.T., M.A. Convery, N.J. Stonehouse, C.J. Adams, L. Liljas, S.E. Phillips, and P.G. Stockley. 2004. The crystal structure of a high affinity RNA stem-loop complexed with the bacteriophage MS2 capsid: further challenges in the modeling of ligand-RNA interactions. *RNA*. 10:1776-1782.

Horvathova, I., F. Voigt, A.V. Kotrys, Y. Zhan, C.G. Artus-Revel, J. Eglinger, M.B. Stadler, L. Giorgetti, and J.A. Chao. 2017. The Dynamics of mRNA Turnover Revealed by Single-Molecule Imaging in Single Cells. *Mol Cell*. 68:615-625 e619.

Hougaard, D.M., H. Hansen, and L.I. Larsson. 1997. Non-radioactive in situ hybridization for mRNA with emphasis on the use of oligodeoxynucleotide probes. *Histochem Cell Biol*. 108:335-344.

Huang, C., J.R. Hepler, A.G. Gilman, and S.M. Mumby. 1997. Attenuation of Gi- and Gq-mediated signaling by expression of RGS4 or GAIP in mammalian cells. *Proc Natl Acad Sci U S A*. 94:6159-6163.

Huang, Y.S., J.H. Carson, E. Barbarese, and J.D. Richter. 2003. Facilitation of dendritic mRNA transport by CPEB. *Genes Dev*. 17:638-653.

Hubstenberger, A., M. Courel, M. Benard, S. Souquere, M. Ernoult-Lange, R. Chouaib, Z. Yi, J.B. Morlot, A. Munier, M. Fradet, M. Daunesse, E. Bertrand, G. Pierron, J. Mozziconacci, M. Kress, and D. Weil. 2017. P-Body Purification Reveals the Condensation of Repressed mRNA Regulons. *Mol Cell*. 68:144-157 e145.

Hutten, S., T. Sharangdhar, and M. Kiebler. 2014. Unmasking the messenger. *RNA Biol*. 11:992-997.

Hyman, A.A., C.A. Weber, and F. Julicher. 2014. Liquid-liquid phase separation in biology. *Annu Rev Cell Dev Biol*. 30:39-58.

Irion, U., J. Adams, C.W. Chang, and D. St Johnston. 2006. Miranda couples oskar mRNA/Staufen complexes to the bicoid mRNA localization pathway. *Dev Biol*. 297:522-533.

Jakymiw, A., K.M. Pauley, S. Li, K. Ikeda, S. Lian, T. Eystathioy, M. Satoh, M.J. Fritzler, and E.K. Chan. 2007. The role of GW/P-bodies in RNA processing and silencing. *J Cell Sci*. 120:1317-1323.

Jambhekar, A., and J.L. Derisi. 2007. Cis-acting determinants of asymmetric, cytoplasmic RNA transport. *RNA*. 13:625-642.

Jangra, R.K., M. Yi, and S.M. Lemon. 2010. DDX6 (Rck/p54) is required for efficient hepatitis C virus replication but not for internal ribosome entry site-directed translation. *J Virol*. 84:6810-6824.

Jaworski, J., L.C. Kapitein, S.M. Gouveia, B.R. Dortland, P.S. Wulf, I. Grigoriev, P. Camera, S.A. Spangler, P. Di Stefano, J. Demmers, H. Krugers, P. Defilippi, A. Akhmanova, and C.C. Hoogenraad. 2009. Dynamic microtubules regulate dendritic spine morphology and synaptic plasticity. *Neuron*. 61:85-100.

Jung, H., C.G. Gkogkas, N. Sonenberg, and C.E. Holt. 2014. Remote control of gene function by local translation. *Cell*. 157:26-40.

Kanai, Y., N. Dohmae, and N. Hirokawa. 2004. Kinesin transports RNA: isolation and characterization of an RNA-transporting granule. *Neuron*. 43:513-525.

Kang, H., and E.M. Schuman. 1996. A requirement for local protein synthesis in neurotrophin-induced hippocampal synaptic plasticity. *Science*. 273:1402-1406.

Kao, D.I., G.M. Aldridge, I.J. Weiler, and W.T. Greenough. 2010. Altered mRNA transport, docking, and protein translation in neurons lacking fragile X mental retardation protein. *Proc Natl Acad Sci U S A*. 107:15601-15606.

Karasmanis, E.P., C.T. Phan, D. Angelis, I.A. Kesisova, C.C. Hoogenraad, R.J. McKenney, and E.T. Spiliotis. 2018. Polarity of Neuronal Membrane Traffic Requires Sorting of Kinesin Motor Cargo during Entry into Dendrites by a Microtubule-Associated Septin. *Dev Cell*. 46:204-218 e207.

Kedersha, N., M.R. Cho, W. Li, P.W. Yacono, S. Chen, N. Gilks, D.E. Golan, and P. Anderson. 2000. Dynamic shuttling of TIA-1 accompanies the recruitment of mRNA to mammalian stress granules. *J Cell Biol*. 151:1257-1268.

Kedersha, N., G. Stoecklin, M. Ayodele, P. Yacono, J. Lykke-Andersen, M.J. Fritzler, D. Scheuner, R.J. Kaufman, D.E. Golan, and P. Anderson. 2005. Stress granules and processing bodies are dynamically linked sites of mRNP remodeling. *J Cell Biol*. 169:871-884.

Kiebler, M.A., and G.J. Bassell. 2006. Neuronal RNA granules: movers and makers. *Neuron*. 51:685-690.

Kiebler, M.A., and L. DesGroseillers. 2000. Molecular insights into mRNA transport and local translation in the mammalian nervous system. *Neuron*. 25:19-28.

Kiebler, M.A., I. Hemraj, P. Verkade, M. Köhrmann, P. Fortes, R.M. Marion, J. Ortin, and C.G. Dotti. 1999. The mammalian staufen protein localizes to the somatodendritic domain of cultured hippocampal neurons: implications for its involvement in mRNA transport. *J Neurosci*. 19:288-297.

Kim-Ha, J., J.L. Smith, and P.M. Macdonald. 1991. oskar mRNA is localized to the posterior pole of the Drosophila oocyte. *Cell*. 66:23-35.

Klann, E., and T.E. Dever. 2004. Biochemical mechanisms for translational regulation in synaptic plasticity. *Nat Rev Neurosci*. 5:931-942.

Knowles, R.B., J.H. Sabry, M.E. Martone, T.J. Deerinck, M.H. Ellisman, G.J. Bassell, and K.S. Kosik. 1996. Translocation of RNA granules in living neurons. *J Neurosci*. 16:7812-7820.

Köhrmann, M., M. Luo, C. Kaether, L. DesGroseillers, C.G. Dotti, and M.A. Kiebler. 1999. Microtubule-dependent recruitment of Staufen-green fluorescent protein into large RNA-containing granules and subsequent dendritic transport in living hippocampal neurons. *Mol Biol Cell*. 10:2945-2953.

Konig, J., S. Baumann, J. Koepke, T. Pohlmann, K. Zarnack, and M. Feldbrugge. 2009. The fungal RNA-binding protein Rrm4 mediates long-distance transport of ubi1 and rho3 mRNAs. *EMBO J*. 28:1855-1866.

Kosik, K.S. 2006. The neuronal microRNA system. *Nat Rev Neurosci*. 7:911-920.

Krichevsky, A.M., and K.S. Kosik. 2001. Neuronal RNA granules: a link between RNA localization and stimulation-dependent translation. *Neuron*. 32:683-696.

Ladomery, M., E. Wade, and J. Sommerville. 1997. Xp54, the Xenopus homologue of human RNA helicase p54, is an integral component of stored mRNP particles in oocytes. *Nucleic Acids Res*. 25:965-973.

Larminie, C., P. Murdock, J.P. Walhin, M. Duckworth, K.J. Blumer, M.A. Scheideler, and M. Garnier. 2004. Selective expression of regulators of G-protein signaling (RGS) in the human central nervous system. *Brain Res Mol Brain Res*. 122:24-34.

Laver, J.D., X. Li, K. Ancevicius, J.T. Westwood, C.A. Smibert, Q.D. Morris, and H.D. Lipshitz. 2013. Genome-wide analysis of Staufen-associated mRNAs identifies secondary structures that confer target specificity. *Nucleic Acids Res*. 41:9438-9460.

Lebeau, G., L.C. Miller, M. Tartas, R. McAdam, I. Laplante, F. Badeaux, L. DesGroseillers, W.S. Sossin, and J.C. Lacaille. 2011. Staufen 2 regulates mGluR long-term depression and Map1b mRNA distribution in hippocampal neurons. *Learn Mem*. 18:314-326.

Lecuyer, E., H. Yoshida, N. Parthasarathy, C. Alm, T. Babak, T. Cerovina, T.R. Hughes, P. Tomancak, and H.M. Krause. 2007. Global analysis of mRNA localization reveals a prominent role in organizing cellular architecture and function. *Cell*. 131:174-187.

Lee, S.J., J.A. Oses-Prieto, R. Kawaguchi, P.K. Sahoo, A.N. Kar, M. Rozenbaum, D. Oliver, S. Chand, H. Ji, M. Shtutman, S. Miller-Randolph, R.J. Taylor, M. Fainzilber, G. Coppola, A.L. Burlingame, and J.L. Twiss. 2018. hnRNPs Interacting with mRNA Localization Motifs Define Axonal RNA Regulons. *Mol Cell Proteomics*. 17:2091-2106.

Levsky, J.M., and R.H. Singer. 2003. Fluorescence in situ hybridization: past, present and future. *J Cell Sci*. 116:2833-2838.

Li, P., X. Yang, M. Wasser, Y. Cai, and W. Chia. 1997. Inscuteable and Staufen mediate asymmetric localization and segregation of prospero RNA during Drosophila neuroblast cell divisions. *Cell*. 90:437-447.

Lian, S., A. Jakymiw, T. Eystathioy, J.C. Hamel, M.J. Fritzler, and E.K. Chan. 2006. GW bodies, microRNAs and the cell cycle. *Cell Cycle*. 5:242-245.

Liu, J., J.Y. Hu, F. Wu, J.H. Schwartz, and S. Schacher. 2006. Two mRNA-binding proteins regulate the distribution of syntaxin mRNA in Aplysia sensory neurons. *J Neurosci*. 26:5204-5214.

Liu, J., M.A. Valencia-Sanchez, G.J. Hannon, and R. Parker. 2005. MicroRNA-dependent localization of targeted mRNAs to mammalian P-bodies. *Nat Cell Biol*. 7:719-723.

Lu, D., and J.J. Yunis. 1992. Cloning, expression and localization of an RNA helicase gene from a human lymphoid cell line with chromosomal breakpoint 11q23.3. *Nucleic Acids Res*. 20:1967-1972.

Ma, B., J.N. Savas, M.S. Yu, B.P. Culver, M.V. Chao, and N. Tanese. 2011. Huntingtin mediates dendritic transport of beta-actin mRNA in rat neurons. *Sci Rep*. 1:140.

Macchi, P., A.M. Brownawell, B. Grunewald, L. DesGroseillers, I.G. Macara, and M.A. Kiebler. 2004. The brain-specific double-stranded RNA-binding protein Staufen2: nucleolar accumulation and isoform-specific exportin-5-dependent export. *J Biol Chem*. 279:31440-31444.

Martin, K.C., and A. Ephrussi. 2009. mRNA localization: gene expression in the spatial dimension. *Cell*. 136:719-730.

Mayr, C. 2017. Regulation by 3'-Untranslated Regions. *Annu Rev Genet*. 51:171-194.

McClintock, M.A., C.I. Dix, C.M. Johnson, S.H. McLaughlin, R.J. Maizels, H.T. Hoang, and S.L. Bullock. 2018. RNA-directed activation of cytoplasmic dynein-1 in reconstituted transport RNPs. *Elife*. 7.

McKenney, R.J., W. Huynh, M.E. Tanenbaum, G. Bhabha, and R.D. Vale. 2014. Activation of cytoplasmic dynein motility by dynactin-cargo adapter complexes. *Science*. 345:337-341.

Medioni, C., K. Mowry, and F. Besse. 2012. Principles and roles of mRNA localization in animal development. *Development*. 139:3263-3276.

Meer, E.J., D.O. Wang, S. Kim, I. Barr, F. Guo, and K.C. Martin. 2012. Identification of a cis-acting element that localizes mRNA to synapses. *Proc Natl Acad Sci U S A*. 109:4639-4644.

Messitt, T.J., J.A. Gagnon, J.A. Kreiling, C.A. Pratt, Y.J. Yoon, and K.L. Mowry. 2008. Multiple kinesin motors coordinate cytoplasmic RNA transport on a subpopulation of microtubules in Xenopus oocytes. *Dev Cell*. 15:426-436.

Meyer, D., T. Bonhoeffer, and V. Scheuss. 2014. Balance and stability of synaptic structures during synaptic plasticity. *Neuron*. 82:430-443.

Micklem, D.R., J. Adams, S. Grunert, and D. St Johnston. 2000. Distinct roles of two conserved Staufen domains in oskar mRNA localization and translation. *EMBO J*. 19:1366-1377.

Miki, T., and Y. Yoneda. 2004. Alternative splicing of Staufen2 creates the nuclear export signal for CRM1 (Exportin 1). *J Biol Chem*. 279:47473-47479.

Mikl, M., G. Vendra, M. Doyle, and M.A. Kiebler. 2010. RNA localization in neurite morphogenesis and synaptic regulation: current evidence and novel approaches. *J Comp Physiol A Neuroethol Sens Neural Behav Physiol*. 196:321-334.

Mollet, S., N. Cougot, A. Wilczynska, F. Dautry, M. Kress, E. Bertrand, and D. Weil. 2008. Translationally repressed mRNA transiently cycles through stress granules during stress. *Mol Biol Cell*. 19:4469-4479.

Molliex, A., J. Temirov, J. Lee, M. Coughlin, A.P. Kanagaraj, H.J. Kim, T. Mittag, and J.P. Taylor. 2015. Phase separation by low complexity domains promotes stress granule assembly and drives pathological fibrillization. *Cell*. 163:123-133.

Monani, U.R. 2005. Spinal muscular atrophy: a deficiency in a ubiquitous protein; a motor neuron-specific disease. *Neuron*. 48:885-896.

Monnier, N., Z. Barry, H.Y. Park, K.C. Su, Z. Katz, B.P. English, A. Dey, K. Pan, I.M. Cheeseman, R.H. Singer, and M. Bathe. 2015. Inferring transient particle transport dynamics in live cells. *Nat Methods*. 12:838-840.

Moon, S.L., T. Morisaki, A. Khong, K. Lyon, R. Parker, and T.J. Stasevich. 2019. Multicolour single-molecule tracking of mRNA interactions with RNP granules. *Nat Cell Biol*. 21:162-168.

Morisaki, T., K. Lyon, K.F. DeLuca, J.G. DeLuca, B.P. English, Z. Zhang, L.D. Lavis, J.B. Grimm, S. Viswanathan, L.L. Looger, T. Lionnet, and T.J. Stasevich.

2016. Real-time quantification of single RNA translation dynamics in living cells. *Science*. 352:1425-1429.

Morisaki, T., and T.J. Stasevich. 2018. Quantifying Single mRNA Translation Kinetics in Living Cells. *Cold Spring Harb Perspect Biol*. 10.

Nicklas, S., S. Okawa, A.L. Hillje, L. Gonzalez-Cano, A. Del Sol, and J.C. Schwamborn. 2015. The RNA helicase DDX6 regulates cell-fate specification in neural stem cells via miRNAs. *Nucleic Acids Res*. 43:2638-2654.

Ortiz, R., M.V. Georgieva, S. Gutierrez, N. Pedraza, S.M. Fernandez-Moya, and C. Gallego. 2017. Recruitment of Staufen2 Enhances Dendritic Localization of an Intron-Containing CaMKIIalpha mRNA. *Cell Rep*. 20:13-20.

Ostroff, L.E., J.C. Fiala, B. Allwardt, and K.M. Harris. 2002. Polyribosomes redistribute from dendritic shafts into spines with enlarged synapses during LTP in developing rat hippocampal slices. *Neuron*. 35:535-545.

Ozgur, S., and G. Stoecklin. 2013. Role of Rck-Pat1b binding in assembly of processing-bodies. *RNA Biol*. 10:528-539.

Pacey, L.K., L. Doss, C. Cifelli, D. van der Kooy, S.P. Heximer, and D.R. Hampson. 2011. Genetic deletion of regulator of G-protein signaling 4 (RGS4) rescues a subset of fragile X related phenotypes in the FMR1 knockout mouse. *Mol Cell Neurosci*. 46:563-572.

Palacios, I.M., and D. St Johnston. 2001. Getting the message across: the intracellular localization of mRNAs in higher eukaryotes. *Annu Rev Cell Dev Biol*. 17:569-614.

Park, H.Y., H. Lim, Y.J. Yoon, A. Follenzi, C. Nwokafor, M. Lopez-Jones, X. Meng, and R.H. Singer. 2014. Visualization of dynamics of single endogenous mRNA labeled in live mouse. *Science*. 343:422-424.

Parker, R., and U. Sheth. 2007. P bodies and the control of mRNA translation and degradation. *Mol Cell*. 25:635-646.

Pfisterer, U., and K. Khodosevich. 2017. Neuronal survival in the brain: neuron type-specific mechanisms. *Cell Death Dis*. 8:e2643.

Pichon, X., A. Bastide, A. Safieddine, R. Chouaib, A. Samacoits, E. Basyuk, M. Peter, F. Mueller, and E. Bertrand. 2016. Visualization of single endogenous polysomes reveals the dynamics of translation in live human cells. *J Cell Biol*. 214:769-781.

Pilaz, L.J., A.L. Lennox, J.P. Rouanet, and D.L. Silver. 2016. Dynamic mRNA Transport and Local Translation in Radial Glial Progenitors of the Developing Brain. *Curr Biol*. 26:3383-3392.

Popper, B., A. Demleitner, V.J. Bolivar, G. Kusek, A. Snyder-Keller, R. Schieweck, S. Temple, and M.A. Kiebler. 2018. Staufen2 deficiency leads to impaired response to novelty in mice. *Neurobiol Learn Mem*. 150:107-115.

R-Core-Team. 2016. R: A language and environment for statistical computing.

Rajgor, D., T.M. Sanderson, M. Amici, G.L. Collingridge, and J.G. Hanley. 2018. NMDAR-dependent Argonaute 2 phosphorylation regulates miRNA activity and dendritic spine plasticity. *EMBO J*. 37.

Ramos, A., S. Grunert, J. Adams, D.R. Micklem, M.R. Proctor, S. Freund, M. Bycroft, D. St Johnston, and G. Varani. 2000. RNA recognition by a Staufen double-stranded RNA-binding domain. *EMBO J*. 19:997-1009.

Riechmann, V., and A. Ephrussi. 2001. Axis formation during Drosophila oogenesis. *Curr Opin Genet Dev*. 11:374-383.

Riechmann, V., and A. Ephrussi. 2004. Par-1 regulates bicoid mRNA localisation by phosphorylating Exuperantia. *Development*. 131:5897-5907.

Rojas, A., and R. Dingledine. 2013. Ionotropic glutamate receptors: regulation by G-protein-coupled receptors. *Mol Pharmacol*. 83:746-752.

Rook, M.S., M. Lu, and K.S. Kosik. 2000. CaMKIIalpha 3' untranslated region-directed mRNA translocation in living neurons: visualization by GFP linkage. *J Neurosci*. 20:6385-6393.

Ross, E.M., and T.M. Wilkie. 2000. GTPase-activating proteins for heterotrimeric G proteins: regulators of G protein signaling (RGS) and RGS-like proteins. *Annu Rev Biochem*. 69:795-827.

Rossoll, W., S. Jablonka, C. Andreassi, A.K. Kroning, K. Karle, U.R. Monani, and M. Sendtner. 2003. Smn, the spinal muscular atrophy-determining gene product, modulates axon growth and localization of beta-actin mRNA in growth cones of motoneurons. *J Cell Biol*. 163:801-812.

Rowsell, S., N.J. Stonehouse, M.A. Convery, C.J. Adams, A.D. Ellington, I. Hirao, D.S. Peabody, P.G. Stockley, and S.E. Phillips. 1998. Crystal structures of a series of RNA aptamers complexed to the same protein target. *Nat Struct Biol*. 5:970-975.

Ryter, J.M., and S.C. Schultz. 1998. Molecular basis of double-stranded RNA-protein interactions: structure of a dsRNA-binding domain complexed with dsRNA. *EMBO J*. 17:7505-7513.

Sahoo, P.K., S.J. Lee, P.B. Jaiswal, S. Alber, A.N. Kar, S. Miller-Randolph, E.E. Taylor, T. Smith, B. Singh, T.S. Ho, A. Urisman, S. Chand, E.A. Pena, A.L. Burlingame, C.J. Woolf, M. Fainzilber, A.W. English, and J.L. Twiss. 2018. Axonal G3BP1 stress granule protein limits axonal mRNA translation and nerve regeneration. *Nat Commun*. 9:3358.

Salman, H., A. Abu-Arish, S. Oliel, A. Loyter, J. Klafter, R. Granek, and M. Elbaum. 2005. Nuclear localization signal peptides induce molecular delivery along microtubules. *Biophys J*. 89:2134-2145.

Saugstad, J.A., M.J. Marino, J.A. Folk, J.R. Hepler, and P.J. Conn. 1998. RGS4 inhibits signaling by group I metabotropic glutamate receptors. *J Neurosci*. 18:905-913.

Saxton, W.M. 2001. Microtubules, motors, and mRNA localization mechanisms: watching fluorescent messages move. *Cell*. 107:707-710.

Schanzenbacher, C.T., J.D. Langer, and E.M. Schuman. 2018. Time- and polarity-dependent proteomic changes associated with homeostatic scaling at central synapses. *Elife*. 7.

Scheuss, V., and T. Bonhoeffer. 2014. Function of dendritic spines on hippocampal inhibitory neurons. *Cereb Cortex*. 24:3142-3153.

Schneider, D., C. Tuerk, and L. Gold. 1992. Selection of high affinity RNA ligands to the bacteriophage R17 coat protein. *J Mol Biol*. 228:862-869.

Schratt, G.M., F. Tuebing, E.A. Nigh, C.G. Kane, M.E. Sabatini, M. Kiebler, and M.E. Greenberg. 2006. A brain-specific microRNA regulates dendritic spine development. *Nature*. 439:283-289.

Schuldt, A.J., J.H. Adams, C.M. Davidson, D.R. Micklem, J. Haseloff, D. St Johnston, and A.H. Brand. 1998. Miranda mediates asymmetric protein and RNA localization in the developing nervous system. *Genes Dev*. 12:1847-1857.

Serman, A., F. Le Roy, C. Aigueperse, M. Kress, F. Dautry, and D. Weil. 2007. GW body disassembly triggered by siRNAs independently of their silencing activity. *Nucleic Acids Res*. 35:4715-4727.

Sharangdhar, T., Y. Sugimoto, J. Heraud-Farlow, S.M. Fernandez-Moya, J. Ehses, I. Ruiz de Los Mozos, J. Ule, and M.A. Kiebler. 2017. A retained intron in the 3'-

UTR of Calm3 mRNA mediates its Staufen2- and activity-dependent localization to neuronal dendrites. *EMBO Rep*. 18:1762-1774.

Sheth, U., and R. Parker. 2003. Decapping and decay of messenger RNA occur in cytoplasmic processing bodies. *Science*. 300:805-808.

Simon, M.I., M.P. Strathmann, and N. Gautam. 1991. Diversity of G proteins in signal transduction. *Science*. 252:802-808.

Smillie, D.A., and J. Sommerville. 2002. RNA helicase p54 (DDX6) is a shuttling protein involved in nuclear assembly of stored mRNP particles. *J Cell Sci*. 115:395-407.

Song, M.S., H.C. Moon, J.H. Jeon, and H.Y. Park. 2018. Neuronal messenger ribonucleoprotein transport follows an aging Levy walk. *Nat Commun*. 9:344.

St Johnston, D. 2005. Moving messages: the intracellular localization of mRNAs. *Nat Rev Mol Cell Biol*. 6:363-375.

St Johnston, D., D. Beuchle, and C. Nusslein-Volhard. 1991. Staufen, a gene required to localize maternal RNAs in the Drosophila egg. *Cell*. 66:51-63.

Stanton, P.K., and J.M. Sarvey. 1984. Blockade of long-term potentiation in rat hippocampal CA1 region by inhibitors of protein synthesis. *J Neurosci*. 4:3080-3088.

Stockley, P.G., N.J. Stonehouse, J.B. Murray, S.T. Goodman, S.J. Talbot, C.J. Adams, L. Liljas, and K. Valegard. 1995. Probing sequence-specific RNA recognition by the bacteriophage MS2 coat protein. *Nucleic Acids Res*. 23:2512-2518.

Sugimoto, Y., A. Vigilante, E. Darbo, A. Zirra, C. Militti, A. D'Ambrogio, N.M. Luscombe, and J. Ule. 2015. hiCLIP reveals the in vivo atlas of mRNA secondary structures recognized by Staufen 1. *Nature*. 519:491-494.

Sutton, M.A., and E.M. Schuman. 2006. Dendritic protein synthesis, synaptic plasticity, and memory. *Cell*. 127:49-58.

Swetloff, A., B. Conne, J. Huarte, J.L. Pitetti, S. Nef, and J.D. Vassalli. 2009. Dcp1-bodies in mouse oocytes. *Mol Biol Cell*. 20:4951-4961.

Tang, S.J., D. Meulemans, L. Vazquez, N. Colaco, and E. Schuman. 2001. A role for a rat homolog of staufen in the transport of RNA to neuronal dendrites. *Neuron*. 32:463-475.

Tantale, K., F. Mueller, A. Kozulic-Pirher, A. Lesne, J.M. Victor, M.C. Robert, S. Capozi, R. Chouaib, V. Backer, J. Mateos-Langerak, X. Darzacq, C. Zimmer,

E. Basyuk, and E. Bertrand. 2016. A single-molecule view of transcription reveals convoys of RNA polymerases and multi-scale bursting. *Nat Commun*. 7:12248.

Taymans, J.M., H.K. Kia, R. Claes, C. Cruz, J. Leysen, and X. Langlois. 2004. Dopamine receptor-mediated regulation of RGS2 and RGS4 mRNA differentially depends on ascending dopamine projections and time. *Eur J Neurosci*. 19:2249-2260.

Tedford, H.W., and G.W. Zamponi. 2006. Direct G protein modulation of Cav2 calcium channels. *Pharmacol Rev*. 58:837-862.

Teixeira, D., U. Sheth, M.A. Valencia-Sanchez, M. Brengues, and R. Parker. 2005. Processing bodies require RNA for assembly and contain nontranslating mRNAs. *RNA*. 11:371-382.

Terenzio, M., S. Koley, N. Samra, I. Rishal, Q. Zhao, P.K. Sahoo, A. Urisman, L. Marvaldi, J.A. Oses-Prieto, C. Forester, C. Gomes, A.L. Kalinski, A. Di Pizio, E. Doron-Mandel, R.B. Perry, I. Koppel, J.L. Twiss, A.L. Burlingame, and M. Fainzilber. 2018. Locally translated mTOR controls axonal local translation in nerve injury. *Science*. 359:1416-1421.

Therneau, T.A., B. 2018. rpart: Recursive Partitioning and Regression Trees. R package version 4.1-13.

Tiedge, H., A. Zhou, N.A. Thorn, and J. Brosius. 1993. Transport of BC1 RNA in hypothalamo-neurohypophyseal axons. *J Neurosci*. 13:4214-4219.

tom Dieck, S., L. Kochen, C. Hanus, M. Heumuller, I. Bartnik, B. Nassim-Assir, K. Merk, T. Mosler, S. Garg, S. Bunse, D.A. Tirrell, and E.M. Schuman. 2015. Direct visualization of newly synthesized target proteins in situ. *Nat Methods*. 12:411-414.

Tritschler, F., A. Eulalio, V. Truffault, M.D. Hartmann, S. Helms, S. Schmidt, M. Coles, E. Izaurralde, and O. Weichenrieder. 2007. A divergent Sm fold in EDC3 proteins mediates DCP1 binding and P-body targeting. *Mol Cell Biol*. 27:8600-8611.

Tsanov, N., A. Samacoits, R. Chouaib, A.M. Traboulsi, T. Gostan, C. Weber, C. Zimmer, K. Zibara, T. Walter, M. Peter, E. Bertrand, and F. Mueller. 2016. smiFISH and FISH-quant - a flexible single RNA detection approach with super-resolution capability. *Nucleic Acids Res*. 44:e165.

Tübing, F., G. Vendra, M. Mikl, P. Macchi, S. Thomas, and M.A. Kiebler. 2010. Dendritically localized transcripts are sorted into distinct ribonucleoprotein particles that display fast directional motility along dendrites of hippocampal neurons. *J Neurosci*. 30:4160-4170.

Turner-Bridger, B., M. Jakobs, L. Muresan, H.H. Wong, K. Franze, W.A. Harris, and C.E. Holt. 2018. Single-molecule analysis of endogenous beta-actin mRNA trafficking reveals a mechanism for compartmentalized mRNA localization in axons. *Proc Natl Acad Sci U S A*. 115:E9697-E9706.

Tutucci, E., M. Vera, J. Biswas, J. Garcia, R. Parker, and R.H. Singer. 2018a. An improved MS2 system for accurate reporting of the mRNA life cycle. *Nat Methods*. 15:81-89.

Tutucci, E., M. Vera, and R.H. Singer. 2018b. Single-mRNA detection in living S. cerevisiae using a re-engineered MS2 system. *Nat Protoc*. 13:2268-2296.

Vershinin, M., B.C. Carter, D.S. Razafsky, S.J. King, and S.P. Gross. 2007. Multiple-motor based transport and its regulation by Tau. *Proc Natl Acad Sci U S A*. 104:87-92.

Vessey, J.P., A. Vaccani, Y. Xie, R. Dahm, D. Karra, M.A. Kiebler, and P. Macchi. 2006. Dendritic localization of the translational repressor Pumilio 2 and its contribution to dendritic stress granules. *J Neurosci*. 26:6496-6508.

Wang, C., B. Han, R. Zhou, and X. Zhuang. 2016. Real-Time Imaging of Translation on Single mRNA Transcripts in Live Cells. *Cell*. 165:990-1001.

Wickham, H. 2009. ggplot2: Elegant Graphics for Data Analysis. Springer-Verlag, New York.

Wickham, H. 2011. The Split-Apply-Combine Strategy for Data Analysis. *Journal of Statistical Software, 40(1), 1-29*.

Wickham, H.F., R. 2016. dplyr: A Grammar of Data Manipulation. R package version 0.5.0.

Wilhelm, J.E., and R.D. Vale. 1993. RNA on the move: the mRNA localization pathway. *J Cell Biol*. 123:269-274.

Willars, G.B. 2006. Mammalian RGS proteins: multifunctional regulators of cellular signalling. *Semin Cell Dev Biol*. 17:363-376.

Williams, A.H., C. O'Donnell, T.J. Sejnowski, and T. O'Leary. 2016. Dendritic trafficking faces physiologically critical speed-precision tradeoffs. *Elife*. 5.

Willis, D., K.W. Li, J.Q. Zheng, J.H. Chang, A.B. Smit, T. Kelly, T.T. Merianda, J. Sylvester, J. van Minnen, and J.L. Twiss. 2005. Differential transport and local translation of cytoskeletal, injury-response, and neurodegeneration protein mRNAs in axons. *J Neurosci*. 25:778-791.

Wu, B., J.A. Chao, and R.H. Singer. 2012. Fluorescence fluctuation spectroscopy enables quantitative imaging of single mRNAs in living cells. *Biophys J*. 102:2936-2944.

Wu, B., C. Eliscovich, Y.J. Yoon, and R.H. Singer. 2016. Translation dynamics of single mRNAs in live cells and neurons. *Science*. 352:1430-1435.

Wu, B., V. Miskolci, H. Sato, E. Tutucci, C.A. Kenworthy, S.K. Donnelly, Y.J. Yoon, D. Cox, R.H. Singer, and L. Hodgson. 2015. Synonymous modification results in high-fidelity gene expression of repetitive protein and nucleotide sequences. *Genes Dev*. 29:876-886.

Yan, X., T.A. Hoek, R.D. Vale, and M.E. Tanenbaum. 2016. Dynamics of Translation of Single mRNA Molecules In Vivo. *Cell*. 165:976-989.

Yang, Z., A. Jakymiw, M.R. Wood, T. Eystathioy, R.L. Rubin, M.J. Fritzler, and E.K. Chan. 2004. GW182 is critical for the stability of GW bodies expressed during the cell cycle and cell proliferation. *J Cell Sci*. 117:5567-5578.

Yoon, Y.J., and K.L. Mowry. 2004. Xenopus Staufen is a component of a ribonucleoprotein complex containing Vg1 RNA and kinesin. *Development*. 131:3035-3045.

Yoon, Y.J., B. Wu, A.R. Buxbaum, S. Das, A. Tsai, B.P. English, J.B. Grimm, L.D. Lavis, and R.H. Singer. 2016. Glutamate-induced RNA localization and translation in neurons. *Proc Natl Acad Sci U S A*. 113:E6877-E6886.

Youn, J.Y., W.H. Dunham, S.J. Hong, J.D.R. Knight, M. Bashkurov, G.I. Chen, H. Bagci, B. Rathod, G. MacLeod, S.W.M. Eng, S. Angers, Q. Morris, M. Fabian, J.F. Cote, and A.C. Gingras. 2018. High-Density Proximity Mapping Reveals the Subcellular Organization of mRNA-Associated Granules and Bodies. *Mol Cell*. 69:517-532 e511.

Zeitelhofer, M., D. Karra, P. Macchi, M. Tolino, S. Thomas, M. Schwarz, M. Kiebler, and R. Dahm. 2008. Dynamic interaction between P-bodies and transport ribonucleoprotein particles in dendrites of mature hippocampal neurons. *J Neurosci*. 28:7555-7562.

Zhang, H.L., T. Eom, Y. Oleynikov, S.M. Shenoy, D.A. Liebelt, J.B. Dictenberg, R.H. Singer, and G.J. Bassell. 2001. Neurotrophin-induced transport of a beta-actin mRNP complex increases beta-actin levels and stimulates growth cone motility. *Neuron*. 31:261-275.

Zhang, H.L., R.H. Singer, and G.J. Bassell. 1999. Neurotrophin regulation of beta-actin mRNA and protein localization within growth cones. *J Cell Biol*. 147:59-70.

Zhang, W.J., and J.Y. Wu. 1996. Functional properties of p54, a novel SR protein active in constitutive and alternative splicing. *Mol Cell Biol*. 16:5400-5408.

Zimyanin, V.L., K. Belaya, J. Pecreaux, M.J. Gilchrist, A. Clark, I. Davis, and D. St Johnston. 2008. In vivo imaging of oskar mRNA transport reveals the mechanism of posterior localization. *Cell*. 134:843-853.

Appendices

Acknowledgments

This dissertation is not only the culmination of my own work, but also that of the people who have accompanied me on this journey. Here I wish to acknowledge those, who have contributed to the success of this research and who have enabled me to reach this point.

First and foremost, I would like to express the greatest gratitude to my supervisor, Michael, Kiebler, who provided me with the opportunity to pursue the research I am fascinated by. Over the years his support, encouragement and confidence in my work has allowed me to refine myself as an individual and as a scientist.
A very special thanks goes to Edouard Bertrand, who has been instrumental to the success of this work. Though situated in Montpelier, France, he was always interested and eager to discuss science and provide exceptional advice, greatly impacting my research and development as a scientist.

A special thanks also goes to the Graduate School of Systemic Neuroscience (GSN), who have accepted me as a PhD student and provided both a rich social environment and the opportunity to learn and exchange new skills and share my research at workshops, meetings and conferences.
I would like to extend a great thanks to Dorothee Dormann and Oliver Griesbeck, who are part of my TAC and have provided valuable scientific advice and support.

I would like to give special credit to all the people who have mentored me and worked with me on these projects. Thank you, first and foremost Inmaculada Segura who has directly worked with me, mentored me and provided both encouragement and scientific support. Thank you, Saskia Hutten, who set up the MS2 imaging system with me and who mentored me during the first part of my PhD. Thank you, Christin Illig, who has shared in my joy, fascination and occasional frustration at the microscope. Thank you, Sabine Thomas for continued mentoring, support and laughs. Thank you, Renate Dombi, for efficient contributions, interest and support. A

special thanks goes to Imre Gaspar, who saw new potential in my data and taught me to approach questions from unexpected angles.

Great thanks to Sandra Fernández-Moya, Janina Ehses, Rico Schieweck, Ulrike Kring and Daniela Rieger. Thank you to all members of the Kiebler lab and the department of *Zellbiologie*. Thank you for scientific discussions, for sharing your knowledge and your friendship.

Finally, I would like to extend greatest thanks to my friends and family, especially my parents Cathy and Karl Bauer, and my partner Gunnar Kuut. Thank you for your love, support and inspiration.

Declaration of Author contribution

Dr. Inmaculada Segura conducted experiments relevant to Supplementary Figure 2.6A, Supplementary Figure 3.1B and Supplementary Figure 3.3. Dr. Segura conducted experiments relevant to manuscript 1 not included in this dissertation and was involved in manuscript and figure editing.

Dr. Imre Gaspar provided analysis relevant to Figure 2.4D-H and Supplementary Figure 2.4E-N.

Dr. Volker Scheuss conducted experiments relevant to Figure 2.5 and Supplementary Figure 2.5.

Christin Illig conducted experiments and analysis relevant to Figure 2.3F-G, Supplementary Figure 2.3A-F and Supplementary Figure 2.4Q-T. Additionally, Christin Illig generated primary rat hippocampal neuronal cell cultures.

Dr. Georg Ammer provided preliminary experiments not included in this dissertation.

Dr. Saskia Hutten provided experiments relevant to Figure 2.1B, Supplementary Figure 2.1D and preliminary experiments not included in this dissertation.

Dr. Eugénia Basyuk designed the 32xMS2 and 128xMS2 sequence used in manuscript 1.

Dr. Sandra M Fernández-Moya cloned lentiviral plasmids and generated lentiviral particles used for experiments relevant to Figure 2.5 and Supplementary Figure 2.5. Additionally, Dr. Fernández-Moya provided experiments relevant to manuscript 1 not included in this dissertation.

Janina Ehses cloned lentiviral plasmids and generated lentiviral particles used for experiments relevant to Figure 2.5 and Supplementary Figure 2.5.

Dr. Edouard Bertrand designed FISH probes used in experiments relevant to Figure 2.1B and Supplementary Figure 2.1B,D. Additionally, Dr. Bertrand provided scientific guidance and was involved in manuscript and figure editing.

Prof. Dr. Michael A Kiebler provided scientific guidance and was involved in manuscript and figure editing.